TRAFFICKING AND FUNCTION OF THE VOLTAGE-GATED SODIUM CHANNEL B2 SUBUNIT

Èric Cortada Almar

Universitat de Girona

DOCTORAL THESIS

Trafficking and Function of the Voltage-Gated Sodium Channel β2 Subunit

Èric Cortada Almar

2020

DOCTORAL THESIS

Trafficking and Function of the Voltage-Gated Sodium Channel β2 Subunit

Èric Cortada Almar

2020

Doctoral Programme in Molecular Biology, Biomedicine and Health

Supervised by:
Marcel Vergés Aiguaviva, Ph.D.
Ramon Brugada Terradellas, Ph.D., M.D.

Tutor:
Ramon Brugada Terradellas Ph.D., M.D.

Presented to obtain the degree of Ph.D. at the
University of Girona

El Dr. Marcel Vergés Aiguaviva, professor agregat de la Facultat de Medicina de la Universitat de Girona.

El Dr. Ramon Brugada Terradellas, catedràtic de la Facultat de Medicina de la Universitat de Girona, director del Centre de Genètica Cardiovascular de l'Institut d'Investigació Biomèdica de Girona i cap de Cardiologia de l'Hospital Trueta i l'Hospital Santa Caterina de Girona.

DECLAREM: Que el treball titulat "Trafficking and Function of the Voltage-Gated Sodium Channel β2 Subunit" que presenta l'Eric Cortada Almar per a l'obtenció del títol de doctor, ha estat realitzat sota la nostra direcció i que compleix els requisits per poder optar a Menció Internacional. I, perquè així consti i tingui els efectes oportuns, signem aquest document.

Marcel Verges, PhD

Ramon Brugada, PhD, MD

Èric Cortada Almar

Girona, 2020

Above all, don't fear difficult moments.
The best comes from them.

Rita Levi-Montalcini (1909-2012)

Acknowledgements

En primer lloc vull donar gràcies al director de la tesi, en Marcel i al co-director i tutor, en Ramon. Gràcies Marcel per donar-me l'oportunitat de fer la tesi i guiar-me tant bé! Vam començar amb el treball de màster amb β2, i experiment rere experiment... n'ha sortit una tesi i bastant més! Posant la curiositat científica i els experiments ben fets com a base, m'has permès participar en totes les etapes del mètode científic. Al teu costat he après molt. A més, sempre m'has donat suport i encoratjat a fer més i millor, i això crea escola.

Ramon, vull agrair-te donar-me l'oportunitat de fer la tesi a Gencardio i guiar la tesi, però també el teu suport i per encomanar-me la teva empenta.

Seguidament, gent del grup, *Gentcardio(?):* Gràcies per ajudar-me en tantes ocasions, però també simplement per ser-hi! Companys de recerca humida: Marta i Mireia, veïnes de bancada i fans del western blot; Rebecca, David i Yajaira, companys elèctrics i *junkies* de cultius; Adrià, clonning master and *E. coli* brewer. També a vosaltres, estudiants d'en Marcel: Gemma, Robert, Laura, Manu, Heleia, Montse i Irene. Hem passat moltes estones, molt llargues, al lab i han sigut molt entretingudes, i és clar, productives. Ens hem trobat amb bandes fantasma, seqüències anòmales, cèl·lules suïcides, esquitxades, petits incendis i demés entrebancs quotidians de la recerca. Però, mica en mica, m'heu ajudat a superar-los i hem fet unes *risses.* Treballar amb vosaltres ha sigut un plaer.

Companys del primer pis: L'Anna amb el *pimple popper*, en Bernat amb *facts* de la URSS, en Txus *deep down the rabbit hole*, l'Adrià amb el *Pokémon Go,* i menys mal, la Mel·lina aportant una mica de sentit comú... un dia qualsevol a les 11 fent el cafè. Gràcies pel vostre suport acadèmic i *in silico,* però sobretot pels bons moments que hem passat esmorzant, carregant forces, i sí, dient moltes bestieses. Gràcies també als sèniors: Sara, Fabiana, Guillermo i Eli, per les bones preguntes, respostes i millors consells i converses!

També a vosaltres, companys de diagnòstic. Alexandra, Ferran, Mònica, Laura, Marta, Anna I, Núria, Òscar, Eli i Carles. Reactius, aparells, mètodes, trucs i humor (a vegades àcid), sempre teniu un as a la màniga i uns minuts per ajudar-me. I també als exmembres del grup: Javi, Anna T, Irene i Helena. Vam coincidir poc temps, però sempre disposats a donar un cop demà.

Gent de l'ICO: Bet i Sara, les investigadores més productives de l'IDIBGI. Hem compartit moltes hores al laboratori, algunes d'intempestives, sobretot a cultius.

Recordo una nit amb tu, Bet, que ens vam quedar tancats a fora de cultius i quasi fem servir la destral per desbloquejar la porta... sort que va venir el senyor de seguretat a temps. Més endavant et vas quedar tancada a la cambra fosca... a vegades em fas patir! Sara, entre moltes altres coses, em vas ensenyar els múltiples usos d'un encenedor al laboratori. I pensar que al principi només l'utilitzava per encendre el bunsen... M'heu ajudat infinitat de vegades i us ho agraeixo de tot cor. Gràcies també a tu Javier.

Maria, Marina, Jèssica, Anna, Ferran, Naiara, Ariadna, Berta, Esther, Rocío, Neus, i tot el personal de l'IDIBGI, gràcies pel bon rotllo i totes les vegades que m'heu ajudat.

Dani i en Vicenç dels serveis tècnics de la UdG, gràcies per l'ajuda amb el confocal. M'ha quedat estrenar el MALDI!

També vull agrair l'ajuda d'en Carles Rentero i en Carles Enrich del "Clínic" amb l'aïllament de DRMs.

I thank Lori Isom for the opportunity of carrying out a research fellowship in her lab, her guidance and support. I also thank Chunling, Allie, Roberto, Heather, Nnamdi, René, Julie and the rest of her team for their critical help. During those three months, I could call Michigan home. I also thank Matt Brody for the rat CMs and Paul Jenkins for his help in detecting ankyrin recruitment.

Fora del laboratori m'han recolzat de manera incondicional, i ho agraeixo profundament. Vull donar gràcies als meus pares, avis i a en David, que sempre m'han donat suport, acceptat les meves decisions i aguantat el meu molt ocasional mal humor. També a n'en Joan, amb qui hem passat molts bons moments i forces aventures, sempre amb moderació. I és clar, als meus amics, amb els quals m'ho passo rebé.

Gràcies a tots vosaltres!

També dono gràcies a les institucions finançadores que han fet possible el desenvolupament d'aquesta tesi: a l'AGAUR, beneficiaria del Fons Social Europeu, amb la Beca FI per a personal investigador; a l'Obra social La Caixa; a la Univ. de Girona, amb la beca MOB19 per a estades de recerca; a la FECYT, del Ministerio de Ciencia, Innovación y Universidades, pel Projecte de micromecenatge (*crowdfunding*), patrocinat per Precipita, sobre "Arritmias cardíacas"; a al al CIBERCV, consorci públic de recerca del Ministerio de Sanidad, Consumo y Bienestar Social.

List of original publications

Dulsat G, Palomeras S, Cortada E, Riuró H, Brugada R, Vergés M. Trafficking and localisation to the plasma membrane of NaV1.5 promoted by the β2 subunit is defective due to a β2 mutation associated with Brugada syndrome. *Biol Cell*. 2017;109(7):273-291. doi:10.1111/boc.201600085

Cortada E, Brugada R, Verges M. N-Glycosylation of the voltage-gated sodium channel β2 subunit is required for efficient trafficking of NaV1.5/β2 to the plasma membrane. *J Biol Chem*. 2019;294(44):16123-16140. doi:10.1074/jbc.RA119.007903

Under review:

Cortada, E., Serradesanferm R., Brugada, R., Verges, M. S-palmitoylation of the voltage-gated sodium channel β2 subunit confers its association with lipid raft domains. *J. Cell Sci*

Abbreviations

ABE	Acyl-biotin exchange
AF	Atrial fibrillation
AIS	Axon initial segment
AMPA	α-amino-3-hydroxyl-5-methyl-4-isoxazole-propionate
ANOVA	Analysis of variance
AP	Action potential
AP-2	Adaptor protein 2
BACE1	β-secretase1
BFA	Brefeldin A
BiP	Binding immunoglobulin protein
BrS	Brugada syndrome
CAM	Cell adhesion molecule
cAMP	Cyclic adenosine monophosphate
CASK	Calcium/calmodulin-dependent serine protein kinase
CCDS	Consensus coding sequence database
CCP	Clathrin-coated pits
CCV	Clathrin-coated vesicles
cDNA	complementary DNA
CD45	Cluster of differentiation 45
CGN	Cis-Golgi network
CHO	Chinese hamster ovary
CM	Cardiomyocyte
CME	Clathrin-mediated endocytosis
CNS	Central nervous system
COP	Coat protein
CPVT	Catecholaminergic polymorphic ventricular tachycardia
CTB	Cholera toxin B subunit
CTCF	Corrected total cell fluorescence
CTX	Cholera toxin
CaMKII	Calcium/calmodulin-dependent protein kinase II
DAPI	4',6-diamidino-2-phenylindole
DMSO	Dimethyl sulfoxide
DNAJC14	DNAJ homolog subfamily C member 14
DRM	Detergent resistant membranes
DTT	Dithiothreitol
EAE	Experimental allergic encephalomyelitis
ECG	Electrocardiogram
ECL	Electrochemiluminescence
EDTA	Ethylenediaminetetraacetic acid
EE	Early endosomes
EEA1	Early endosomes antigen 1
ERAC	ER-associated compartment
ERAD	ER-assisted degradation

ERGIC	ER-Golgi intermediate compartment
ERO	ER oxidoreductases
ERP	Effective refractory period
FBS	Fetal bovine serum
FRAP	Fluorescence recovery after photobleaching
GFP	Green fluorescent protein
GLUT4	Glucose transporter type 4
GM1	Monosialotetrahexosylganglioside
GM130	Golgi matrix protein 130
GPI	Glycosylphosphatidylinositol
GRASP	Golgi reassembly-stacking protein
GT	Glycosyltransferase
HAM	Hydroxylamine
Hc	Heavy chain
HEK	Human embryonic kidney
HSD	Honest significance difference
HSP70	70 KDa heat shock proteins
HSP90	90 KDa heat shock proteins
ICD	Intracellular domain
ID	Intercalated disc
Ig	Immunoglobulin
I_{Na}	Sodium current
JACoP	Just another co-localization plug-in
KDa	Kilodaltons
LAMP2	Lysosome-associated membrane protein 2
LBPA	Lysobisphosphatidic acid
Lc	Light chain
LE	Late endosomes
LM	Lateral membrane
LQTS	Long QT syndrome
MAGUK	Membrane-associated guanylate kinase
MCDK	Madin-Darby canine kidney
MF	Mobile fraction
MFI	Mean fluorescence intensity
NEB	New England biolabs
NEM	*N*-ethylmaleimide
Na_V	Voltage-gated sodium channel
OST	Oligosaccharyltransferase
PAT	Palmitoyl-acyl transferases
PCR	Polymerase chain reaction
PDI	Protein disulfide isomerase
PM	Plasma membrane
PNGase	Peptide:*N*-glycosidase F
PTM	Post-translational modification
PVDF	Polyvinylidene difluoride
SAP97	Synapse-associated protein 97
SCD	Sudden cardiac death

SDS	Sodium dodecyl sulfate
SNX	Sortin nexin
SRP	Signal recognition particle
ST	Sialyltransferase
TCA	Trichloroacetic acid
TFR	Transferrin receptor
TGN	Trans Golgi network
TGN46	Trans-Golgi network integral membrane protein 2
TM	Transmembrane
TMD	Transmembrane domain
TTX	Tetrodotoxin
TUN	Tunicamycin
TW	Transwell
U18666A	(3β)-3-[2-(Diethylamino)ethoxy]androst-5-en-17-one hydrochloride
VGIC	Voltage-gated ion channel
VTC	Vesicular tubular clusters
WT	Wild type
YFP	Yellow fluorescent protein
ZO-1	Zonula occludens 1

Index of figures

Index of tables

Table of contents

Resum

La subunitat β2 és un component del canal de sodi dependent de voltatge (Na_V), un complex proteic multimèric. Al cor està compost principalment per una subunitat α, formadora del porus, i dues subunitats β associades. Na_V és vital pel funcionament dels cardiomiòcits. Na_V s'obre en resposta a canvis de voltatge al sarcolemma, deixant entrar sodi a la cèl·lula i provocant la seva contracció. Així, Na_V és clau per traduir els potencials d'acció cardíacs en la contracció sincronitzada dels cardiomiòcits, que resulta en el batec del cor.

Els complexes Na_V es concentren en dominis especialitzats al sarcolemma dels cardiomiòcits, conferint-los propietats elèctriques úniques. Les fallides en la correcte localització de Na_V són la base d'un conjunt de canalopaties amb alta incidència de mort sobtada. D'aquesta manera, la localització funcional de Na_V és tant important com el seu correcte funcionament. El paper exacte que juga β2 en el canal encara és un misteri. Tot i això, s'han descrit mutacions en β2 associades a fibril·lació atrial i síndrome de Brugada, ambdues arrítmies letals. En particular, l'efecte de D211G, la mutació associada a síndrome de Brugada, indica que β2 està involucrada en regular a localització a la membrana plasmàtica (MP) de $Na_V1.5$.

En aquesta tesi, explorem el tràfic polaritzat de β2 i descrivim la seva funció en promoure la localització de $Na_V1.5$ al domini apical de cèl·lules Madin-Darby canine kidney. Per aconseguir-ho, utilitzem una combinació de tècniques bioquímiques i de microscòpia de fluorescència. β2 exhibeix tres *N*-glicans complexes, dels quals només un (Asn-42) és sialilat. La glicosilació permet l'arribada eficient de β2 a la MP. A més, β2 glicosilada promou la localització de $Na_V1.5$ a la MP. Sense glicosilació, β2 pot arribar a la MP esquivant l'aparell de Golgi, via *Golgi bypass.* En aquestes condicions, però, ho fa a un terç de la taxa del WT i exhibint glicosilacions simples, provinents del reticle endoplasmàtic (RE). A més, la falta de glicosilació anul·la l'efecte de β2 en la localització de $Na_V1.5$ i resulta en la major part de β2 i $Na_V1.5$ acumulades al RE. Per altra banda, el mutant β2 D211G es localitza al domini apical de cèl·lules polaritzades de la mateixa manera que β2 WT, però no té cap efecte en la localització de $Na_V1.5$. Així, co-expressar β2 D211G amb $Na_V1.5$ produeix un resultat similar a expressar $Na_V1.5$ tot sol: $Na_V1.5$ es queda retingut al RE. Aquesta observació dóna una pista clara del mecanisme patogènic darrere de la mutació.

També hem descobert que β2 és *S*-palmitoïlada a Cys-182. Aquesta modificació post-traduccional concentra β2 a dominis de membrana de baixa densitat. Aquests

dominis són bioquímicament similars als *lipid rafts*, que són subdominis de membrana rics en colesterol. β2 es localitza en *lipid rafts* al domini apical. De fet, hem determinat que aquesta distribució polaritzada de β2 és dependent de la seva associació a dominis de la MP rics en colesterol i al tràfic intracel·lular de colesterol. També hem analitzat la dinàmica de β2 a la MP. β2 és una proteïna molt estable a la MP, donat que no n'hem detectat endocitosi. Mitjançant microscòpia de fluorescència en cèl·lula viva, hem detectat que aproximadament la meitat de la fracció de β2 a la MP és mòbil, exhibint una difusió lenta. L'altra meitat és immòbil i està ancorada a la MP a través de la cua citoplasmàtica.

En resum, els nostres resultat donen suport a la idea que β2 promou la localització funcional de $Na_V1.5$ a subdominis específics de la MP. D'aquesta manera, β2 assegura una densitat de canals de sodi suficient i disminueix el potencial arritmogènic.

Resumen

La subunidad β2 es un componente del canal de sodio dependiente de voltaje (Na_V), un complejo proteico multimérico. En el corazón está compuesto principalmente por una subunidad α, formadora del poro, y dos subunidades β asociadas. Na_V es vital para el funcionamiento de los cardiomiocitos. Na_V se abre en respuesta a cambios en el voltaje del sarcolema, permitiendo entrar sodio a la célula y provocando su contracción. De esta manera, Na_V es clave para traducir los potenciales de acción cardiacos en la contracción sincronizada de los cardiomiocitos, que resulta en latido del corazón.

Los complejos Na_V se concentran en dominios especializados del sarcolema de los cardiomiocitos, confiriéndoles sus propiedades eléctricas únicas. Los fallos en la correcta localización de Na_V son la base de un conjunto de canalopatías con una alta incidencia en muerte súbita. De esta forma, la localización funcional de Na_V es tan importante como su correcto funcionamiento. El papel exacto que β2 juega en el canal es aún un misterio. Aun así, se han descrito mutaciones en β2 asociadas a fibrilación atrial y síndrome de Brugada, ambas arritmias letales. En particular, el efecto de D211G, la mutación asociada a síndrome de Brugada, indica que β2 está involucrada en regular la localización a membrana plasmática (MP) de $Na_V1.5$.

En esta tesis, exploramos el tráfico polarizado de β2 y describimos su función en promover la localización de $Na_V1.5$ al dominio apical de células Madin-Darby canine kidney. Para lograrlo, utilizamos una combinación de técnicas bioquímicas y de microscopía de fluorescencia. β2 exhibe tres *N*-glicanos complejos, de los cuales sólo uno (Asn-42) está sialilado. La glicosilación permite la llegada eficiente de β2 a la MP. Además, β2 glicosilada promueve la localización de $Na_V1.5$ a la MP. Sin glicosilación, β2 puede llegar a la MP saltándose el aparto de Golgi, a través de *Golgi bypass*. Pero, en estas condiciones, lo hace a un tercio de la tasa del WT y exhibiendo glicosilaciones simples, provenientes del retículo endoplasmático (RE). Además, la falta de glicosilación anula el efecto de β2 en la localización de $Na_V1.5$, y resulta en la mayor parte de β2 y $Na_V1.5$ acumuladas en el RE. Por otro lado, el mutante β2 D211G se localiza en el dominio apical de células polarizadas de la misma forma que β2 WT, pero no tiene efecto alguno en la localización de $Na_V1.5$. Así, co-expresar β2 D211G con $Na_V1.5$ produce un resultado similar a expresar solamente $Na_V1.5$: $Na_V1.5$ queda retenido en el RE. Esta observación da una pista clara del mecanismo patogénico detrás de la mutación.

También hemos descubierto que β2 es *S*-palmitoilada en Cys-182. Ésta modificación post-traduccional concentra β2 en dominios de membrana de baja densidad. Estos dominios son bioquímicamente similares a los *lipid raft*, que son dominios de membrana ricos en colesterol. β2 se localiza en *lipid rafts* en el dominio apical. De hecho, hemos determinado que esta distribución polarizada de β2 es dependiente de su asociación a dominios de la MP ricos en colesterol y al tráfico intracelular de colesterol. También hemos analizado la dinámica de β2 a la MP. β2 es una proteína muy estable a la MP, de la cual no hemos detectado endocitosis. Mediante microscopía de fluorescencia en célula viva, hemos detectado que aproximadamente la mitad de la fracción de β2 en la MP es móvil, exhibiendo una difusión lenta. La otra mitad es inmóvil y está anclada a la MP a través de su cola citoplasmática.

En resumen, nuestros resultados respaldan la idea que β2 promueve la localización funcional de $Na_V1.5$ en subdominios específicos de la MP. De esta forma, β2 asegura una densidad de canales de sodio suficiente y disminuye el potencial arritmogénico.

Summary

The sodium channel β2 subunit is a component of the voltage-gated sodium channel (Na_V), a large multimeric protein complex. In the heart, Na_V is mainly composed of a pore-forming α subunit, $Na_V1.5$, and two associated β subunits. Na_V is vital for cardiomyocyte function. Na_V opens in response to voltage changes at the sarcolemma, allowing sodium to enter into the cell and triggering its contraction. Thus, the channel is critical for coupling cardiac action potentials with synchronous cardiomyocyte contraction, resulting in blood pumping.

Na_V complexes concentrate in specialized subdomains of the cardiomyocyte sarcolemma, conferring its unique conduction properties. Deficient Na_V sarcolemma localization underlies a subset of channelopathies with high incidence in sudden death. This way, the functional localization of the Na_V is as important as its correct functioning. The precise role of β2 in the Na_V complex is still a mystery. However, there have been described mutations in β2 linked to Brugada Syndrome (BrS) and Atrial Fibrillation, both deadly cardiac arrhythmias. In particular, the effect of the BrS-associated mutant D211G indicates that β2 has a role in regulating the plasma membrane (PM) localization of $Na_V1.5$.

In this thesis, we explore the polarized trafficking of β2 and describe its function in promoting the localization of $Na_V1.5$ to the apical domain of polarized cells. To do so, we use a combination of biochemistry and fluorescence microscopy approaches. β2 displays three complex *N*-glycans, of which only one (Asn-42) undergoes sialylation. Glycosylation in β2 allows the protein to efficiently reach the PM and promotes $Na_V1.5$ trafficking to the PM. Without glycosylation, β2 can still reach the PM by bypassing the Golgi apparatus, although at a rate of 1/3rd to that of the WT and displaying simple, endoplasmic reticulum (ER)-made glycans. Despite that, lack of glycosylation in β2 abolishes its effect on $Na_V1.5$ localization and results in the bulk of β2 and $Na_V1.5$ retained in the ER. The mutant β2 D211G localizes indistinguishably to its WT counterpart, however, it fails to promote $Na_V1.5$ localization, resulting in $Na_V1.5$ stuck in the ER. This provides clear insight of the pathogenic mechanism behind the mutation.

We found that β2 is *S*-palmitoylated at Cys-182. This post-translational modification partitions β2 into detergent-resistant membranes. These are biochemically similar to lipid rafts, which are subdomains of the PM rich in cholesterol. β2 colocalizes with lipid rafts at the apical domain. In fact, we determined that β2 polarized distribution is dependent on its association to cholesterol-rich domains at the PM and the intracellular trafficking of cholesterol.

We also analyzed the dynamics of β2 at the PM. β2 is highly stable at the PM, displaying no measurable endocytosis. By live cell fluorescence microscopy, we detected that about half the fraction of the protein undergoes slow diffusion, while the other half is immobile, bound to the PM through its intracellular domain.

Overall, our findings support the idea that β2 promotes the functional localization of $Na_V1.5$ to specific subdomains of the PM, thereby ensuring enough sodium channel density and decreasing arrhythmogenic potential.

1.INTRODUCTION

1. Introduction

Proteins are large biomolecules that participate virtually in every process of life. From composing cells to their functioning, proteins are part of the engines, gears, and chassis of the cell.

The present work will focus on a discreet yet important transmembrane (TM) protein, the sodium channel β2 subunit (*SCN2B*). β2 is a component of the voltage-gated sodium channel (Na_V), a large multimeric protein complex. In the heart, the channel is mainly composed of a pore-forming α subunit and two associated β subunits. In response to action potentials, the channel is critical for the synchronous contraction of the cardiomyocytes (CM), resulting in the beating of the heart [1].

β2 precise functions are still a mystery. However, the current understanding points at regulatory roles within the channel complex as a modulator of α subunit functioning; in addition, it may also act as a cell adhesion molecule (CAM) [2]. Despite this limited knowledge, pathogenic mutations in β2 have been linked with deadly cardiac conditions [3,4].

In the next pages we are going to dive deep into β2 biology, explore its structure and even discover a novel function for this protein.

1.1 The secretory pathway

The making of a TM protein starts in the cytosol when a ribosome begins translating a messenger RNA into a polypeptide chain. The first synthesized amino acids often conform the signal peptide, which is recognized by the Signal Recognition Particle (SRP) and brought to the rough endoplasmic reticulum (ER) membrane. At this point, the ribosome inserts the nascent peptide into the ER lumen [5].

During translation (or sometimes once completed), a signal peptidase cleaves the signal peptide, releasing the protein free into the ER lumen in the case of secreted proteins. For TM proteins, the long stretch of hydrophobic amino acids that constitutes their TM domain (TMD) is detected. At this point, the protein is pushed aside and becomes anchored in the ER membrane [6,7].

1.1.2 N-linked glycosylation

Also co-translationally, glycans are attached to an asparagine residue (Asn or N) within the consensus sequence Asn-X-Ser/Thr – where X is any amino acid but proline. For this reason, the process is known as *N*-glycosylation. *N*-glycosylation is a common and conserved modification in eukaryotes. About a quarter of eukaryotic proteins are *N*-glycosylated, and the *N*-glycosylation consensus sequence (or sequon) appears ~ 4-10 times every 1000 residues [8–10].

N-glycosylation occurs in two phases. It starts in the cytosol, where specific glycosyltransferases assemble a branched oligosaccharide onto dolichol pyrophosphate, a lipid carrier. This oligosaccharide is always the same, $Glc_3Man_9GlcNAc_2$ (Glc: glucose; Man: mannose; and GlcNAc: *N*-acetylglucosamine), and identical among many species. The simplicity of this initial glycosylation is in contrast with the vast heterogeneity that mature proteins display after modifications. The second phase continues in the ER lumen. Oligosaccharyltransferase (OST) detects the *N*-glycosylation sequon and transfers $Glc_3Man_9GlcNAc_2$ as a single unit to the asparagine side chain amine (Figure 1), by binding it through an *N*-glycosidic bond [8].

$Glc_3Man_9GlcNAc_2$ is also known as a high mannose oligosaccharide, given the elevated number of mannoses that compose it. These early *N*-glycans enable the protein folding process. They are bulky and hydrophilic, and these properties shield regions of the polypeptide chain prone to hydrophobic aggregation. They also ease the acquisition of secondary structure elements like turns [11]. In this regard, they may be considered as available chemical chaperones. In addition, *N*-glycans display critical information regarding the folding status and age of proteins. During the folding process, $Glc_3Man_9GlcNAc_2$ is digested by several enzymes that sequentially erode and modify its composition and affinity for enzymatic chaperones. These changes are used to organize and regulate the folding process [9,12].

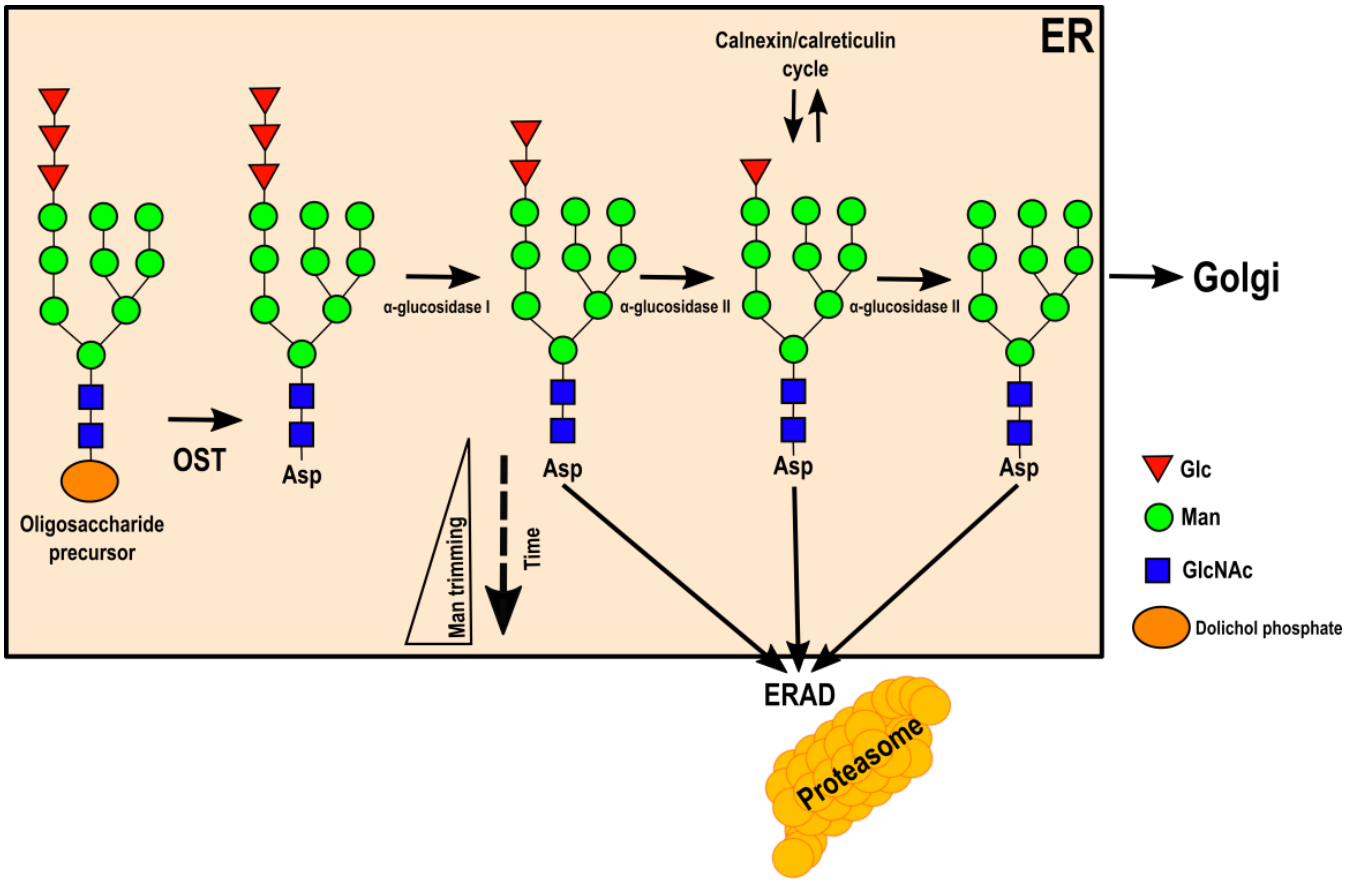

Figure 1. Overall view of ER glycosylation. From left to right: A dolichol-linked oligosaccharide precursor is attached to a nascent polypeptide by OST. α-glucosidases sequentially remove glucoses from the glycan until is ready to be exported to the Golgi apparatus; along this process, proteins undergo through calnexin/calreticulin cycles, which help in their folding. Slowly-folding proteins are subjected to mannose trimming, which increases their likelihood of being discarded through ERAD.

1.1.3 Oxidative folding

Still in the ER, chaperones further assist in the folding of proteins whose cysteine residues are linked together to lock conformations. The majority of proteins require disulfide bonds to achieve proper structure and folding. The ER has an oxidizing environment that facilitates their formation. Disulfide bond formation precedes definitive conformational folding and is prioritized over achieving the most stable conformation. This is especially important for proteins that allow several conformations, as incorrect disulfide bonds would lock improper folding. Formation of native disulfide bonds is a relatively slow process and largely occurs by random encounters of reactive groups. These encounters are determined by peptide chain loops entropies and steric hindrances [12,13].

For the formation of the thioester bond, the thiols of the involved cysteine residues must oxidize. The reaction is catalyzed by protein disulfide isomerases (PDIs) and ER oxidoreductases (ERO). The electrons are transferred from the substrate thiols to the PDI, then to the ERO, and finally are given to oxygen. The process is also called oxidative folding and is coupled with chaperoning, as many PDIs have chaperone activity or form complexes with chaperones (Figure 2). For many proteins, the native conformation is the most stable one. Chaperones facilitate folding by shielding the protein from interactions and aggregation with other proteins. To do so, chaperones create an exclusive folding environment or "Anfinsen cage" [7,13]. There are at least three hierarchical chaperone machineries for this purpose: Hsp70 (70 kDa heat shock proteins), which prefers completely unfolded proteins; Hsp90 (90 kDa heat shock proteins); and calnexin/calreticulin cycle chaperones, which are dedicated to partially folded proteins. Hsp70 and Hsp90 are chaperone protein families [13].

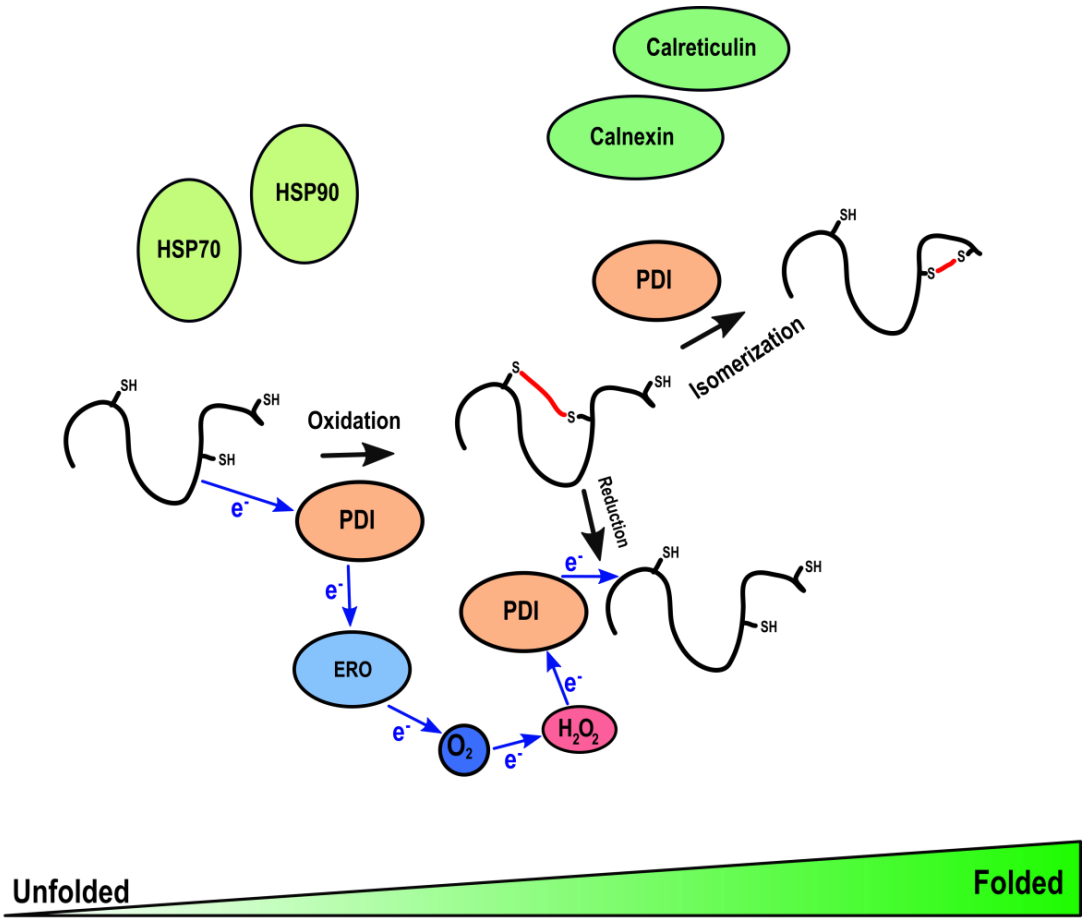

Figure 2. Oxidative folding in the ER. PDIs catalyze the formation of disulfide bonds between cysteine residues. In addition, PDIs can isomerize the folding protein or reduce its disulfide bonds with the help of EROs. Throughout the process, Hsp70 and Hsp90 help to

fold completely unfolded proteins, while calnexin and calreticulin handle partially folded proteins. Disulfide bonds are in red. The flow of electrons is represented with blue arrows.

The calnexin/calreticulin cycle is considered well understood, although some details of its function remain unsolved. While calnexin is a peripheral membrane protein, both calnexin and calreticulin are lectin-like chaperones, therefore they recognize glycans and act post *N*-glycosylation. These have affinity for monoglucosylated glycans, so after glucose trimming of $Glc_3Man_9GlcNAc_2$, where two of the three terminal glucoses are removed by ER glucosidases, the chaperones interact with the partially folded proteins. Calnexin has a specific binding domain for this purpose, and calreticulin, aside from its high affinity for the single glucose, has a hydrophobic binding domain that prevents aggregation with other proteins [12,13]. Alongside glucose trimming and chaperoning, the ER resident glucosyltransferase (GT) competes to reglycosylate the protein attempting to be folded. GT identifies misfolded proteins by recognizing glycans in unstructured regions of the protein with exposed hydrophobic patches. This sends the slowly-folding protein back, to start over the calnexin/calreticulin cycle. Partially folded proteins undergo repeated cycles of folding until a native structure is reached. PDIs cooperate with chaperones to achieve proper folding [12,14].

Once a protein has acquired native disulfide bonds and is properly folded, it is generally ready for ER exit. However, protein synthesis is a hectic task, and despite a diverse array of enzymatic machinery dedicated to ensure proper folding, a fraction of proteins remain misfolded or aggregated. To remove slowly folding and unfoldable substrates, which would block the ER folding machinery, two mechanisms are involved: ER-assisted degradation (ERAD) and autophagy. The first one is activated constitutively to deal with the expected portion of proteins failing to fold. Nonetheless, under ER stress, ERAD capacity increases. The second one is activated under ER stress, but it is unknown if it plays a role in basal conditions [13].

In the ERAD pathway, unfolded proteins are translocated out of the ER and degraded in the cytosol by the proteasome. Slowly folding substrates are identified due to their prolonged time in folding cycles. Evidence suggests that elements of the folding machinery can directly dispatch substrates to ERAD [15]. When protein folding turns difficult, proteins with oligosaccharides in which glucose residues have been cleaved, further mannose cleavage follows. Mannosidases label slowly folding proteins by removing their mannoses from *N*-linked oligosaccharides. Next, lectins, checking for the extent of mannose trimming, detect the slow folding polypeptides and hand these over to ERAD. In addition, mannose trimming creates poor substrates for cleavage by α-glucosidase II (cleaves terminal glucoses of *N*-glycans), and with low affinity to calnexin and calreticulin. This probably results in a

slowdown of the calnexin/calreticulin cycle, eventually leading to protein degradation. Regeneration of PDIs occupied with a slowly folding substrate by EROs may also signal a deficient folding conformation and target the PDI-substrate pair for ERAD [13].

1.1.4 Autophagy

During ER stress, autophagy handles high volumes of unfoldable and aggregated proteins. Autophagy involves the formation of an isolation membrane, the phagophore, which engulfs cytosol and several organelles. The phagophore fuses with lysosomes and gets degraded. When synthesis of a particular protein becomes problematic (e.g. when forcing the expression of an aberrant protein), selective substrate degradation takes place. The ER is compartmentalized, triggering the formation of an ER-associated compartment (ERAC), which is then recognized and absorbed by the phagophore. When misfolded proteins and chaperones accumulate in the ER, the ERAC, stacked ER cisternae and the ER-Golgi intermediate compartment (ERGIC) are generated and detected to be sorted for autophagocytic degradation. If ER stress is prolonged or severe, it can lead to apoptosis [9,13].

1.1.5 ER to Golgi transport

Only properly folded and assembled proteins can leave the ER. Proteins destined for the Golgi apparatus or beyond are packaged into small COP II-coated transport vesicles. COP II (coat protein) are multimeric protein complexes that mediate vesicle budding from the ER. It is a loosely selective process, since ER-resident proteins can get packaged and leak out of the ER. This is redressed by sorting receptors. ER-outgoing vesicles shed the COP II coat after budding and fuse together to form the vesicular tubular clusters (VTC). VTCs move along microtubules to fuse with the Golgi compartment and deliver its cargo [16,17].

COP I is another coat protein complex, but instead enables retrograde transport from the Golgi back to the ER. COP I-coated vesicles bud off from the VTC and go back to the ER to return proteins involved in ER budding, such as subunits of the COP II complex and other resident ER proteins that must be retrieved back to the ER. This process is known as the ER retrieval (or retrograde) pathway. An equivalent process exists for returning leaked out Golgi proteins [17]. This establishes a constant bidirectional transport of cargo between ER and Golgi, with the COP II machinery mediating budding of vesicles from the ER and the COP I

machinery mediating budding of vesicles from Golgi and VTC back to the ER (Figure 3) [18,19].

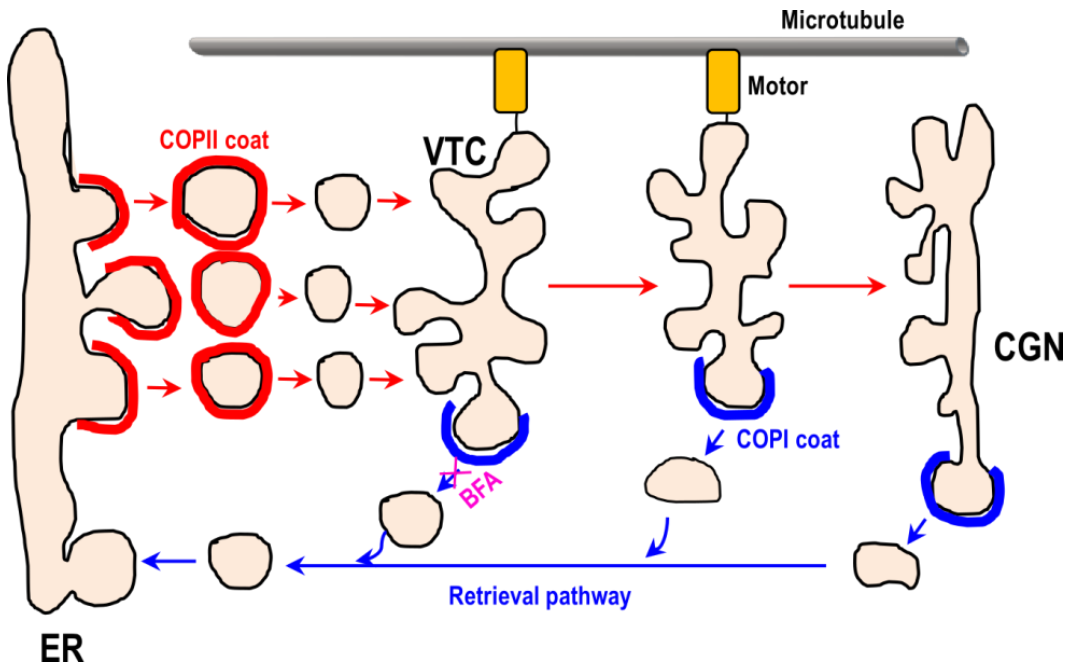

Figure 3. ER to Golgi transport. COPII-coated vesicles enable the anterograde transport from the ER to the Golgi apparatus. Vesicles movement is powered my motors on microtubule tracks. COPII coats and leaked ER resident proteins are brought back to the ER through the retrieval or retrograde pathway, a process mediated by COPI, which allows the budding of vesicles from the VTC and the CGN. The effect of the fungal drug BFA is represented in pink. BFA prevents the assembly of COPI coats, which indirectly prevents the recycling of COPII. This in turn blocks ER-Golgi communication.

The ER retrieval pathway relies on sorting signals. To identify and return ER-specific cargo, resident ER membrane proteins have signals that bind to COP I subunits. A known signal is the KKXX sequence (Lys-Lys-X-X; where X is any amino acid), located at the C-terminus of ER membrane proteins. Soluble ER proteins (like the Hsp70 chaperone 5) have sequences KDEL-like (Lys-Asp-Glu-Leu). The binding of these proteins to their carriers is likely pH-dependent, as different compartments have a different lumenal pH. There is a pH gradient from the ER (more neutral) to the Golgi (more acidic). Aside from the complex ER retrieval pathway, another simpler mechanism exists to retain ER and Golgi-resident proteins in their respective compartments. It involves aggregation of resident proteins to form complexes too large to enter into transport vesicles. This process is called *kin recognition* [16–18].

Yet another even simpler and more elegant strategy to maintain membrane proteins in their designed organelles is based on their TMD length. TMD length determines specific membrane location. Transport vesicles connecting the Golgi and the plasma membrane (PM) are rich in cholesterol. Cholesterol forces a tighter alignment of phospholipid hydrocarbon chains of the lipid bilayer, effectively increasing membrane thickness. TM proteins residing at the plasma membrane have longer TMDs than Golgi and ER-resident TM proteins, permitting their entry into vesicles destined to the PM. This is thought to be a mechanism to keep intracellular membrane proteins within their designated compartment, as ER and Golgi membrane proteins with an artificially long TMD are transported to the PM [20,21]. This aspect will be further explored in section 1.1.9.

The Golgi complex consists of an ordered stack of flattened cisternae. Many of the stacks are connected by tubules. The Golgi is oriented in two faces, the entry or *cis* face and the exit or *trans* face. Both faces are interconnected with a mesh of tubules and cisternae, the cis Golgi network (CGN) and the trans Golgi network (TGN), with the *medial* Golgi in between. The two networks participate in bidirectional protein sorting; in general, proteins move from the ER to the Golgi to then be sorted at the TGN to their final destinations: to the PM, by means of secretory vesicles, or sometimes to an internal organelle. This is noteworthy in cells specialized in secretion, like the globet cells of the intestinal epithelium. These secrete heavy amounts of glycoproteins and proteoglycans, and show very large vesicles at the TGN, highlighting the role of the Golgi in glycosylation and secretion [17,22].

1.1.6 Glycosylation in the Golgi apparatus:

While some mature glycoproteins exhibit ER-made high mannose glycosylation and pass through the Golgi without extra processing, many others undergo complex oligosaccharide modifications. This is mostly because of the location of their oligosaccharides within the protein, which allows or prevents access to a wide array of glycan-editing machinery. These enzymes function in a sequential manner. After a first mannose is removed by ER-mannosidase I, Golgi mannosidase I removes three additional mannoses. Then, GlcNAc transferase I adds a GlcNAc. Next, mannosidase II removes another two mannoses. This sets a common core for complex oligosaccharides, which at this point become resistant to endoglycosidase H (Endo H), an enzyme used to differentiate complex from simple *N*-glycans. From this stage on, galactoses, GlcNAc and sialic acid moieties can be added on top of the core oligosaccharide (Figure 4). Some proteins also have fucose attached to their glycan GlcNAc stem [17].

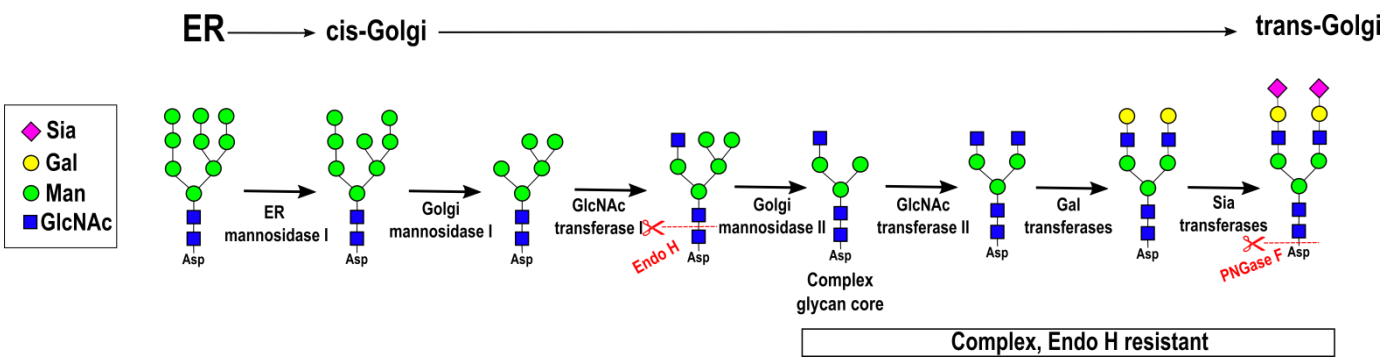

Figure 4. Golgi glycosylation. Overview of the glycosylation steps in the Golgi apparatus. Cleavage sites by glycosidases are in red. Peptide:N-glycosidase F (PNGase F) completely removes all N-glycans. Endo H only removes high mannose glycans. Sia, sialic acid; Gal, galactose; Man, mannose.

In the Golgi apparatus, some proteins undergo O-linked glycosylation. In this type of post-translational modification (PTM), glycosyltransferases attach oligosaccharides to hydroxyl groups of serine and threonine residues. In this case, though, sugar moieties are added one by one and their location is harder to predict, as there is no known O-glycosylation sequon [17].

If simple glycosylation confers enhanced solubility and increases protein half-life by limiting the exposure to proteases, the vast diversity of Golgi glycosylation provides another layer of complexity to the proteins properties. Complex glycans function as specific labels, recognized by lectins that participate in protein sorting at the TGN. In addition, complex glycans on cell surface proteins mediate cell-cell adhesion processes and play regulatory roles [16,17]. For instance, fucosylation facilitates cellular adhesion and immune regulation, and increased protein fucosylation has been associated with inflammatory processes and cancer [23,24].

1.1.7 Post-Golgi trafficking

Newly synthesized cargo going from the ER to the Golgi is concentrated and moves mostly in the same direction. In contrast, the bulk of transport beyond the TGN occurs in many fast-moving transient carriers. On top of that, these pathways are often varied and customized in different cell types. After the TGN, protein cargo intersects with the endosomal pathway before finally arriving to their target organelles or PM subdomains [25].

Constitutive transport derived from the TGN:

Derived from the TGN, there is a continuous transport of (mostly) newly-synthesized and (some) recycling proteins that are headed to the PM and to other multiple destinations. Protein transport through these pathways usually involves continuous traffic of small amounts of cargo in vesicles that bud off at the TGN and fuse with the destination membrane for cargo delivery. Multiple carriers and routes are required for constitutive transport; these fuel major cell functions, like secretion, signaling, cell adhesion, migration and proliferation. The diversity and amount of cargoes of constitutive transport varies extremely among different cell types. For example, maintenance of mature parenchymal cells typically requires minimal transport. On the other end, virtually all constitutive transport in plasma B cells is focused on secreting antibodies [25].

Constitutive transport can be adjusted to cope with periods of increased demand for secretion and protein expression at the PM. To satisfy this larger workload, the expression of trafficking machinery is upregulated and the frequency of constitutive budding at the TGN increased. Another way to deal with increased trafficking requirements is the existence of specialized post-Golgi vesicles. For instance, in adipocytes, upon activation of the insulin receptor, cells need to translocate a large quantity of GLUT4 transporters held in specialized post-Golgi vesicles, i.e. the GLUT4 storage vesicles, to the PM. These arrive to the cell surface and are released in large numbers [26].

Polarized trafficking:

In cells displaying separate membrane domains, distribution of proteins from the TGN to those domains becomes a more complex endeavor. On top of that, in migrating cells, or during the immunological synapse in lymphocytes, polarity is transient and dedicated trafficking routes must be established and suppressed on demand. In apico-basolateral polarity, basolateral transport is mediated by protein carriers that rely on sorting signals, adaptors and clathrin or non-clathrin-dependent mechanisms. Apical transport is less understood and mostly uses lipid-based carriers [25].

The cytoskeleton has ubiquitous roles in all pathways of post-Golgi traffic. Motors on microtubule tracks provide direct transport to membrane domains of polarized cells. A noteworthy fact is that the Golgi apparatus orients and projects the TGN face towards the apical membrane in epithelial cells, to the axon in neurons, to the moving front edge in migrating cells, and to the immunological synapse in lymphocytes. The Golgi and post-Golgi trafficking pathways rely on motors on microtubules to rotate and reorient traffic to the proper direction [25,27].

Endosomal hubs in constitutive transport:

Many post-Golgi pathways intersect with endosomes, especially with recycling endosomes (RE), both during transit to the PM and for redirection to other destinations. RE form a dynamic tubular reticulum where recycled PM proteins converge with newly synthesized proteins coming from the TGN. This way, RE serve as hubs to time, reorganize and direct transport. For example, cargo destined to the basolateral domain goes through RE after leaving the TGN [25,28].

Lipid-based sorting and traffic:

In post-Golgi trafficking pathways, membrane lipids help determine protein destination. Lipid rafts are patches of concentrated cholesterol and glycosphingolipids in biological membranes. These are dynamic, fluid and of different sizes. Because of its hydrophobic properties, lipid rafts attract lipophilic proteins. This promotes the assembly of multimeric complexes and signaling events [29–31].

Lipid rafts form at the TGN to facilitate clustering of specific cargo. Well-known examples of these cargo are glycosylphosphatidylinositol (GPI)-anchored proteins, which localize to lipid rafts and cluster together at the TGN to be delivered to the apical PM, among other destinations. The apical domain of polarized epithelial cells is enriched in lipid rafts and their associated molecules, compared to the basolateral domain. Their biochemical properties help the formation of vesicular carriers: lipid rafts merge together into larger patches, which generate biophysical forces that favor membrane curvature and budding of vesicles and tubules. The same mechanism also participates in clustering of components participating in vesicle transport, such as SNAREs (Soluble *N*-ethylmaleimide sensitive factor attachment protein receptor), Ras-like Rab GTPases, adaptors, coats and cytoskeleton linkers. This way, lipid rafts play critical roles in sorting, packaging, and delivery of cargo between the TGN and the PM [25,32].

Protein-based sorting at the TGN:

Protein-based sorting relies on a diverse array of cytoplasmic mechanisms to sort TM proteins. These mechanisms are based on the interaction of adaptors with the cytosolic domain of cargo proteins and packaging them into vesicular and tubular carriers. Amino acid sequences in the cytosolic tail of cargo proteins are recognized as sorting signals by cytoplasmic adaptors; then, coat proteins sort cargo into specific carriers. At the TGN, sorting signals with tyrosine and dileucine motifs are known for translocating proteins to endosomes or to the basolateral domain of epithelial cells. Phosphorylation and ubiquitination can direct trafficking

as well. Finally, lumenal O-glycosylation can direct proteins to the apical domain [25,32].

1.1.8 Golgi bypass

Some TM proteins can reach the PM skipping a key step of the conventional secretory pathway: The Golgi compartment. Golgi bypass is often the result of cellular stress such as ER and mechanical stress. Stress may impair the functionality of the classical secretory pathway and Golgi bypass may be an efficient alternative to deal with it. PM glycoproteins undergoing Golgi bypass display high mannose ER glycosylation, as they skipped oligosaccharide complex processing. Point mutations in TM proteins can prevent proper folding, which can result in accumulation in the ER and subsequent activation of the ER stress response. Pharmacological inhibition of ER *N*-glycosylation with tunicamycin yields similar results [33]. Brefeldin A (BFA) has an equivalent effect but through a different mechanism. BFA is a commonly used drug to study Golgi bypass since it disturbs ER to Golgi transport by preventing association of the COP-I coat onto Golgi membranes (see Figure 3). BFA targets GBF1 (Golgi-specific Brefeldin A-resistance guanine nucleotide exchange factor 1), a nucleotide exchange factor of the Arf family recruited to Golgi membranes [34,35].

Golgi bypass triggered by ER stress relies on detection of the cargo to be redirected by ER sorting machineries. Two pathways have been described. The first one is based on GRASP (Golgi reassembly-stacking protein). Upon ER stress, GRASP55 (GRASP of 55 KDa) is phosphorylated and relocated from the Golgi to the ER. In the ER, GRASP55 detects the PDZ domain of substrates that undergo Golgi bypass, such as the CFTR (Cystic Fibrosis Transmembrane Conductance Regulator). This enables a sorting mechanism that packs the proteins into carriers destined to the PM, likely via the endosomal compartment [36–38]. The second sorting mechanism is based on Hsp70 and its co-chaperone DNAJC14, and it is well exemplified by pendrin: Hsp70 interacts with mutated H723R pendrin, which under normal conditions would send it to degradation. However, under ER stress, DNAJC14 expression is upregulated, removing the mutated protein from the ERAD pathway and mediating its PM delivery [39].

Golgi bypass triggered by mechanical stress could also be a way to regulate the localization of certain proteins to PM subdomains. In *Drosophila*, ciliary beating may provoke shear stress and subsequent Golgi bypass. This results in integrins and ciliary proteins being delivered to subdomains of the PM, while the classical secretory pathway delivers proteins to other PM subdomains [38,40].

A clear purpose for Golgi bypass is still unknown. However, at least five hypotheses arise: (i) Golgi bypass is a mechanism to bring critical and likely functional proteins to the PM under stress conditions. (ii) Golgi bypass allows proteins that under normal conditions would have complex glycans to display simple glycosylation. This may change the protein function or prevent it from establishing interactions that otherwise require complex glycosylation. (iii) It is a mechanism to sort the same protein to different subcellular locations depending on cellular stress. (iv) It speeds up protein delivery to the (axon) PM of neurons without relying on the Golgi apparatus in the cell body, which could be at a considerable distance [41,42]. (v) Lastly, it could preserve Golgi function and save Golgi processing mechanisms for critical proteins, minimizing the post-translational processing of other, less important, substrates [33,43].

So far, all eukaryotic organisms examined exhibit Golgi bypass mechanisms [44], suggesting that such conserved mechanisms must provide some advantages.

1.1.9 *S*-palmitoylation of membrane proteins

S-acylation is a PTM that consists in the addition of the acyl chain of a saturated fatty acid, usually a palmitate (C16) to a cysteine residue in a protein's TMD or intracellular domain (ICD) via a thioester linkage. For this reason, the names *S*-acylation and *S*-palmitoylation are often used interchangeably. It is a reversible modification and thus is suitable to regulate protein function. *S*-palmitoylation is catalyzed by palmitoyl-acyl transferases (PATs), which are multipass membrane proteins that share a conserved cytoplasmic DHHC (Asp-His-His-Cys) motif. PATs localize to the ER, the Golgi, PM, and endosomes, with the Golgi hosting most of them. However, both increased and lack of palmitoylation can result in Golgi retention. Knowledge about palmitoylation-removing enzymes (palmitoyl-protein thioesterases) is scarce in comparison. Since the thioester bond holding palmitoylation appears to be rather stable, as some proteins stay palmitoylated their entire life cycle, palmitoyl-protein thioesterases should play a critical role in the palmitoylation cycle [45–47].

To date, there is no known consensus sequence for palmitoylation, suggesting that PATs identify specific structural features instead of amino acid sequence motifs. Palmitoylation is involved in regulation of membrane protein folding, trafficking, targeting, and protein-protein interactions. Many palmitoylated TM proteins reside in the PM; despite this, palmitoylation alone rarely is a critical requirement for PM targeting. Instead, it may help to regulate intracellular trafficking steps and partition of proteins in PM microdomains. It has been proposed that palmitoylation may

determine the mode of endocytosis – either clathrin-dependent or independent – and transfer to the RE or the TGN. An example of this is the transferrin receptor, which undergoes clathrin-mediated endocytosis. In the absence of palmitoylation, its rate of endocytosis accelerates [48]. Similarly, palmitoylation increases the PM residence time of anthrax toxin receptor 1 [45].

Protein palmitoylation is known to affect protein-protein interactions via changes in conformation, subcellular localization and steric hindrances (Figure 5). For instance, palmitoylation of the mannose-6-phosphate receptor is required for its interaction with the retromer, a protein complex participating in endosome to TGN transport [49,50]. Examples of negative regulation also exist: C-terminus palmitoylation of α-amino-3-hydroxyl-5-methyl-4-isoxazole-propionate (AMPA) receptors prevents their anchorage with the cytoskeleton through protein 4.1N. This results in AMPA receptors internalization [51].

Palmitoylation can regulate the formation of protein platforms; tetraspanins are a good example of this. These associate to form microdomains containing integrins, signaling molecules and DHHC PATs, regulating integrin-dependent adhesion. Palmitoylation of tetraspanins promotes heterologous associations [47,52].

Palmitoylation and lipid rafts

Palmitoylation partitions many TM proteins into lipid rafts; this is supported by biochemical isolation of detergent-resistant membranes (DRMs), often considered equivalent to lipid rafts given their insolubility in cold non-ionic detergents and their equivalent cholesterol and glycosphingolipids composition. Lipid raft association of a TM protein is likely dependent of one or more of the following: amino acid composition of the TMD(s), whether or not the protein is palmitoylated, its interaction with other proteins, and if these interacting proteins localize to lipid rafts. In spite of this uncertainty, palmitoylation near or at the TMD of a protein does have at least one effect on the protein: it will increase the effective hydrophobicity of the TMD. For instance, this could make TMDs hydrophobic enough to enter into lipid rafts [51]. In addition, in TMD helices bearing bulky amino acids, which usually partition into liquid-disordered (Ld) membranes, palmitoylation may hide part of the helix surface and favor association with liquid-ordered (Lo) membranes microdomains. Palmitoylation may also prolong the TMD hydrophobic stretch (Figure 5) [46]. Palmitoylation on juxtamembrane regions (Figure 5D) may force single pass TM proteins to tilt relative to the plane of the membrane. Tilting could favor protein folding and help the protein to temporarily allocate in intracellular membranes during biosynthesis, as those membranes are thinner than the PM. Studies with mutant, single-pass TM proteins in which their TMDs have been shrunk show that these are retained intracellularly, likely because it becomes too

short and not hydrophobic enough to localize properly to the PM ([47] and our unpublished data).

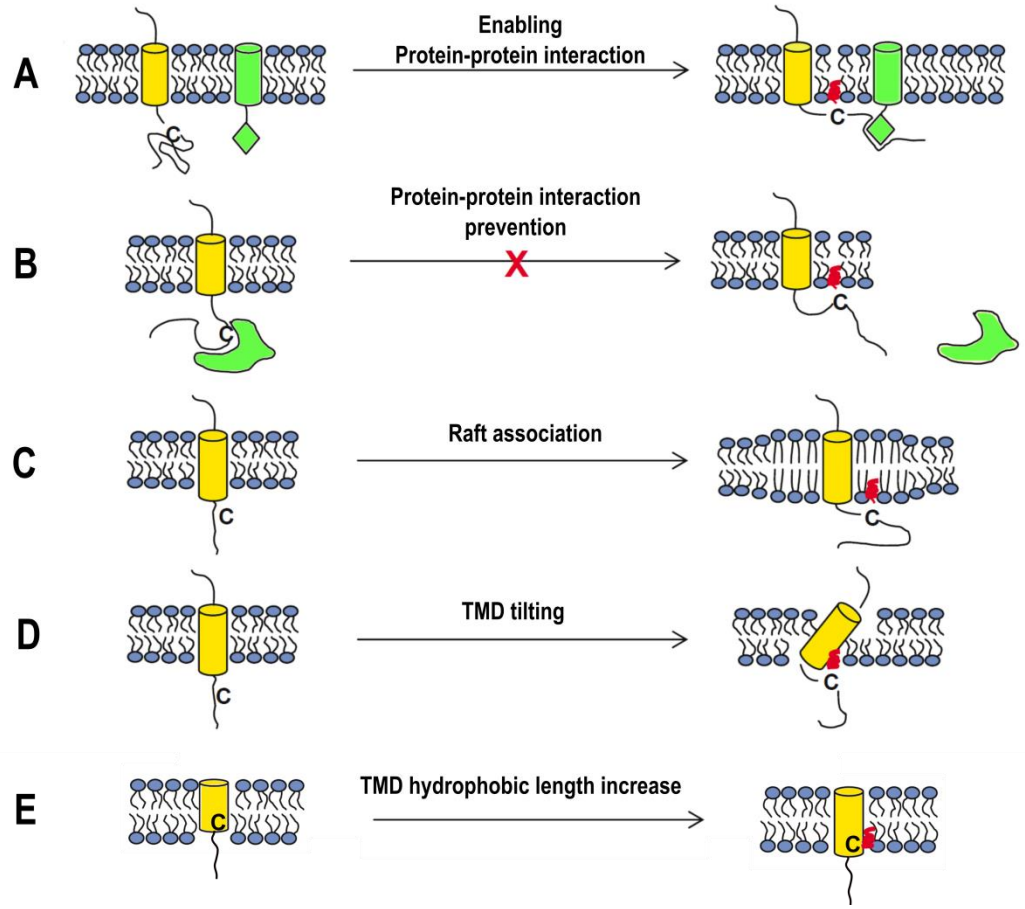

Figure 5. Palmitoylation effects on TM proteins. Palmitoylation can modify the conformation of a protein's ICD, enabling (A) or preventing (B) interaction with other proteins. When palmitoylation is at the juxtamembrane region, it modifies the hydrophobic properties of the TMD, associating the protein with lipid rafts (C), tilting the protein (D) or increasing the TMD's hydrophobic length, better allocating the protein in the lipid bilayer (E). C denotes the palmitoylable cysteine. Adapted from [47].

1.1.10 Endocytic pathway

Cells internalize PM proteins and other macromolecules via endocytosis. PM proteins recycling and degradation is almost as important as their synthesis. This way, endocytic pathways become essential for surface protein turnover, but also to regulate cell surface expression of important proteins and mediate signaling events triggered at the PM. The endocytic pathway was once considered as a fairly passive and non-specific process, where most proteins internalized through "the

bulk membrane flow". Nonetheless, the discovery of specific sorting motifs and cargo adaptors challenged this view and proposed a rather more complex and organized process [53].

Two main modes of endocytosis exist: clathrin-mediated endocytosis (CME) and caveolae uptake.

After proteins and other cargoes have been internalized, the vesicles containing them fuse together to form early (sorting) endosomes (EE). From there, cargoes can be recycled back to the PM via the RE, sent to the TGN via retrograde trafficking mechanisms, or transported through the late endosomes (LE) to the lysosomes for degradation. In polarized cells, cargoes can also be transported across the cell to the other domain of the PM through transcytosis [54].

CME involves clathrin-coated pits (CCP) and clathrin-coated vesicles (CCV). Well-known proteins undergoing CME are the receptors for low density lipoprotein protein and transferrin. CME is carried out in several stages. First, a shallow invagination, the CCP, is formed. Next, cargo is selected and brought to the growing CCP. Among other cargo-specific adaptor proteins, adaptor protein 2 (AP2) recruits and concentrates cargo. Polymerization of clathrin regulates the curvature of the maturing spherical pit. When the CCP is deeply invaginated, dynamin (a large GTPase) encircles the neck of the pit and provokes membrane fission to release a CCV. Finally, clathrin is disassembled and the uncoated vesicle can fuse with an existing endosome [54,55].

Caveolae uptake is important for transcytosis, mechanosensing and lipid regulation. It occurs in caveolae, i.e. flask-shaped PM invaginations that are present in most eukaryotic cells. Caveolae are resistant to cold detergent extraction, very hydrophobic and enriched in cholesterol and sphingolipids [56,57]. Aside from endocytosis, caveolae are considered signaling platforms, regulators of lipid metabolism, and involved in sensing cell surface tension [58]. The principal structural element of caveolae are caveolins, which are integral membrane proteins of the inner leaflet of the PM bilayer. Their cytosolic domain binds to cholesterol and serves as a scaffold to bind to signaling molecules. Compared to CCP, caveolae are rather static, but endocytosis via caveolae is similarly triggered by ligand binding. Caveolae budding is mediated by kinases and phosphatases and, like CME, dynamin releases them from the PM [54,55,59].

In addition to CME and caveolae uptake, a few other endocytic mechanisms are known, but the volume of cargo that they handle is significantly smaller than in CME and caveolae uptake, and their roles and importance are far less understood [54].

Endosomal trafficking

After cargo internalization by any of the mentioned endocytic mechanisms, cytosolic vesicles fuse with the EE, which mature into LE. Their internal pH gradually decreases thanks to proton pumps in their membranes. The lowering pH allows for a gradual release of ligands from their internalized receptors. PM receptors release their ligands in the LE, so that empty receptors can be recycled back to the cell surface, while ligands can be destined to the TGN or to lysosomes, where the lumenal pH is even lower [60]. In addition, each compartment is differentially labeled with specific phosphatidylinositol phospholipids by lipid kinases and phosphatases, and recruits different Rab family GTPases involved in directing the endosomes to fuse with their precise destination organelle (Figure 6) [54].

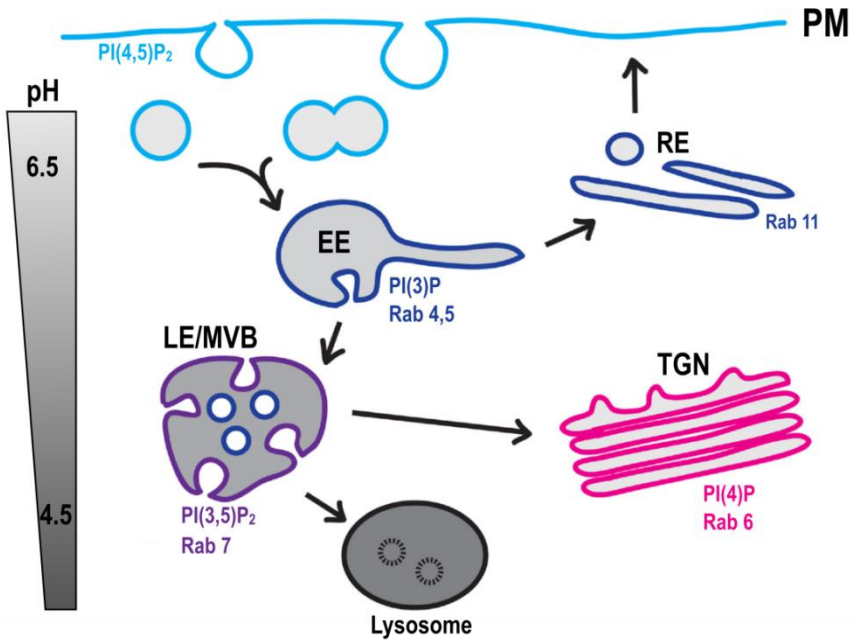

Figure 6. Overview of the endocytic pathway. After internalization, vesicles fuse with the EE, which mature into LE. Gradual acidification allows release of ligands from their internalized receptors. Receptors are recycled back to the PM and ligands are destined to the TGN or the lysosomes. Membrane-specific phosphatidylinositol (PI) phospholipids and Rab family GTPases are indicated. Adapted from [54].

1.2 The voltage-gated sodium channel

Voltage-gated ion channels (VGIC) are TM proteins that allow selected ions to cross the PM in response to changes in the voltage between the two faces of the membrane. This allows a coordinated and lightning fast response to electrical signals within the body. A type of VGIC are the Na_V. Ten genes compose the family of the Na_V (*SCN1A* to *SCN5A* and *SCN7A* to *SCN11A*), which encode channel α subunits $Na_V1.1$ to $Na_v1.9$. Na_X (*SCN7A*) is a voltage-insensitive isoform, which is sensitive to sodium concentration instead, and is considered part of the family [61]. These are present in excitable cells of electrically active tissues. $Na_V1.1$, $Na_V1.2$, $Na_V1.3$ and $Na_V1.6$ are neuronal channels mainly expressed in the central nervous system (CNS); $Na_V1.7$, $Na_V1.8$ and $Na_V1.9$ are expressed in the dorsal root ganglia; $Na_V1.4$ is the skeletal muscle channel; and $Na_V1.5$ is the major cardiac channel[62,63]. Na_X is expressed in the heart, and in glial cells, where has a role in sensing sodium in body fluid [64].

All Na_V (excluding Na_X) isoforms have similar structures, although $Na_V1.5$ is the only one resistant to tetrodotoxin (TTX), e.g. TTX EC50 (half maximal effective concentration) is ~1.2 nM for $Na_V1.2$ while it is ~1-2 mM for $Na_V1.5$. Given its importance on cardiac physiology [63], $Na_V1.5$ is, after β2, an important character in the present work. All nine Na_V have 24 α-helical TM segments organized in four domains (DI to DIV), within a single polypeptide chain of ~2000 amino acids. Every domain is similar but not identical to the other three. Each one consists of six TM segments (S1 to S6). The first four make up the voltage sensing domain and S5-S6 and the linker connecting these two constitute the pore domain (Figure 7). A selectivity filter is formed by a ring of four residues, one from each domain (from DI to DIV: DEKA). The filter makes the channels selective for sodium ions, with more than ten sodium ions entering the cell for each potassium ion [65]. Interestingly, if the DIII lysine (K) is replaced, the selectivity is lost and both sodium and potassium ions can cross the channel [62,66].

When the extracellular face of the PM becomes positively charged, it has been proposed that the charged S4 segment moves toward the cell surface. The movement is transferred to the pore domain through the intracellular linker, changing the conformation and opening the channel for an instant. Next, the channel undergoes fast inactivation, when the voltage sensor is still active, closing the pore again. The brief time in which the channel is open allows a large influx of sodium ions into the cell. The fast inactivation is mediated by four amino acids in the linker between DIII and DIV (IFMT) [67]. When the cytosol is depolarized, these amino acids act like a lid in the intracellular side of the channel (Figure 8). After the

cell repolarizes, the inactivation lid IFMT detaches from the pore's cytosolic end, effectively turning off the fast inactivation mechanism [62].

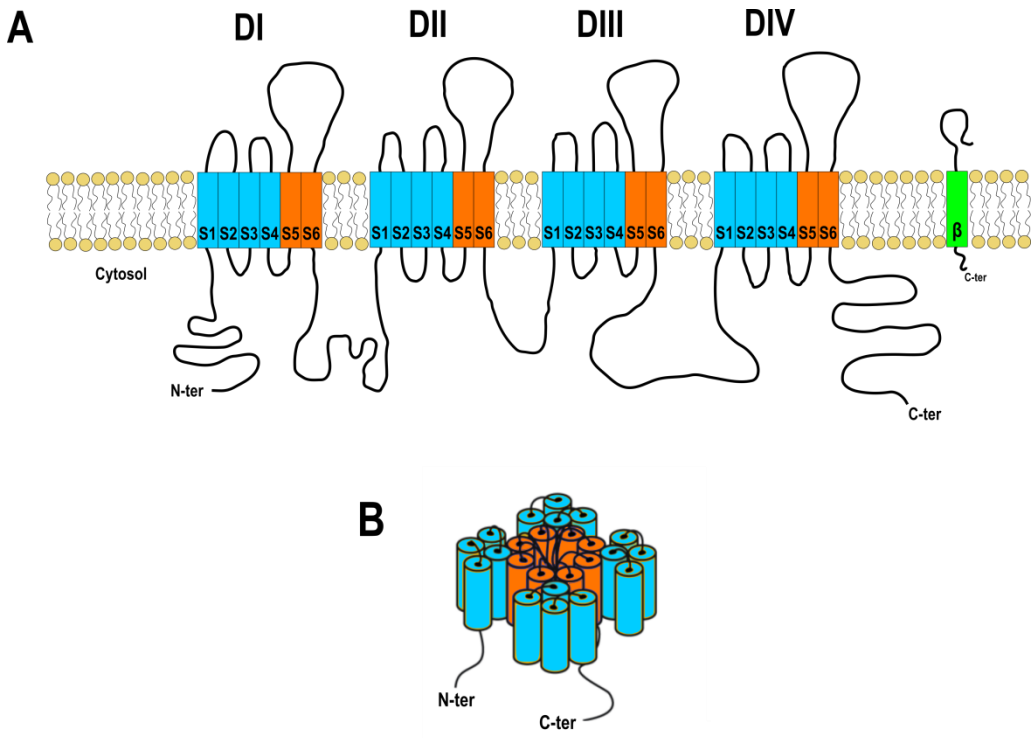

Figure 7. $Na_V1.5$ topology. A. $Na_V1.5$ is composed of a single polypeptide chain, organized into four domains (DI to DIV), each one with six TM segments (S1 to S6). S1 to S4 (in blue) form the voltage-sensing domain, and S5 and S6 constitute the pore domain. β subunits usually accompany the channel. B. Spatial organization of the TM segments.

Another layer of control for channel opening is slow inactivation. In contrast to the fast inactivation, which shuts the channel for milliseconds, slow inactivation closes it for seconds. Slow inactivation occurs during repetitive or prolonged depolarization cycles, limiting channel function over longer time periods. The precise mechanism of slow inactivation is not yet understood, however, it has been suggested that repetitive channel conformational changes during prolonged depolarization may lead to the collapse of the pore and selectivity filter, temporarily blocking conduction. Like fast inactivation, slow inactivation starts during depolarization and ends at repolarized potentials. This way, channels have three functional states: resting (closed), active (open) and inactivated, and they alternate these states cyclically. The inactivated state is the longest and is also called refractory. Channels go back to the open state when the PM has returned to the initial membrane potential (Figure 8) [62,68].

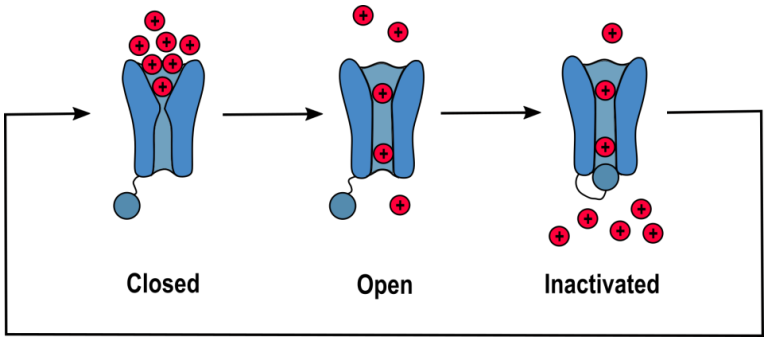

Figure 8. Na_V conformational states. After opening for an instant, the channel becomes inactivated by the blockade of the cytosolic end of the pore thanks to the closure by a "hinged lid". This proposed mechanism of inactivation is also called ball and chain inactivation. Sodium ions are in red.

Sodium channel α subunits dimerize and associate with many interacting partners to form huge multimeric complexes (channelosomes), but it is worth mentioning that, on their own, α subunits are functional and indispensable [69]. The nine $Na_V1.X$ isoforms work in a similar manner but their ultimate functionality is different among the tissues they are expressed in. In neuronal cells, depolarization initiated in the AIS propagates the action potential (AP) along the axon to target cells. In cardiac and skeletal muscle, the AP serves to trigger contraction in a synchronized manner. There, the AP activates a calcium cascade that results in cellular contraction. In the skeletal muscle, contraction produces body movements, while in the heart, blood pumping. In all these locations and roles, α subunits interact with other proteins that modify their biophysical properties, subcellular localization and abundance [62,70].

1.3 Cardiac channelopathies

The heart is an organ that must remain in perfect conditions throughout life. Its abnormal function is a sign of disease and can lead to an early grave. Cardiomyopathies are diseases affecting the function of the heart muscle, are associated with arrhythmia (irregular heart rhythm) and can result in sudden cardiac death (SCD), that is, unexpected heart arrest when, suddenly, arrhythmia prevents sufficient blood flow. In the US, SCD affects up to 400,000 people every year, with coronary heart disease being present in 80% of the cases [71]. In the world, it is estimated that approximately 6 million people die annually of SCD due to ventricular arrhythmia. Worryingly, the survival rate of cardiac arrest is less than 1%. This represents a third of deaths from cardiovascular diseases of any kind, which are the main cause of death worldwide [72]. That said, understanding the

mechanisms by which arrhythmias arise, from inherited and environmental factors, is a top priority in life sciences in order to prevent those and design treatments [1].

SCD occurs in people under 50 and it is often the first and fulminant symptom of an inherited heart disease that has remained undiagnosed by conventional clinical practice [73]. A known arrhythmia is Brugada Syndrome (BrS), a disorder characterized by an abnormal electrocardiogram (ECG) that causes ventricular fibrillation. It is inherited by an autosomal dominant trait and its prevalence in the general population is estimated to be 35/100,000 people, and although it can affect individuals of any age, young men (<40-year-old) are the most affected (75%) [73]. In BrS, the ventricular muscle quivers, instead of contracting in a coordinated manner. Such tachycardia prevents the blood from flowing efficiently in the body; as a result, the individual faints (syncope) and can die in a matter of minutes [1,74].

Since genetics and molecular biology intertwined with clinical biology, multiple genes and variants have been associated with SCD. A fundamental hypothesis is that many SCD cases are the manifestation of rare hereditary diseases caused by mutations in the ion channels that generate the cardiac AP. With this premise, the definition of channelopathies emerged, and comprises diseases linked to the dysfunction of ion channels and the proteins that regulate these. Along with BrS, other channelopathies that cause SCD include long QT syndrome (LQTS) and catecholaminergic polymorphic ventricular tachycardia (CPVT) [1,75].

The Na_V many times shows alterations that lead to cardiac channelopathies. For example, 20-25% of BrS cases are caused by mutations in the *SCN5A* gene, encoding $Na_V1.5$ [73]. In the heart, $Na_V1.5$ is responsible for generating the rising phase of the AP, therefore playing a fundamental role in myocardial excitability. The abnormal ECG observed in BrS is due to a loss-of-function of the Na_V. It is characterized by an ST segment elevation of the V1-V3 precordial leads and occurs in the absence of structural heart disease (Figure 9) [1,74].

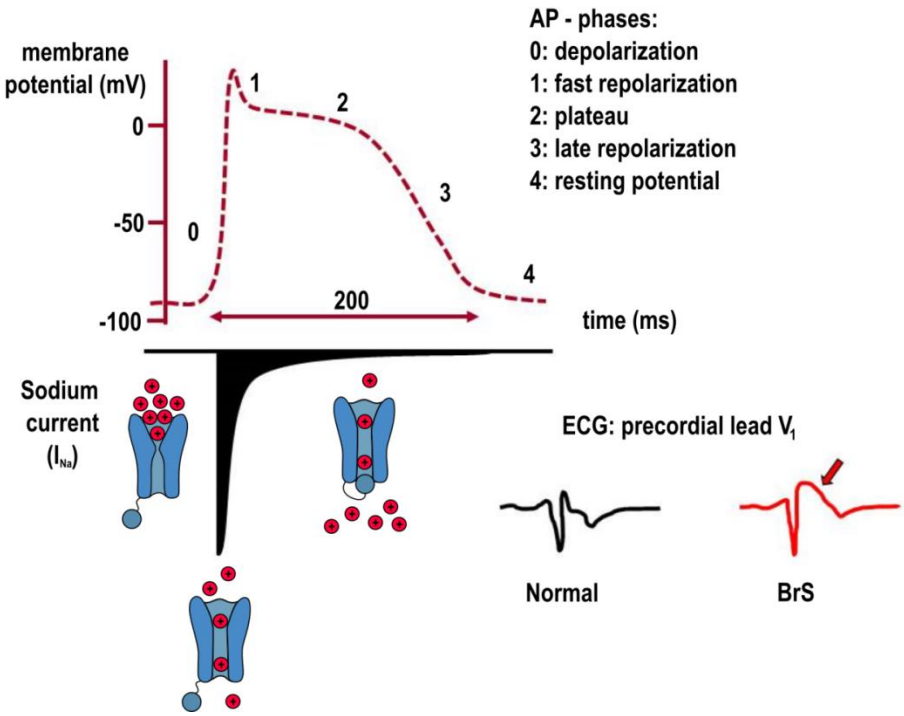

Figure 9. Role of $Na_V1.5$ in the generation of the cardiac AP. Representation of the cardiac AP and the contribution of the sodium current (I_{Na}) generated by $Na_V1.5$, which is responsible for the depolarization phase. The three states of the channel, contributing to the I_{Na} profile, are represented; from left to right, these are closed, open and inactivated. The electrical pattern of precordial lead V1 of a normal ECG and one with an ST segment elevation typical of BrS are shown (arrow). Adapted from [1].

Mutations in *SCN5A* have also been associated with atrial fibrillation (AF), LQTS, CPVT and other channelopathies. In LQTS, the repolarization of the heart is delayed through a characteristically longer QT segment in the ECG [76]. In AF, the atrial chambers of the heart beat rapidly and irregularly [77]. In CPVT, the ventricles beat abnormally fast and irregularly in response to physical activity or emotional stress [78]. Although via different mechanisms, in all these conditions underlying alterations in electrical conduction lead to potentially fatal arrhythmias.

However, mutations in several genes encoding proteins interacting with the Na_V have been associated to channelopathies.

1.4 β subunits

Na_V α subunits interact with a multifarious array of partners, but sodium channel β subunits are the first that come to mind. At first, β subunits were described as mere auxiliary subunits of the big mighty α subunit. However, as research on these thrived, several other roles outside the context of the pore-forming α subunit arose. Nowadays it is common knowledge that β subunits are multifunctional proteins with conducting and non-conducting functions; besides, they are expressed in excitable cells throughout the nervous system and the heart and in non-excitable cells [79]. As partners of the α subunit, β subunits modulate the biophysical properties of the channel and its subcellular localization. β subunits also interact with other components of the channel complex, serving as linkers and anchors. Since all β subunits have an extracellular immunoglobulin (Ig)-like domain, they are considered CAMs. Outside the context of the α subunit, β subunits play roles in extracellular and intracellular signaling pathways, migration, proliferation, neuron axon outgrowth, path-finding and fasciculation in the CNS. In addition, their cleavage products regulate gene expression [2].

β subunit genes appeared later in evolution than α subunit genes. Their genes are found in zebrafish and mammals, but are not present in invertebrates [80]. There are four β subunit genes, (*SCN1B* to *SCN4B*), translating into five proteins: β1, β1B, β2, β3 and β4. β1B is a splice variant of *SCN1B* that lacks the TMD, resulting in a soluble secreted protein. All full length β subunits are type I, single pass TM proteins with three topological domains: the largest one is the extracellular domain containing the Ig-like loop. The other two are the TMD and a short cytoplasmic tail at the C-terminus (Figure 10) [81].

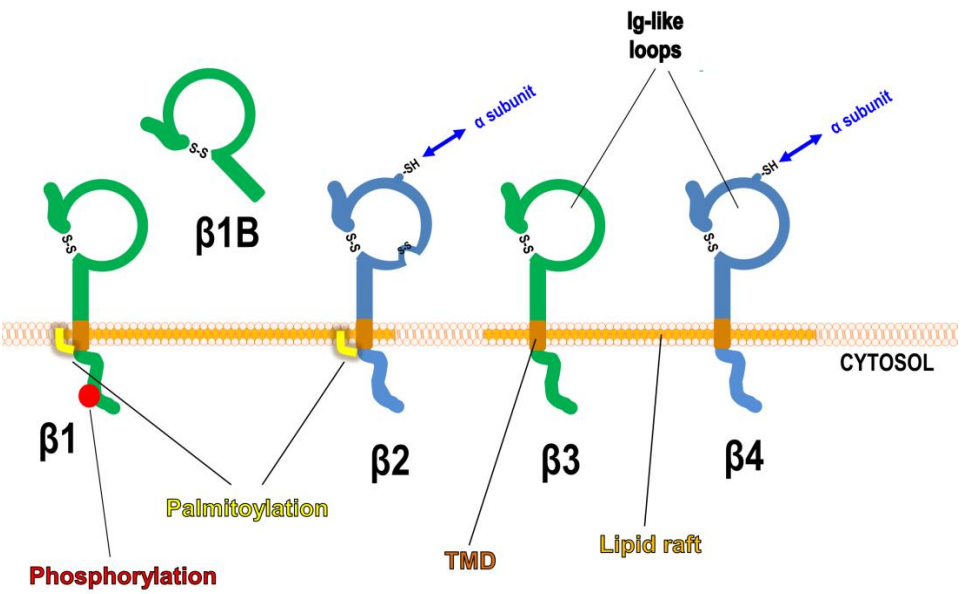

Figure 10. Topology of β subunits. β subunits can be classified in two groups by sequence homology: On the one hand, β1 and β3 (in green), and on the other, β2 and β4 (in blue), which interact with the α subunit through a disulfide bond. β1B is a splice variant of the β1 gene, which lacks the TMD and it is soluble. Structural motifs and PTMs are indicated.

The four TM subunits can be classified by sequence homology and interaction with the α subunit in two groups: β1 and β3, which are similar and interact with α through hydrophobic interactions; and β2 and β4, which are also similar but interact with α covalently via an extracellular disulfide bond (Figure 10) [81].

1.4.1 Multifunction proteins

In conjunction with α, β subunits modify the subcellular localization and gating properties of the channel. For instance, the heterologous co-expression of $Na_V1.2$ with β1 or β2 in Xenopus oocytes increased I_{Na}. Even more interesting, co-expression β1 and β2 with $Na_V1.2$ had a synergistic effect, further increasing the currents compared to $Na_V1.2$ alone, or along with either β1 or β2 [82,83]. Similar to β1 and β2, β3 and β4 also have modulatory effects on sodium channels in heterologous systems [81]. However, their effect is not limited to Na_V, at least for β1, which can also modulate voltage-gated potassium channels [84].

Beside the roles directly related to α subunit function, β subunits display a number of diverse functions on their own. As connectors, β1 and β2 interact homophilicaly (with themselves) and heterophilicaly (with one another), and with the extracellular

matrix proteins tenascin C and R [85,86]. Tenascins are expressed in the developing CNS of vertebrates and reappear in wound healing, regenerative and tumorigenic processes. They influence shape, growth and migration of cells [87]. This supports the implication of β1 and β2 in migration, neurite outgrowth, and their interplay with proteins outside the channel complex.

Interestingly, all full-length β subunits are sequentially cleaved by β and ɣ secretases, releasing their extracellular and intracellular domains respectively [88]. This suggests a potential signaling role for the released CAM domain in the extracellular space. On the intracellular side, downstream signaling effects have been reported for β2. In β2-expressing Chinese Hamster Ovary (CHO) cells, migration and cell-cell adhesion was dependent on β2 cleavage of its ICD [89]. More interestingly, after β-secretase 1 (BACE1) and subsequent ɣ-secretase cleavage of β2, the β2 ICD upregulated transcription and translation of $Na_V1.1$ in neuroblastoma cells. This is relevant since Alzheimer's disease (AD) patients and an AD mouse model (with overexpression of BACE1) have increased levels of BACE1 and β2 cleavage products in neurons. In the mouse, this resulted in increased neuronal expression of $Na_V1.1$ that however accumulated intracellularly, since PM levels and I_{Na} where markedly reduced. This indicates that β2 negatively regulates the cell surface expression of sodium channels and currents in neurons [90].

Other functions of β subunits are closely related to the cellular environment they are expressed in and often regulated by PTMs.

1.4.2 *Glyco*-β subunits

All five β subunits are glycosylated, with 3 - 4 *N*-glycans in their extracellular Ig-like domain, accounting for approximately a third of their molecular weight. Although the implication of glycosylation on β subunit trafficking remains largely unexplored, these PTMs could be involved in their subcellular localization in polarized cells. Their intracellular trafficking could be mediated by recognition of their glycan epitopes by lectins[1]. Glycosylation also appears to be an important modification of β subunits, as in sialylation-deficient (CHO) cells β1 failed to modify the gating of $Na_V1.2$, $Na_V1.5$ and $Na_V1.7$ [91]. Similarly, β2 effect on α subunit gating changed according to its sialylation status and depending on which α was co-expressed with. Namely, β2 sialylation affected the gating of $Na_V1.5$ but not that of $Na_V1.2$, indicating an isoform-specific regulatory effect. [92]. Whether glycosylation is required for β subunits CAM function (at least, regarding to β1 and β2) remains untested, but it is highly likely, as their Ig-like domains are heavily glycosylated.

1.4.3 Subcellular localization and function of β subunits

β subunits can sense the extracellular milieu and react intracellularly. Specifically, this is the case of β1 and β2, whose homophilic interaction with adjacent cells results in ankyrin recruitment at points of cell-cell contact. For β1, this effect was abolished upon phosphorylation. It is worth noting the differential localization of phosphorylated β1 in highly polarized CMs, where it co-localizes with $Na_V1.5$ at the intercalated discs (IDs), while non-phosphorylated β1 co-localizes with TTX-sensitive channels at the T-tubules (Figure 11) [85]. It has been proposed that, at the T-tubules, β1 modulates the channel while, in the IDs, it only has adhesion functions, as phosphomimetic (mutant that simulates phosphorylation) β1 fails to modulate channel function [86]. At the IDs, β1B, which lacks the TMD and therefore cannot be phosphorylated, would modulate the channel [93].

This differential localization of β1 in polarized cells is a common feature of β subunits. They are usually detected in channelosomes, in which are membrane subdomains enriched in the cytoskeleton adaptor ankyrin-G, Na_V and other β subunits. In neurons, β1, β2 and β4 localize to the axon initial segment (AIS), i.e. a membrane domain between the cell soma and the axon [94–96], and at the nodes of Ranvier (specialized regions of the axon membrane that establish gaps in the myelin sheath) of some myelinated neurons. A proposed role for β subunits at the nodes of Ranvier is to stabilize channel complexes and maintain cell-cell contacts, as *scn1b* null mice display fewer channels and neuronal contacts with glia, along with demyelination [85,97]. In the case of β2 (and likely β4), it requires disulfide bonding with the α subunit for their localization at the neuron AIS [96].

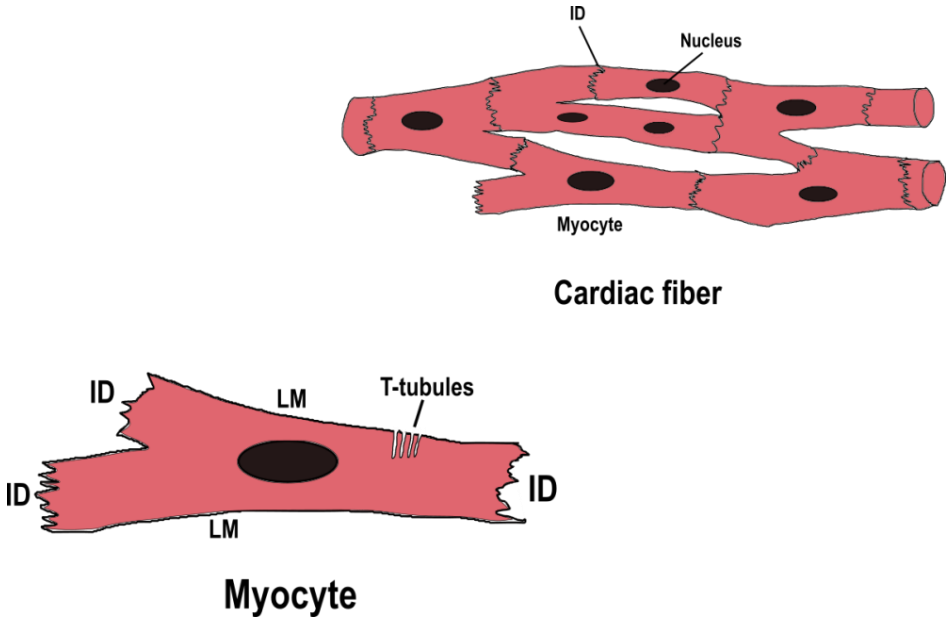

Figure 11. Cardiac fiber and CM representation. CMs are highly polarized cells, displaying three main subdomains at the PM (or sarcolemma). CMs sarcolemma has distinct domains, the LM and the IDs. The T-tubules are a subregion of the LM. CMs are connected through the IDs to constitute cardiac fibers.

In ventricle CMs, β1 localizes at T-tubules and IDs, while in atrium CMs, it only localizes to the IDs [85,98]. More specifically, in the IDs, β1 is enriched at the perinexus, an intercellular space flanking ID gap junctions of two adjacent cells. Through trans-homophilic interaction, it holds together the perinexus and clusters Na_Vs, contributing to cardiac AP propagation [99]. β2 has been detected in T-tubules and IDs in several animal models, but a clear consensus for its precise localization in CMs is still missing [85,98,100]. β3 localizes to T-tubules in mouse ventricular CMs and to the IDs and cell surface puncta in human atrium. β4 mainly localizes to the IDs in mouse ventricle CMs and to cell surface puncta in human atrium CMs [98,100].

1.4.4 Study models for β subunits

Limitations due to the use of heterologous cellular models are apparent, since they lack important channelosome proteins and a specialized and polarized cell architecture. Differences in cell background, specific combination and expression of Na_V subunits, and other interacting partners are also important shortcomings.

However, these models are relatively straightforward to work with and provide useful data to understand Na_V biology. With the ever growing availability of more relevant and complex model systems, like more accurate transgenic animal models and patient-derived, induced pluripotent stem cells, the diverse roles carried out by

Na_V β subunits become more apparent. In particular, transgenic mice are providing strong evidence of β subunit importance in human health.

1.4.5 Discreet proteins, severe diseases

The importance of β subunits is highlighted by their association with disease. Pathogenic mutations in *SCN1B* are linked to various epileptic and arrhythmogenic disorders. *SCN2B* and *SCN3B* mutations are associated with AF and BrS, and *SCN4B* variants are linked to AF and LQTS [79]. Such pervasive connection to devastating diseases establishes these proteins as potential therapeutic targets.

1.4.6 Asymmetric functional redundancy

KO mice for all β subunit genes have been generated, and β2, β3 and β4 KO mice are relatively healthy. In striking contrast, β1 null mice die perinatally [81,101]. In addition, pathogenic mutations in *SCN1B* are associated with more severe and developmental diseases. This could be due to the lack of an analog for β1B. While β2 and β4 may compensate for each other, given their similarity, and β1 may similarly compensate for β3 in its absence, β3 cannot compensate for the lack of the unique β1B, which has no known analogue. An evidence to support the hypothesis of some β subunits being functionally redundant is the case of a double β1 and β2 KO mouse, which has a worse phenotype and dies younger than the *scn1b* KO mice [81].

1.4.7 Neurodegeneration

There may be a link between Na_V and neurodegeneration. A proposed neurodegenerative mechanism is the accumulation of intra-axonal sodium that results in calcium overload, leading to axonal loss and cell death [102]. Thus, persistent I_{Na} (or non-inactivating current, a result of opened Na_V) is associated with increased intracellular calcium concentration, which leads to neuron death. In support of this premise, β2 KO is neuroprotective in experimental allergic encephalomyelitis, a mouse model of multiple sclerosis[103]. In addition, β2 KO mice have reduced I_{Na} density in central and peripheral nervous systems [97,104]. However, this contradicts the findings of another study, which describes β2 as a negative regulator of channel cell surface expression in neurons [90]. This suggests that the link between neurodegeneration and Na_V is not that simple, and that β2 effect on Na_V cell surface expression is likely cell type-dependent, among many other

factors. Nonetheless, I_{Na} reduction might be a suitable therapeutic approach against neurodegeneration [103].

1.5 Ion channel trafficking, cardiac excitability and arrhythmia

The function of the heart is governed by electrical and mechanical activity of CMs. Several types of ion channels, differentially distributed in specialized domains of the sarcolemma, determine the shape and duration of the cardiac AP and therefore control the effective refractory period (ERP). The ERP is the segment of the cardiac AP when the sodium channels remain closed until the cell fully repolarizes. The ERP prevents the spontaneous aperture of the channels, helps coordinating contraction of the cardiac fibers, and regulates the heart rate. Therefore, alterations in the ERP often provoke arrhythmia [105]. Many anti-arrhythmic drugs often prolong the ERP, buying time for all heart cells to repolarize before the new depolarization wave arrives [106].

The majority of arrhythmias are caused by mutations that alter the biophysical properties of the channels, such as their ERP or their sensitivity to voltage changes. These types of arrhythmias are often treated with ion channel blockers. However, some arrhythmias arise from dysfunctional trafficking and stabilization of the channels to their functional subcellular localization. In those cases, effective therapies to restore proper expression of the channels at the CMs sarcolemma are missing [105].

1.6 Channel density and arrhythmias

Alterations in ion channel trafficking are important factors in both acquired and inherited arrhythmias. Channel density at sarcolemma subdomains depends on the organized interplay of anterograde and retrograde trafficking mechanisms. Swings in this equilibrium can lead to overexpression of surface channels, resulting in gain-of-function phenotypes such as LQTS or, more often, in insufficient channel density, leading to loss-of-function phenotypes, like AF and BrS [105].

From synthesis to degradation, including stabilization at the PM, ion channels can fail to achieve proper localization anywhere in their intracellular trafficking routes. However, most mutations provoking trafficking alterations involve ER exit defects, resulting in retention and ERAD of the channel early in the secretory pathway [107].

Another important factor is the interaction of ion channels with β subunits, chaperones, scaffolds and anchors, as the association with these partners regulates subcellular localization and thereby can influence the conducting properties of the CMs and cardiac fibers [108]. Still, we lack deep understanding of these interactions and trafficking routes in native CMs [105]. Nonetheless, a growing volume of research is unveiling the pathogenic molecular mechanisms affecting ion channel trafficking and paving the way for the design of novel therapeutic approaches.

1.6.1 Lipid content

Cellular lipid content can regulate cardiac excitability, as cholesterol directly influences the transport and properties of several cardiac ion channels [109,110]. For instance, depletion of PM cholesterol with methyl-β-cyclodextrin (MβCD) increased the levels of cell surface voltage-gated potassium channel 5 (Kv1.5), while reducing its mobility (as seen by fluorescence recovery after photobleaching, FRAP). This was the result of increased endosome-to-PM recycling of channels stored in submembrane compartments, likely RE, as RE are especially sensitive to cholesterol depletion [111,112]. Although acute modification of cholesterol content is an invasive approach, unparalleled with physiological conditions, the rapid changes in the number of ion channels at the PM highlights the existence of an underlying mechanism modulating the electrical properties of CMs.

1.6.2 Mechanical stress

CMs are constantly subjected to mechanical stress causing stretch, shear and strain. The two main sources of CMs shear stress are the CMs sheets sliding relative to each other and the blood flow [113,114]. This mechanical stimulation triggers APs in monolayers of ventricular CMs [115]. Interestingly, shear stress can also regulate ion channel trafficking, at least for $K_v1.5$. Shear stress increases $K_v1.5$ trafficking from the RE to the PM, and generates a large associated outward current [105].

1.6.3 Multichannel complexes

Ion channels and associated proteins form complexes that regulate their own trafficking and stabilization at the PM. Perhaps the most prominent example is Synapse-associated protein 97 (SAP97), a MAGUK family, scaffold protein that

forms macromolecular complexes with several ion channel families, including $K_V1.5$, Inward Rectifier Potassium Channels (Kir2.x) and $Na_V1.5$ [105]. In particular, SAP97 promotes the formation of $Na_V1.5$ and Kir2.1 complexes. Kir2.1 maintains the resting membrane potential and $Na_V1.5$ initiates the rapid depolarization during APs. The $Na_V1.5$/Kir2.1 complex thus allows these two processes to be tightly regulated to ensure proper cardiac excitability. Moreover, $Na_V1.5$ reduces internalization of Kir2.1 [116].

1.6.4 Partner proteins, polarity and conduction

A result of the highly polarized structure and distribution of ion channels in CMs is their conduction anisotropy. The IDs are highly enriched in $Na_V1.5$, while the lateral membrane (LM) has a considerably lower density of sodium channels (3-8 times less current). This way, APs are transmitted between CMs through the IDs, but APs are conducted along the LM [117,118]. Perhaps for this reason, $Na_V1.5$ has multiple partners (connexin-43, plakophilin-2, ankyrin-G and SAP97) at the IDs, and only two (syntrophin and ankyrin-G) have been reported at the LM (Figure 12) [119]. KO or KD of any of these partners resulted in reduced I_{Na} and altered localization of $Na_V1.5$, implying their positive regulation of $Na_V1.5$ targeting [105]. However, the MAGUK family CASK (calcium/calmodulin-dependent serine protein kinase) associates with the syntrophin/dystrophin/$Na_V1.5$ complex at the LM and prevents $Na_V1.5$ trafficking to the LM, negatively regulating I_{Na} intensity [120]. More importantly, CASK expression is reduced in dilated human atria associated with AF. In this case, CASK would fail to downregulate the expression of $Na_V1.5$ at the CMs LM, altering CM conduction anisotropy and resulting in tissue remodeling and arrhythmia [105].

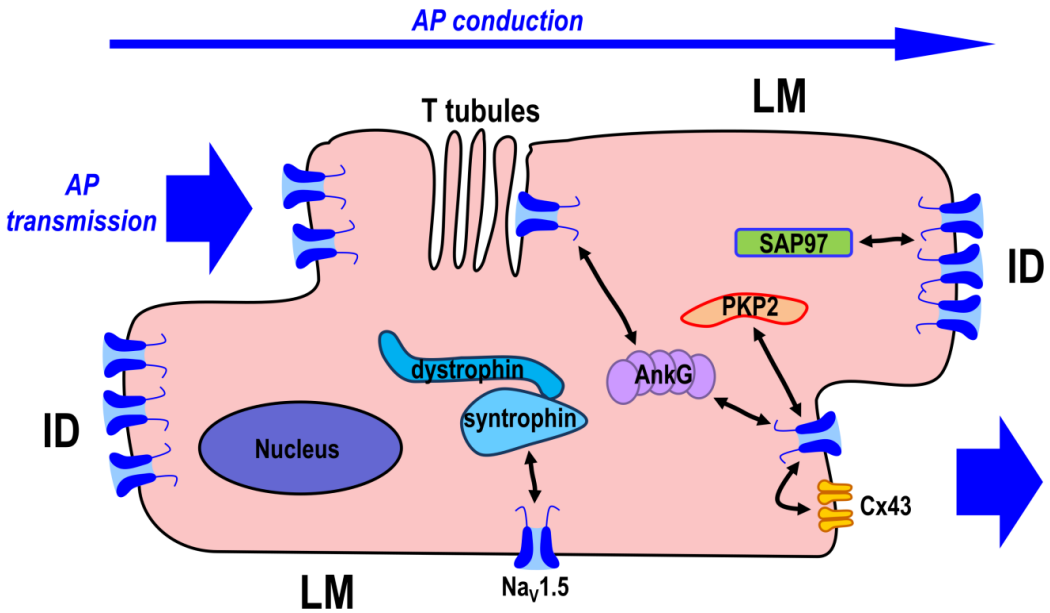

Figure 12. $Na_V1.5$ distribution in the CM. $Na_V1.5$ interaction with other proteins defines different pools of the channel, which distribute in specific subregions of the CM sarcolemma; this is the basis of the CM conduction anisotropy, represented by blue arrows. While the LM is oriented along the AP direction, the IDs are perpendicular to it; this results in different AP conduction velocities. The IDs hold more $Na_V1.5$ than the LM, which results in a more intense I_{Na}, represented by thick arrows. Adapted from [1].

1.6.5 Sarcolemma scaffolds and anchors

$Na_V1.5$ has an ankyrin-G binding domain in the DII-DIII cytoplasmic loop. In CMs, ankyrin-G targets $Na_V1.5$ to the sarcolemma and associates it with other proteins, such as the scaffold protein β4-spectrin and the signaling molecule calcium/calmodulin-dependent protein kinase II (CaMKII), among others, to form multimeric complexes [121]. However, a BrS-associated mutation in $Na_V1.5$ abolishes its association with ankyrin-G. This prevents $Na_V1.5$ accumulation at the IDs. Interestingly, in HEK293 cells the mutation does not affect $Na_V1.5$ cell surface expression [122], highlighting the differences in trafficking machineries of different cell types and a reminder for the need of physiologically relevant model systems.

1.6.6 Ubiquitin-mediated endocytosis

Another mechanism regulating PM expression of ion channels is ubiquitination. Ubiquitin is a small (8,6 kDa) regulatory protein that it is attached to proteins in a three steps process by three types of enzymes; ubiquitin-activating enzymes (E1s), ubiquitin-conjugating enzymes (E2s) and ubiquitin ligases (E3s). This protein modification often marks proteins for proteasomal degradation, but can also affect their subcellular localization, activity and interaction with other proteins [123]. The addition of ubiquitin to PM ion channels by E3s is followed by their internalization and degradation, usually in the lysosome [124]. For instance, $Na_V1.5$ has a PY motif (Pro-Pro-X-Tyr) that can be recognized by the E3 ubiquitin-protein ligase neural precursor cell-expressed developmentally downregulated protein 4-2 (Nedd4-2). Upon ubiquitination at the PM, $Na_V1.5$ is internalized and targeted for degradation [125]. Curiously, pathogenic mutations altering PY motif formation in $Na_V1.5$ are associated with both gain and loss-of-function channelopathies. Recent evidence for this was provided by Wang and colleges. They described two mutations, at and near the PY motif of $Na_V1.5$, associated to LQTS type 3 and BrS, respectively. The LQTS-associated mutation modifies the PY motif, rendering it dysfunctional. This prevented $Na_V1.5$ ubiquitination and subsequent removal from the PM, resulting in an accumulation of channels at the cell surface and thus a gain-of-function phenotype. At the other end, the BrS-associated mutation creates an additional PY motif, which resulted in increased ubiquitination and clearance of $Na_V1.5$ from the PM, leading to a loss-of-function phenotype. Internalization of $Na_V1.5$ was likely followed by proteasomal degradation, as proteasome inhibitors restored mutant channel levels to those similar in the WT (Figure 13) [126,127].

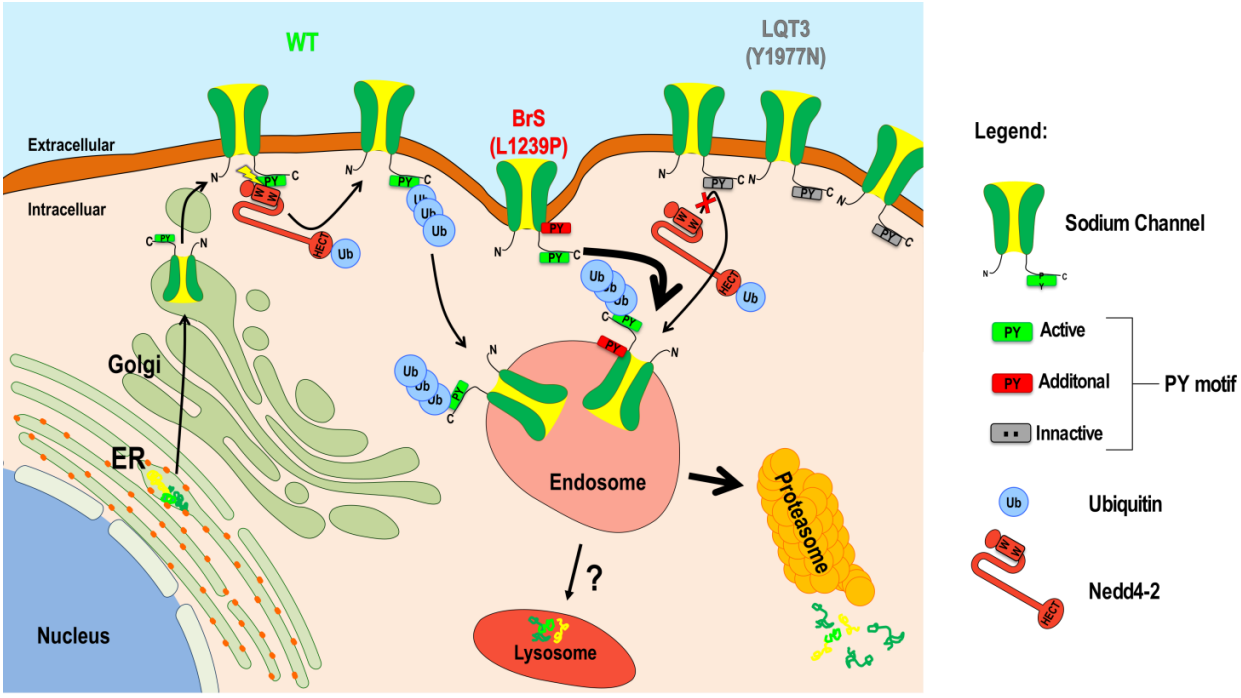

Figure 13. Alterations in ubiquitin-mediated endocytosis of $Na_V1.5$. $Na_V1.5$ is synthesized in the ER and exported to the Golgi apparatus to reach the PM. Once at the PM, its PY motif can be recognized by the WW domain of the HECT-type E3 ubiquitin ligase Nedd4-2, which binds to proline-rich motifs. Ubiquitination (Ub) of $Na_V1.5$ promotes its internalization and targeting to degradation at the proteasome, or perhaps in the lysosome. BrS- and LQTS type 3-associated mutations, respectively, create an additional $Na_V1.5$ PY motif, or remove the existing one, leading to lack or surplus of channels at the PM. Adapted from [127].

1.7 Pathogenic Na_V β2 subunit

In current genetic counseling, *SCN2B* is regularly screened for potentially pathogenic variations [73]. So far, three *SCN2B* variants, resulting in amino acid changes, have been linked to two diseases. On the one hand, R28Q and R28W, located at the signal peptide of β2, were found associated with AF. In CHO cells, co-expression of $Na_V1.5$ and mutated β2 reduced ~30% the I_{Na} peak and affected the voltage dependence of activation compared to the WT [4]. On the other hand, D211G, in the β2 ICD, was found associated with BrS. In CHO cells, co-expression of $Na_V1.5$ and mutant β2 reduced ~40% the I_{Na} peak, and also cell surface $Na_V1.5$ levels in comparison to the WT, suggesting a trafficking defect [3].

Aside from these three variants, a growing number of *SCN2B* variants are potentially associated with cardiac diseases, often detected in combination with

other potentially pathogenic variants, as seen in ClinVar [128]. For the aforementioned evidence regarding β2 function and association with disease, it becomes a key requirement to understand the molecular mechanisms governing β2 biology and how the disruption of these may underlie AF, BrS and the alterations seen in transgenic animals and model cell systems.

β2 is a protein of 215 amino acids: the first 29 amino acids correspond to the signal peptide, residues 30-159 are the extracellular domain, residues ~160-180 are the TMD, and residues 181-215 comprise the ICD (UniProt O60939) [129]. Within this relatively simple architecture, several sites stand out. On the extracellular domain, there are three predicted *N*-glycosylation sites, i.e. at Asn N42, N66 and N74. Cys C55 is available to form a disulfide bond with the Na_V α subunit. A disulfide bond from C50 to C127 holds the Ig-like loop. An additional disulfide bond between C72 and C75, a unique feature among β subunits, has also been described [96,129,130]. In the intracellular side, C182 may be *S*-acylated/palmitoylated, based on β1 analogy [2,131]. S192 and T204 are putative phosphorylation sites [129]. Flanking the TMD, on the extracellular face, β secretase then cleaves likely between L147 and M148, and γ secretase cleaves the ICD (Figure 14) [90].

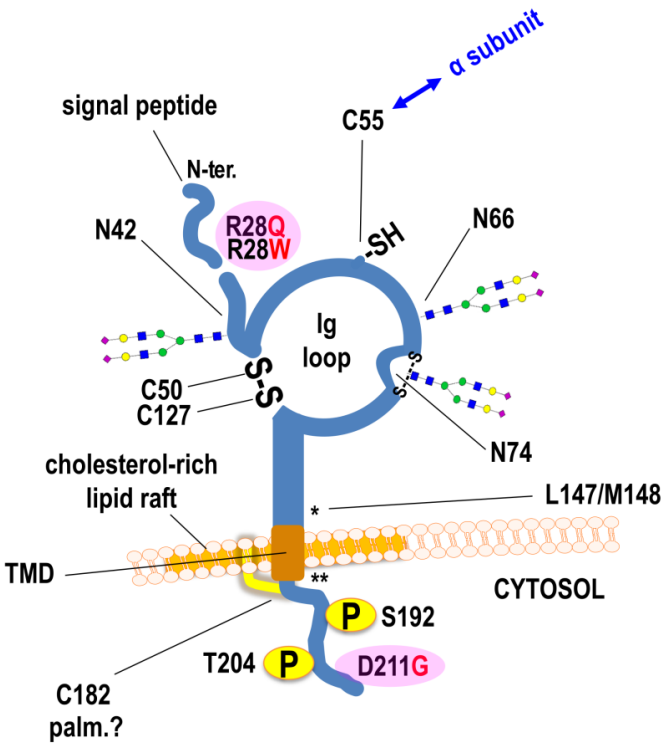

Figure 14. Sequence and domain architecture of the β2 subunit. Of its 215 amino acids, the first 29 correspond to the predicted N-terminal (N-ter.) signal peptide. It is worth noting the extracellular Ig-like loop. The TMD, which expands along ~ 20 residues, and is probably associated with lipid rafts, is followed by a short C-terminal domain. Asterisks denote the approximate location of cleavage sites by β-secretase (L147/M148; *) and ɣ-secretase (**). Pathogenic mutations, i.e. the AF-associated R28Q and R28W, and the BrS-associated D211G are shown in pink background; see the text for more details. Adapted from [1].

Although mutations in β2 have a modest influence on the biophysical properties of the Na_V, so far the literature suggests a role by β2 in promoting trafficking of the Na_V to the cell surface. In order to rigorously explore this function of β2, one must first dissect the mechanisms governing trafficking and localization of β2, to then assess β2 influence on the main cardiac Na_V.

2.HYPOTHESES

2. Hypotheses

The dysfunctional trafficking and localization of the Na_V and other ion channels define a subset of channelopathies with a high risk of sudden death. This way, the functional localization of the Na_V to the CM sarcolemma is as important as its correct functioning. The intracellular transport pathways that establish the highly specialized CM polarity are poorly understood; however, it is well known that at the CM sarcolemma different pools of VGIC confer the CM with its unique conduction and excitability properties. Evidence from a BrS-associated variant indicates that the Na_V β2 subunit has a role in regulating PM localization of $Na_V1.5$. Despite this, even a basic understanding of β2 and $Na_V1.5$ trafficking and localization in a relevant model of cell polarity is missing. Other β subunits, namely β1, have been found to exert different roles, both in and outside the context of the Na_V α subunit. Such effects are mediated by their functional architecture and PTMs.

Thus, we hypothesize that β2 displays a specialized subcellular distribution in polarized cells. More precisely, we propose that specific sequence motifs in the topology of β2 determine its polarized trafficking to the PM and regulate its effect on $Na_V1.5$ subcellular localization. Specifically, we propose that (1) glycosylation at predicted sites allows its exit from the ER and arrival to the PM; (2) *S*-palmitoylation facilitates β2 partitioning to subcellular domains of the PM; and (3) the ICD anchors β2 to the submembrane actin cytoskeleton. Importantly, we suggest that some of these elements in β2 are important to promote cell surface localization of $Na_V1.5$.

3.OBJECTIVES

3. Objectives

In the present work, we aim to dissect the polarized trafficking and localization of the Na_V β2 subunit in polarized Madin-Darby canine kidney (MDCK) cells, and its role in regulating the subcellular localization of the $Na_V1.5$. Specifically, we aim:

- To determine the subcellular localization of β2 and $Na_V1.5$ in polarized MDCK cells.
- To determine the glycosylation pattern of β2 and its effect on the subcellular localization of β2 and $Na_V1.5$.
- To assess whether β2 is *S*-palmitoylated and if this PTM partitions the protein to subdomains of the PM.
- To determine if cholesterol association and transport underlies β2 polarized trafficking.
- To explore β2 stability and dynamics at the PM.
- To investigate trafficking and effect on $Na_V1.5$ localization in polarized cells of the BrS-linked β2 mutant D211G.

4.MATERIALS AND METHODS

4. Materials and methods

4.1 Plasmid vectors, cDNA cloning and site directed mutagenesis

The vector with FLAG-tagged human *SCN5A* cloned in pcDNA3.1 has been described. The FLAG tag, located in the extracellular loop between segments S1 and S2 of domain I (between Pro154 and Pro155), does not alter the biophysical properties of $Na_V1.5$ [132,133]. Vectors containing the *SCN5A-yfp* cDNA, or that of *SCN2B* fused to *cfp* (generated from vectors pEBFPN1-β1 and pEGFPN2-β2, from rat and human, respectively), have also been described. In all these, the fluorescent protein was fused to the C-terminal end, and in neither case the tag alters Na_V properties ([134] and our unpublished data). The *SCN2B-yfp* vector was made by double digestion of the *SCN2B-cfp* vector with NheI/NotI and subcloning of the *SCN2B* insert into a pcDNA3-*yfp* plasmid (Addgene). Following the manufacturer's instructions, the QuikChange Lighting Site-Directed Mutagenesis Kit (Agilent Technologies) was used to introduce the BrS-linked mutation D211G in *SCN2B*, as previously [3].

The same method was used to change Asn for Gln at predicted β2 N-glycosylation sites [135], thus preventing potential N-glycosylation of the expressed protein. Human *SCN2B* (designated in the Consensus Coding Sequence database (CCDS) with ID 8390.1), containing the desired mutation, was used as a template. Complementary primer pairs for PCR were designed with the QuikChange® Primer Design Program (Agilent) and synthetized by Metabion International AG. Sequences were sense: 5'-CCCTCAACGTCCTC**CA**GGGCTCTGACGCCCG-3' and antisense: 5'-CGGGCGTCAGAGCC**CT**GGAGGACGTTGAGGG-3' (N42Q); sense: 5'-CACAAACAGTTCTCCCTG**CA**GTGGACTTACCAGGAGTGC-3' and antisense: 5'-GCACTCCTGGTAAGTCCA**CT**GCAGGGAGAACTGTTTGTG-3' (N66Q); sense: 5'-ACTTACCAGGAGTGCAAC**CA**GTGCTCTGAGGAGATGTTC-3' and antisense: 5'-GAACATCTCCTCAGAGCA**CT**GGTTGCACTCCTGGTAAGT-3' (N74Q). (Mutated bases are marked in bold and underlined.) All possible combinations of mutant β2 were generated: N42Q, N66Q, N74Q, N42Q / N66Q, N42Q / N74Q, N66Q / N74Q, and N42Q / N66Q / N74Q.

SCN2B Cys-182 was changed for Ser (changing to Ser intends to avoid affecting the protein's tertiary structure); Cys-182 is the single intracellular Cys in β2, which appears to be conserved among species [80] and we hypothesized that it could be *S*-acylated by analogy to similar single pass TM proteins [47]. Both *SCN2B-yfp* and *SCN2B-cfp* vectors were made to express β2 C182S. Sequences were as follows:

5'-GTGCTGATGGTGGTCAAG**A**GTGTGAGGAGAAAAAAAG-3' (sense) and 5'-CTTTTTTTCTCCTCACAC**T**CTTGACCACCATCAGCAC-3' (antisense); mutated bases are marked in bold and underlined.

To generate a tail-minus β2-YFP, the following primer pairs were used to remove the ICD, equivalent to amino acids 182-215: 5'-GCTGATGGTGGTC-----GCGGCCGCGATGG-3' (sense) and 5'-CCATCGCGGCCGC-----GACCACCATCAGC-3' (antisense); the location of the sequence removed is indicated with a dashed gap. Since β2 lacking the ICD (181X) was poorly expressed, we added a $(Gly\text{-}Gly\text{-}Ser\text{-}Gly)_2$ linker between residue 181 and the YFP tag, using the following primer pairs: 5'-GCTGATGGTGGTC**GGTGGTTCTGGTGGTGGTTCTGGT**GCGGCCGCGATGG-3' (sense) and 5'-CCATCGCGGCCGC**ACCAGAACCACCACCAGAACCACC**GACCACCATCAGC-3' (antisense); introduced bases are marked in bold and underlined.

Construction of the IRES-containing bicistronic vector encoding human *SCN2B* with *gfp* (*SCN2B*:*gfp*), WT or bearing the D211G mutation, has been previously published [3].

All constructs were verified by sequencing.

4.2 Cell culture techniques

MDCK cells II and transfectant derivatives were maintained in Minimum Essential Medium with Earl's salts, supplemented with 10% FBS and 1% GlutaMAX™ (Gibco). To generate a fully polarized monolayer, cells were grown in polycarbonate Transwell filters of 12 mm diameter and 0.4 µm of pore size for at least 3 days (Corning-Costar), as described [136]. Transfections were performed following the manufacturer's instructions with Lipofectamine® 2000 in Gibco Opti-MEM™ I reduced-serum medium (Invitrogen), as described [137]. Briefly, cells were seeded and immediately transfected – in suspension – with plasmid DNA at 1 µl transfection reagent/µg DNA. Unless otherwise specified, cells were seeded as follows: 400,000 cells/Transwell; 350,000 cells/22 mm well (12-well plates), $1.2 \cdot 10^6$ cells/35 mm well (6-well plates).

To analyze β2 surface localization, by immunofluorescence or by cell surface biotinylation, we transfected 2 µg DNA vector per 22 mm well or Transwell to express β2. To analyze β2 and $Na_V1.5$ surface localization by cell surface biotinylation, and for immunoprecipitation and immunofluorescence experiments,

we transfected, per 35 mm well, 2 µg of DNA vector to express β2 and/or 3 µg *SCN5A*-FLAG vector; or, per Transwell, 1 µg of DNA vector to express β2 and/or 2 µg *SCN5A*-FLAG vector. When indicated, in cotransfections of $Na_V1.5$ and β2, the pEGFP-N1 vector (Clontech) was used as a control for β2-YFP.

For experiments of Fluorescence recovery after photobleaching (FRAP), 180,000 cells were seeded on ibidi® µ-slides with 4 wells Ph+ and a glass bottom, and transfected with 1.5 µg DNA vector to express β2.

4.2.1 Generation of stable cell lines

Transfections were performed by calcium phosphate co-precipitation, as described [138], and single-cell clones then selected with 200 µg/ml G418 (Sigma). Positive clones for β2-YFP, β2-CFP, β2:GFP (WT and mutants), and for $Na_V1.5$-YFP, were identified visually using the appropriate filter under a fluorescence microscope, and then confirmed by Western blotting. $Na_V1.5$-FLAG-expressing clones were identified by Western blotting. Proper distribution of surface markers (gp114, apical; p58, basolateral) and tight junctions (ZO-1) was then verified by immunofluorescence, ensuring normal cell polarity. The cell lines expressing WT or mutant $Na_V1.5$-YFP, $Na_V1.5$-FLAG, β2-CFP, β2:GFP [139], β2-YFP [137] and BACE1 [140] have been described.

4.2.2 Pharmacological inhibition of glycosylation

To block N-linked protein glycosylation, cells were treated with TUN (Sigma T7765). TUN inhibits the initial events in glycosylation of Asn residues, resulting in the synthesis of totally unglycosylated proteins. TUN was first dissolved at 10 mg/ml in dimethyl sulfoxide (DMSO). Cells were treated ~ 2 h after transfection with 0.3 µg/ml TUN for 24 h in complete medium; in untreated samples, an equivalent volume of solvent was added (0.003%).

To inhibit O-linked protein glycosylation, cells were treated with benzyl-2-acetamido-2-deoxy-α-D-galactopyranoside (Gal-NAc-α-O-benzyl; Sigma B4894), a competitive inhibitor of the glycosyltransferase incorporation of glucosamine into *O*-glycans [141]. Gal-NAc-α-O-benzyl was first dissolved at 100 mg/ml in DMSO. Cells were treated ~ 2 h after transfection with 2 mM Gal-NAc-α-O-benzyl for 24 h in complete medium; in untreated samples, the equivalent volume of solvent was added (0.6%).

4.2.3 Treatment with Brefeldin A (BFA)

To block transport from the ER to the Golgi, cells were treated with the fungal drug BFA (Thermo Fisher Scientific 00-4506-51). BFA reversibly inhibits a GTPase activity necessary for coat formation on Golgi membranes, which ultimately induces a redistribution of Golgi components to the ER [142]. Cells were treated ~ 2 h after transfection with 1.5 µg/ml BFA o/n in Opti-MEM (BFA was purchased already dissolved at 3 mg/ml in methanol); in untreated samples, an equivalent volume of solvent was added (0.05%).

4.2.4 Pharmacological depletion of cholesterol

In all treatments, cells were first rinsed twice in $DPBS^+$ (DPBS with divalent cations) and the drug was added in Opti-MEM, which lacks cholesterol and lipoproteins, thus preventing cells from obtaining exogenous cholesterol. In untreated controls, an equivalent volume of the drug solvent was added.

Except when otherwise indicated, cells were treated for 1 h with 10 mM methyl-β-cyclodextrin (MβCD, Sigma 332615) to acutely deplete cell surface cholesterol [143]. MβCD was dissolved directly in Opti-MEM and prepared fresh at the indicated concentration; dose and time of incubation were previously titrated by ensuring absence of non-specific effects in localization of surface markers.

Cells were treated for 24 h with U18666A (Sigma U3633) to inhibit intracellular cholesterol transport [144]. U18666A was added at the indicated concentration from a stock solution at 10 mg/ml in DMSO, previously aliquoted and stored at -20ºC.

To inhibit cholesterol synthesis [145], cells were pretreated overnight in some experiments with lovastatin (aka mevinolin, Sigma PHR1285) at the indicated concentration, prepared from a stock solution, as follows. Hydrolysis of its lactone ring to get the β-hydroxy acid open ring form, i.e. the active form, was done in ethanolic NaOH, as described [146]. Briefly, lovastatin was first dissolved at 40 mg/ml in ethanol. Then, 0.1 N NaOH at 1.5-fold the volume of ethanol was added, and the mixture heated for 2 h at 50°C. The solution was rapidly cooled on ice until r.t. and the pH then adjusted to 7.2 with HCl. It was then brought to 10-fold the initial volume of ethanol with sterile H_2O. The resulting solution (4 mg/ml, i.e. 10 mM) was aliquoted and stored at -20°C.

4.3 Biochemistry

4.3.1 *In vitro* protein deglycosylation

Deglycosylation was performed in whole cell lysates. Reactions were stopped with Laemmli buffer. To remove completely N-glycans, we used PNGase F (NEB P0708), which cleaves off the bond between Asn and the first GlcNAc moiety, liberating the entire N-glycan. The protocol by New England Biolabs (NEB) was used. Briefly, 10 µg protein were denatured for 10 min at 100ºC in 10 µl Glycoprotein Denaturing Buffer (0.5% SDS with 40 mM DTT). The reaction with 1 µl PNGase F (500 units) was then performed in 20 µl total volume, including GlycoBuffer 2 (50 mM sodium phosphate at pH 7.5) and containing 1% Nonidet P-40, by o/n incubation at 37°C.

To discern between simple and complex *N*-glycosylation, we used Endo H (NEB P0702), which cleaves N-glycans between the two GlcNAc moieties in the core region of the glycan chain on high-mannose and hybrid, but not complex, glycans. Similarly, 7.5 µg protein were denatured for 10 min at 100ºC in 10 µl Glycoprotein Denaturing Buffer. The reaction with 1 µl Endo H (500 units) was then performed in 20 µl total volume, including GlycoBuffer 3 (50 mM sodium acetate at pH 6), by o/n incubation at 37°C.

To cleave terminal sialic acids, from *N*- and *O*-glycans, we used α2-3,6,8 neuraminidase (NA; NEB P0720), which hydrolyzes α2-3, α2-6, and α2-8-linked sialic acid residues from glycoproteins and oligosaccharides. Here, 2 µl NA (100 units) were added to 3.5 µg protein in 20µl GlycoBuffer 1 (5 mM $CaCl_2$ in 50 mM sodium acetate at pH 5.5) and incubated o/n at 37°C. To ensure proper visibility in gels with samples from double mutants, twice the amount of protein and enzyme were used in digestions with Endo H and NA.

In experiments addressing the effect of BFA, material obtained by surface protein biotinylation (see below) was also digested with Endo H. Here, o/n NeutrAvidin pulldowns were resuspended in 20 µl Glycoprotein Denaturing Buffer and denatured as above to release the protein from beads. Beads were then spun down and 10 µl of supernatant were deglycosylated in GlycoBuffer 3 as above using 3-times as much enzyme.

4.3.2 Isolation of detergent-resistant membranes (DRM)

The procedure followed has been described [147], which we modified slightly, as follows. The whole process was performed at 4ºC and buffers were supplemented

with a cocktail of protease inhibitors. Confluent cells – 4 x 10-cm dishes per condition – were homogenized in 20 mM HEPES/NaOH pH 7.4, containing 1 mM EDTA and 250 mM sucrose (4 ml in total), by 30 passages through a 22-gauge needle. The homogenate was centrifuged at 255,000 g_{max} for 90 min in a Beckman MLA-130 rotor. The pellet was then resuspended in 1 ml MBS buffer (25 mM MOPS/NaOH pH 6.5 with 150 mM NaCl), containing 1% Triton X-100, and left on ice for 20 min. This solubilized material was then resuspended with 30 passages through a 22-gauge needle and mixed with an equal volume (1 ml) of 90% (w/v) sucrose (in H_2O), which was then overlaid with 35% sucrose (2 ml) and 5% sucrose (1 ml), both prepared in detergent-free MBS. Samples were centrifuged at 235,000 g_{av} overnight in a Beckman SW 55 Ti Rotor, and 0.5 ml fractions were collected from top to bottom. The upper 2-3 fractions are those detergent-insoluble and thus defined as DRM.

4.3.3 Acyl-Biotin Exchange (ABE) assay

Detection of protein *S*-acylation (which we will refer to here as palmitoylation, as the most common form of *S*-acylation) was done by immunoprecipitation and acyl-biotin exchange (ABE). 400,000 cells/35-mm well (6-well plates) were seeded and allowed to grow until confluence for 3 days. Immunoprecipitation was done essentially as described [139]. Here, cells were lysed at 4ºC with 1% (w/v) IGEPAL® CA-630 (formerly, Nonidet P-40) in 20 mM Hepes/NaOH at pH 7.2 containing 150 mM NaCl; all buffers were prepared fresh and supplemented with a protease inhibitors cocktail. To ensure exhaustive blocking of free sulfhydryl groups (thiols), 50 mM *N*-ethylmaleimide (NEM; Thermo Fisher Scientific 23030) was included, essentially as described [148]. Immunoprecipitation of β2-YFP was performed for at least 1 h with an anti-GFP antibody previously conjugated to Protein A-agarose beads (Thermo Fisher Scientific 15918-014) at 0.5 µg IgG per sample. Extensive washing of immunoprecipitates at 4ºC was required to ensure total removal of residual NEM, as described [149]. Next, cleavage of the acyl-thioester bond with 1 M hydroxylamine (HAM·HCl; Thermo Fisher Scientific 26103) in DPBS was performed for 1 h at r.t. after adjusting the pH to 7.2 with NaOH. Then, the free sulfhydryl residues generated were specifically labeled with EZ-Link™ BMCC-Biotin (Thermo Fisher Scientific 21900) at 40 µM in DPBS, previously adjusted to pH 7.0 with HCl, for 2 h at r.t.; an 8 mM stock solution of BMCC-Biotin in DMSO was prepared immediately before use. Finally, beads were washed, immobilized proteins were eluted in Laemmli buffer, and then analyzed by anti-biotin western blot to detect biotinylated (acylated) and total β2 in immunoprecipitates.

Various controls were performed. First, NEM was not included. Without NEM, several non-specific bands appear as a result of the presence of free, unblocked thiol groups in proteins that are subsequently biotinylated and detected; including NEM in immunoprecipitations, such bands are absent. Second, the assay was performed omitting HAM cleavage. Without HAM, palmitoyl chains are not removed and their otherwise free thiols cannot be biotinylated and detected; this serves as a control for potential contaminants of the immunoprecipitation and for unspecific biotinylation. Third, as a negative control for palmitoylation, an irrelevant, not palmitoylated protein was immunoprecipitated, and the sample was subjected in parallel to ABE; we chose Vps26, which is enriched in the endosomal compartment of MDCK cells [150]. And fourth, metabolic labeling with the palmitate analog 2-bromopalmitate (aka 2-bromohexadecanoic acid, 2-BP; Sigma 238422) was performed to inhibit palmitoylation in cells. Prior to the experiment, cells were grown for 1 h in medium containing 2% serum, and 2-BP was added at increasing concentrations (within the μM range, from a 100 mM stock prepared fresh in ethanol), and left for 1 h more; an equivalent volume of solvent was added in untreated controls.

4.3.4 Cell surface biotinylation and endocytosis

Surface protein biotinylation was done with EZ-Link™ Sulfo-NHS-SS-Biotin (Thermo Fisher Scientific 21441), a water-soluble and membrane impermeable reagent. The procedure followed has been described previously in detail [139,140]. Unless otherwise specified, 9/10th of cell lysate were subjected to overnight pulldown with NeutrAvidin (Thermo Fisher Scientific 53150) and analyzed by western blot along with the remaining 10% (referred to as lysate). Quantitation of blotted protein bands in lysates and pulldowns was performed as described [139], using the ImageJ program, as follows. We first estimated the relative presence of a protein at the cell surface over its total amount in the lysate by dividing arbitrary units/μg obtained from quantitations of each band in the pulldown over its corresponding lysate. This variable (efficiency of arrival to the cell surface or pulldown) was expressed over 1. This was done for $Na_V1.5$ or β2, and the corresponding internal controls, i.e. gp114 or Na/K-ATPase, as apical and basolateral markers in MDCK cells, respectively, or simply using the latter in non-polarized MDCK cells. Next, the ratio of pulled down $Na_V1.5$ or β2 (at the surface) over each control protein was obtained by dividing their efficiencies. This ratio was also expressed over 1. To control for specificity, untransfected MDCK cells were always processed in parallel, and we only considered those experiments in which bands for $Na_V1.5$ and β2 were clearly visualized only in lysates and pulldowns of transfected cells and with comparable intensity levels.

To examine endocytosis of β2 from the apical surface, we proceeded as described [140]. Briefly, the apical surface of polarized MDCK cells was biotinylated. We then examined β2 endocytosis at 37ºC upon glutathione cleavage of surface-exposed, biotinylated proteins. By reducing the disulfide bond of the biotin reagent, glutathione removes the biotin tags from the labeled membrane proteins. Since glutathione does not permeate into cells, intracellular biotin moieties of endocytosed proteins remain protected, being then detected by western blot. An additional Transwell was left untreated, representing at time zero the total amount of biotin reagent bound to surface proteins.

4.3.5 Sample preparation and western blot

Protein determination from cell lysates was done with the bicinchoninic acid assay (Thermo Pierce). Samples for SDS-PAGE were prepared in Laemmli buffer by heating at 95°C for 5 min and protein transfer to polyvinylidene difluoride (PVDF) membranes was done overnight without SDS. Samples analyzing $Na_V1.5$ were prepared in Laemmli buffer by heating at 70°C for 10 min, and protein transfer to PVDF membranes was done for 30 h in the presence of 0.01% SDS to optimize $Na_V1.5$ solubilization and transfer. The immunoreactive bands were visualized using enhanced chemiluminescence (Pierce) on GE Amersham ECL Hyperfilm or using the image analyzer Bio-Rad ChemiDoc MP. Stripping for antibody reprobing was done for 30 min by gentle shaking in 25 mM glycine/HCl pH 2.0 containing 1% SDS.

Protein from DRM fractions was concentrated by precipitation with trichloroacetic acid (TCA, Sigma T6399), as follows. The procedure was performed at 4ºC. To a given volume of each collected fraction, all containing an identical amount of protein, e.g. 6 µg, $1/10^{th}$ of a 100% (w/v) TCA solution was added (previously prepared by dissolving 220 g TCA in 100 ml H_2O). After vigorous vortex, the mixture was left on ice for 10 min and microfuged for 15 min at maximum speed. After removing the supernatant, 1 ml acetone (stored at -20ºC) was added, without loosen up the pellet, and spun again. The pellet was then allowed to dry, dissolved in Laemmli buffer, and processed as above, ensuring here to reach an adequate pH for SDS-PAGE by adding, if needed, 1 M Tris/HCl at pH 8.8.

4.4 Antibodies

Some antibodies were provided by other researchers and have been previously described. These include the rabbit polyclonal antibodies to BACE1 [151], to Vps26

and to Vps35 [152]; the mouse monoclonal antibodies to gp114 (a cell adhesion molecule) and to p58 (the Na/K-ATPase β subunit) [153]; and the rat monoclonal antibody against ZO-I [154].

Commercial mouse monoclonal antibodies used were: From BD Transduction Laboratories, to flotillin-1 (610820), to EEA1 (610457), to GM130 (610822), and to SNX2 (611308); from Abcam, to the Na/K-ATPase α1 subunit (ab7671), to GFP (ab1218), and to TGN46 (ab7671); and from Sigma, to FLAG (F3165).

Commercial rabbit polyclonal antibodies used were: From BD Transduction Laboratories, to caveolin-1 (610060); from Abcam, to biotin (ab53494), to calnexin (ab75801), and to GFP (ab290); from Alomone, to Na_V β2 (ASC-007) and to Na_V1.5 (ASC-013); from Sigma, to actin (A2066); and from Thermo Fisher, the antibody included in the Vybrant® Lipid Raft Labeling Kit V-34405 to the cholera toxin (CTX) B subunit.

Secondary antibodies HRP-conjugated for western blot were from Jackson ImmunoResearch (codes 111-035-003 and 115-035-003), and Alexa Fluor®-labeled for immunofluorescence were from Molecular Probes-Invitrogen (excitation wavelength peak – in nm – Ex 488, goat anti-rabbit A-11008; Ex 594, goat anti-mouse A-11005; Ex 633, goat anti-rabbit A-21070; and Ex 633, goat anti-rat A-21094).

4.5 Confocal Imaging and Quantitative Image Analysis

MDCK cells were analyzed at subconfluence on glass coverslips or grown polarized in 12 mm Transwells. Cells were fixed with paraformaldehyde and immunostained, essentially as described [139,140]. When indicated, the cell surface was outlined with Alexa Fluor 633®-labeled phalloidin (Molecular Probes), and DAPI (4',6-diamidino-2-phenylindole) was used to stain the nuclei.

High magnification images were taken on a Nikon A1R confocal microscope with an oil-immersion objective (Plan-Apo 100X, 1.4 NA) at 512 x 512 pixel (0.9 µm/pixel) using the NIS-Elements AR software, as described [150]. As previously, images were exported to TIFF format and 3D volume co-localization was analyzed throughout the entire cell without image preprocessing. Since the ratio of two potentially co-localizing probes was expected to vary widely, and their intensities not to be related by a simple, linear relationship, we estimated co-localization by calculating the Manders' M1 and M2 coefficients. Defined as the fraction of the total amount of a probe localizing to compartments labeled with a second probe,

these coefficients are unaffected when signals change not proportionally and are useful when the two probes distribute into different sort of compartments [155,156].

Image analysis was performed with Fiji, the ImageJ-based package that includes the JACoP plugin for co-localization analysis. For determination of Manders' coefficients, and to avoid underrepresentation of the correlation between two probes when one was not uniformly represented, such as in transiently transfected cells, images were cropped prior to analysis; this ensured that the region of interest analyzed contained essentially structures expressing the exogenous protein [156]. Incorporation of negative controls and adjustment of threshold values for image noise correction were done as described [150]. Random overlap was considered negligible and thus not subtracted from measurements.

To analyze the effect of β2 in surface localization of $Na_V1.5$, polarized MDCK cells co-expressing measurable levels of both proteins were selected for analysis. Optical slice thickness of apical-to-basal *z*-stacks was 0.5 µm. To analyze localization of $Na_V1.5$ close to, and at the apical membrane, we calculated the corrected total cell fluorescence (CTCF) along 3D reconstructions, as previously; CTCF is based on the integrated density, i.e. the product of the average fluorescence in each section and its area [150]. In non-polarized cells, we first determined the presence of β2 at the PM, and then its effect on Nav1.5 localization, as follows. Cells were processed for immunofluorescence to localize the PM marker Na/K-ATPase. A *z*-stack of images was taken at 0.25 µm optical slice thickness. Using a Fiji tool created by our Research Technical Services, which was named *plot3colors*, we drew 4 straight lines per cell, each of 30 pixels long (0.1 µm/pixel). Lines were drawn from the PM into the cytoplasm, approximately perpendicular to perfectly identifiable cell surface regions, as assessed by well-defined labeling of the Na/K-ATPase and/or β2. To achieve a broad representation of each cell, lines were distanced between each other ≥ 100 pixels along the membrane perimeter. For each linear region individually, we calculated the fraction of fluorescence intensity/pixel over the pixel with maximum intensity (≥ 3 cells analyzed). We refer to this average percentage as mean fluorescence intensity (MFI); this was done for each channel and MFIs were then represented as line charts. The 5 most peripheral pixels were then considered as the cell end, or PM region, and the rest as intracellular localization. The rationale for this 5 pixel-limit was as follows: first, it was beyond this point that the Na/K-ATPase MFI decreased by ≥ 50%; secondly, the axial resolution obtained in confocal microscopy is nearly 500 nm [155], matching the 5 pixels taken; and third, it fits within the range in which proteins localizing to the cell end have been previously identified [157].

4.5.1 Fluorescent labeling of membrane lipid rafts with the cholera toxin (CTX) B subunit (CTB)

Cells were incubated with 10 µg/ml cholera toxin (CTX, Sigma C8052) for 10 min in complete medium at 4ºC; the CTX B subunit binds to lipid raft-associated ganglioside GM1 [158]. After extensive rinsing with ice-cold medium, cells were incubated at 4ºC with an anti-CTB antibody (at 1:200) for 15 min in complete medium. After extensive rinsing with ice-cold $DPBS^+$, cells were fixed at r.t. with 4% paraformaldehyde for 10 min. Then, we proceeded with a 30 min incubation with an Alexa Fluor®-labeled secondary antibody in complete medium at r.t., nuclei staining with 4',6-diamidino-2-phenylindole (DAPI), and mounting of the slide for fluorescence microscopy analysis, as described [140].

4.5.2 Fluorescence recovery after photobleaching (FRAP)

Dynamics of fluorescently tagged β2 was monitored by fluorescence recovery after photobleaching (FRAP) essentially as described [137], with a few modifications. MDCK cells, transiently or stably expressing β2-YFP, were grown subconfluent (for 2 days or as otherwise indicated) on ibidi® glass supports. For treatment with MβCD, and prior to the experiment, cells were incubated with increasing concentrations of the drug in Opti-MEM for 10 min. FRAP was performed in the presence of MβCD for up to an additional 30 min.

Cells were placed in a live-cell imaging chamber at 37ºC and 5% CO2, and imaged through a water-immersion objective (Plan-Apo 60X, 1.2 NA) on a Nikon A1R confocal microscope. Confocal images were taken at 512 x 512 pixel (0.21 µm/pixel). An argon laser with emission at 514 nm was used to image the YFP fluorescence and a 405 nm diode laser was used for photobleaching. The pinhole radius was set to 3 Airy Units, except when imaging large perinuclear ER structures, when the pinhole was set to 1 Airy Unit. 3 regions-of-interest were drawn: a bleached area, in which fluorescence recovery was recorded along time; a background area, outside obvious fluorescence labeling; and a non-bleached (reference) area, in a different cell displaying similar fluorescence intensity as the bleached cell. Both bleached and reference areas were circular regions with a nominal radius (r_n) of 2 µm, except when imaging perinuclear ER structures, where r_n was 1 µm, and also when otherwise indicated.

Images were collected at a rate of 1 frame per second, as follows. First, 10 pre-bleaching images were taken, and then bleaching was done for 5 seconds at 100% laser transmission. Immediately, post-bleaching images were captured until

fluorescence recovery reached a plateau, with a few exceptions: when comparing dynamics of β2-YFP WT with C182S, post-bleaching images were captured for 1 min at 1 frame each 2 s; then, for 4 min at 1 frame each 8 s; and subsequently, at 1 frame each 20 s until fluorescence recovery had reached a plateau. Finally, when comparing bleached area, post-bleaching images were captured for 1 min at 1 frame each 7 s, and at 1 frame each 15 s until reaching the plateau.

Similarly as described [159], we used the NIS-Elements AR software to measure average fluorescence intensities and to correct for background and acquisition photobleaching, taking into account background and reference fluorescence values, respectively. Next, data were normalized as follows. First, the lowest fluorescence value, obtained from the first post-bleaching recording, was subtracted from each time point value to set bleach depth to zero. Then, all values were divided by the value from the last pre-bleaching (10th) frame, i.e. right before photobleaching. From each curve, we then obtained three parameters: [1] the mobile fraction (MF), determined by averaging the fluorescence values of the first 30 time-points throughout which the curve reaches a plateau (30 s), and expressing this value as a percentage of the maximum fluorescence at pre-bleaching, indicates the portion of molecules that can undergo diffusion during the experiment; [2] the half-time of recovery ($\tau_{1/2}$), i.e. the time-point in which half of total fluorescence recovery has occurred (this value inversely correlates to the rate of diffusion, and therefore to the speed of molecule movement in the area analyzed); and [3] the diffusion coefficient (D), indicating rate of diffusion, and calculated applying the simplified Soumpasis equation [160]:

$$D = 0.25 \cdot (r_n^2 / \tau_{1/2})$$

4.6 Statistics

All experiments were performed a minimum of three times. Data are expressed as mean ± SD or SEM, as indicated in figure legends and tables, and displayed as curves or bar graphs superimposed to scatter plots showing all the individual data points (when these are included). Statistical significance was calculated by the two-tailed Student's *t*-test, or by one-way ANOVA with Tukey's honest significant difference (HSD) or Dunnett's post hoc tests, by using the R software for statistical computing [161], when differences among groups needed to be tested. *P* values are also specified in figure legends.

5.RESULTS

5. Results

5.1 *N*-glycosylation is required for β2 trafficking to the plasma membrane

In order to study the trafficking and function of β2 in the context of the heart, CMs would indeed be the most physiologically relevant model system. However, primary cultures of CMs do not divide and do not survive most biochemical treatments and assays. In addition, an important limitation to study trafficking in CMs is that their functional PM domains cannot be independently manipulated and analyzed *in vitro*. To get insights into the regulation of $Na_V1.5$ targeting and localization by β2 to the CM sarcolemma, we used epithelial MDCK cells as a model system, an archetype for studying membrane trafficking and polarized sorting. MDCK cells grow polarized in Transwells, developing two well differentiated apical and basolateral membrane domains separated by tight junctions [162]. Although MDCK cells have little resemblance to CMs, both are polarized cells, and the apical domain of MDCK cells may have important similarities to highly specialized membrane domains of excitable cells, like the neuron AIS and certain regions of the CM sarcolemma [1].

5.1.1 β2 localizes to the apical domain of polarized MDCK cells

To assess the distribution of β2 in our cell model of choice, we exogenously expressed β2-CFP in polarized MDCK cells. By immunofluorescence, β2 was almost exclusively found at the apical surface. Cell surface biotinylation confirmed the observation, with virtually no β2 detected at the basolateral domain (Figure 15).

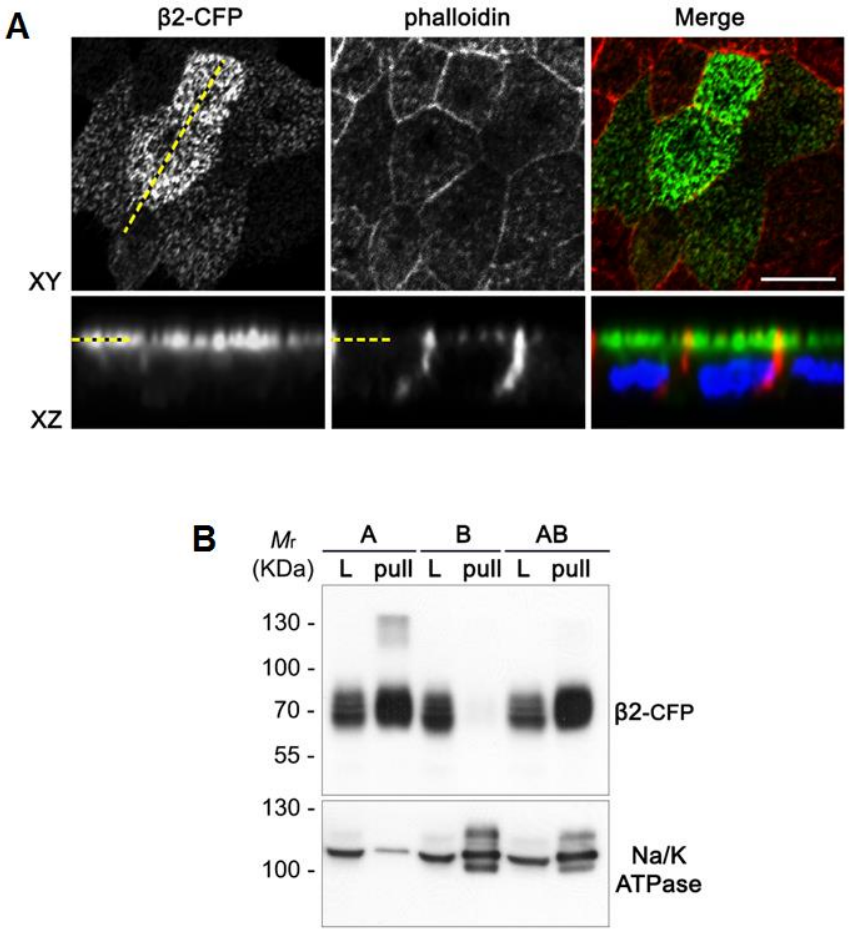

Figure 15: In polarized MDCK cells, β2-CFP is at the apical surface. MDCK cells were transiently transfected with the *SCN2B-cfp* vector to express WT β2 and grown polarized in Transwells. (A) Cells were fixed and immunostained with a rabbit polyclonal antibody against β2 (green). Phalloidin (red) outlines the PM, and nuclear staining by DAPI is in blue. Images were obtained by confocal microscopy. Representative XY sections, taken at the apical level, and *z*-axis reconstructions (reciprocal XZ and XY sections are marked by a yellow dashed line) show that β2-CFP is restricted to the apical surface. Scale bar is 10 µm. (B) Cells were biotinylated at 4ºC at the apical (A) or basolateral (B) surface, or simultaneously at both (AB). Representative western blots show β2-CFP enrichment over the lysate (L; 20 µg) in biotin-NeutrAvidin pulldowns (pull; ~ 200 µg protein) obtained from the apical but not the basolateral surface, contrasting with the basolateral localization of Na/K-ATPase. Molecular weight markers are shown in kilodaltons (kDa).

5.1.2 β2 is *N*-glycosylated and sialylated

As exogenously expressed β2 localizes almost exclusively at the apical domain in polarized MDCK cells, we first addressed how β2 is preferentially targeted to this surface domain. Both *N*- and *O*-linked glycosylation are common apical sorting signals [163,164]. The extracellular domain of β2 has three predicted *N*-glycosylation sites, i.e. Asn-42, Asn-66 and Asn-74 [165], that follow the Asn-X-Ser/Thr (NxS/T) motif, being x any amino acid except Pro [135]. We therefore systematically mutated these to Gln, which is never glycosylated due to its different conformation, and transiently expressed YFP-tagged β2 in MDCK cells. Consequently, all mutants showed increased electrophoretic mobility, with N42Q displaying the highest increase, followed by N74Q and N66Q, the latter, with a minor, albeit measurable shift. This variable mobility may be due to different degrees of glycosylation on each specific site and/or changes on overall glycoprotein size or charge; the triple (fully) unglycosylated mutant showed complete reduction in apparent mass, no longer appearing as a smear, with double mutants migrating in between (Figure 16A). To verify that β2 variants were indeed *N*-glycosylated, cells were lysed and treated with peptide:*N*-glycosidase F (PNGase F), which cleaves off the bond between Asn and the first GlcNAc moiety, liberating the entire *N*-glycan [166]. Upon treatment, WT and mutants displayed identical mobility to that of fully unglycosylated β2 (Figure 16B). To confirm that β2 glycosylation takes place in cells, these were treated with TUN, or with Gal-NAc-α-*O*-benzyl, to block *N*- or *O*-glycosylation, respectively. As a result, β2 WT became fully deglycosylated only with TUN, remaining unaffected with Gal-NAc-α-*O*-benzyl (Figure 16C). These data show that β2 is *N*-glycosylated, but does not undergo *O*-glycosylation.

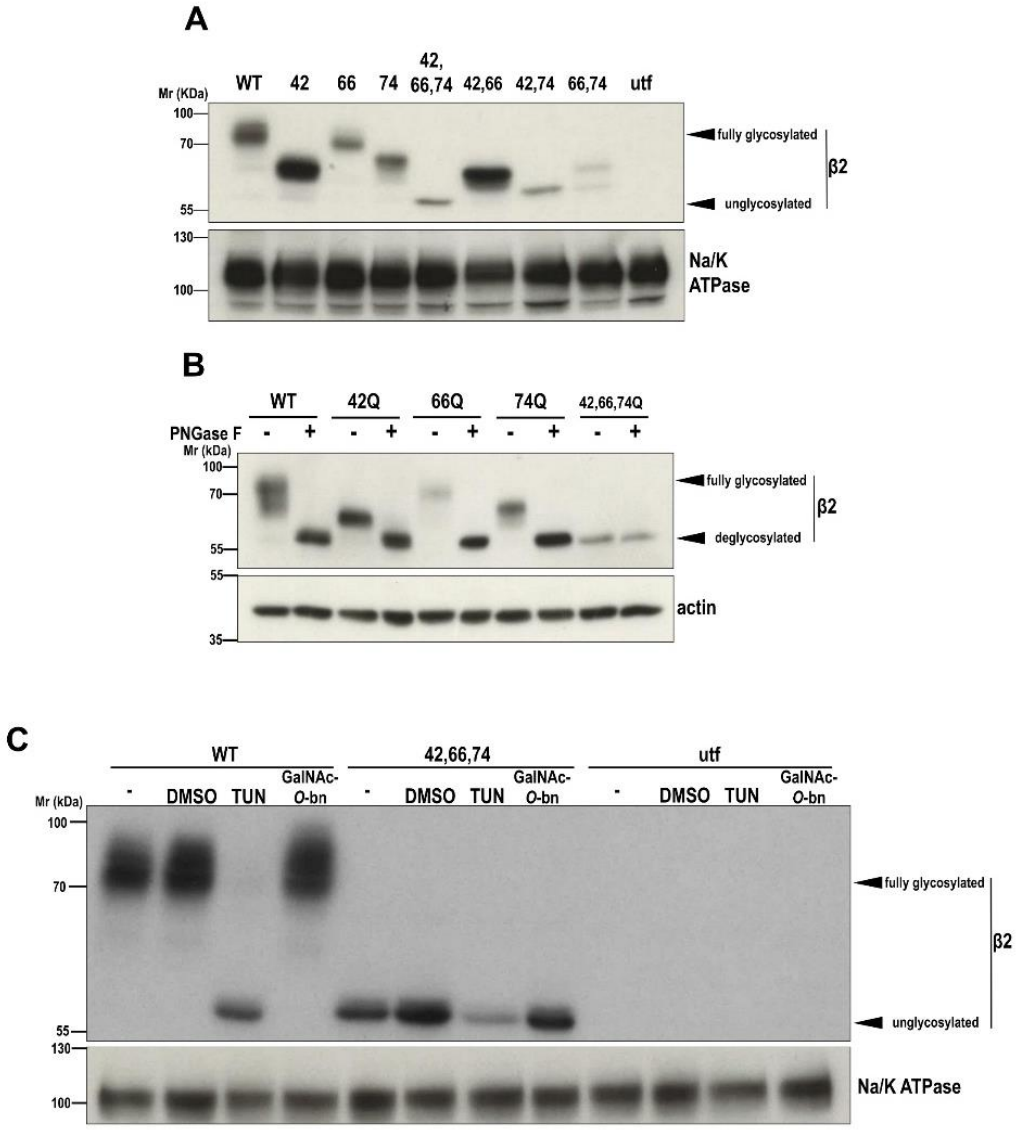

Figure 16. β2 is *N*-glycosylated at positions Asn-42, Asn-66 and Asn-74. MDCK cells were transiently transfected with the *SCN2B-yfp* vector to express WT, partially or fully unglycosylated β2, or left untransfected (utf). (A, B) Cells were grown for 2 days in wells. Representative western blots are shown with the same amount of protein lysate loaded into each lane. (A) All glycosylation-defective mutants display increased electrophoretic mobility, with N42Q as the single mutant with the greatest change, and triple (fully) unglycosylated β2 showing complete shift. (B) Denatured protein from cell lysates was treated o/n at 37°C with PNGase F to cleave off all *N*-glycans. (C) Cells were treated with TUN, or with Gal-NAc-α-*O*-benzyl (GalNAc-*O*-bn), to block *N*- or *O*-glycosylation, respectively, and grown for 1 day in wells; β2 WT remains unglycosylated only with TUN. DMSO: indicates cells with the equivalent volume of solvent added, and "-", untreated cells. Blots for Na/K-ATPase or actin are included as loading controls. Molecular weight markers are in kilodaltons (kDa).

We next investigated the complexity of β2 *N*-glycosylation with Endo H, which cleaves high-mannose and hybrid, but not complex glycans, characteristic of late-Golgi glycosylation [166]. When cells were analyzed early (1 day) after transfection, a faster-migrating band, also visible in single and double mutants, suggested the presence of immature β2-YFP still unprocessed in the ER. Endo H treatment effectively increased the mobility of this band, which then coincided with unglycosylated β2, but did not affect mature β2 (Figure 17A and B). Thus, at that moment a considerable fraction of β2 had not yet undergone processing by Golgi α-mannosidase II [166].

To further assess *N*-glycans complexity, cells were treated with a sialidase of broad substrate specificity, i.e. NA, which cleaves terminal sialic acids from both *N*- and *O*-glycans [166]. In consequence, the slower-migrating band displayed a noticeable increase in mobility in β2 WT, N66Q and N74Q mutants, but not in β2 N42Q. Similarly, no effect was seen in double mutants including the N42Q mutation, but it was clear in β2 N66Q / N74Q (Figure 17C and D). Because all variants with the N42Q mutation were insensitive to NA, we conclude that β2 is sialylated uniquely at Asn-42.

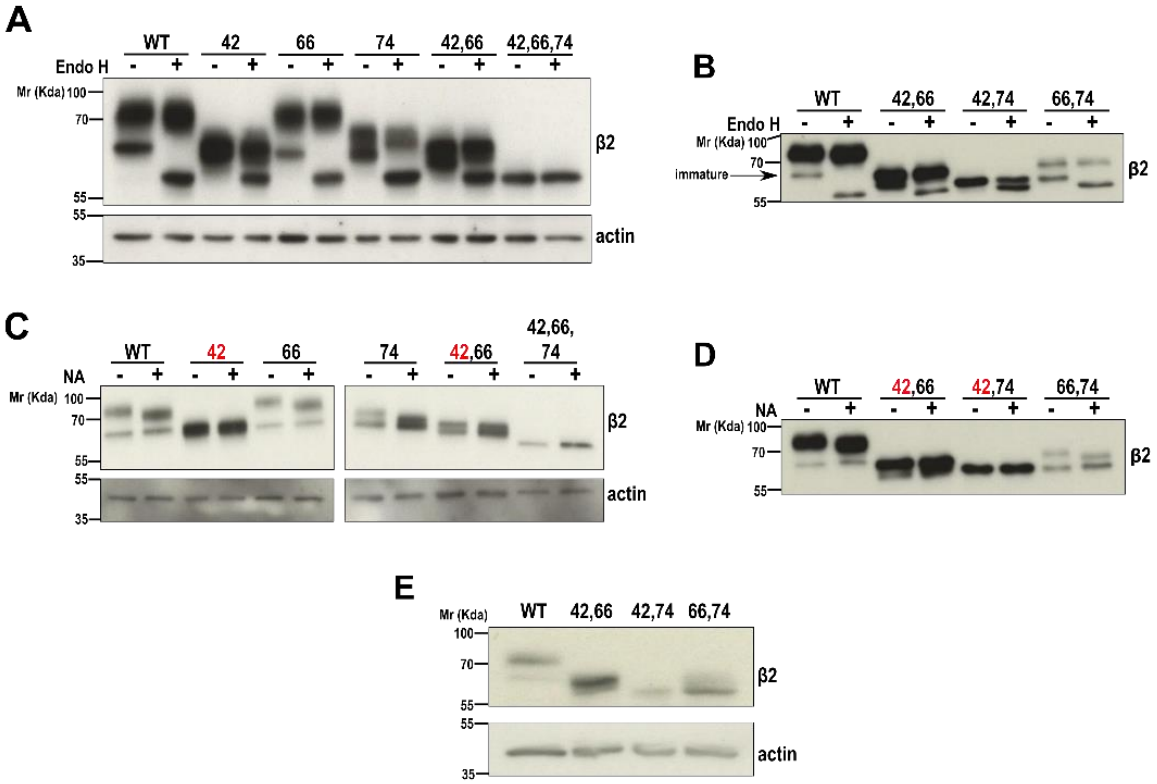

Figure 17. β2 undergoes complex *N*-glycosylation and is sialylated at Asn-42. MDCK cells were transiently transfected with the *SCN2B*-yfp vector to express WT, partially or fully unglycosylated β2, and grown for 1 day in wells. Representative western blots are

shown with the same amount of protein lysate loaded into each lane. Note that immature (unprocessed) β2 is clearly discernible from the slow-migrating mature form (compare with Figure 16). (A, B) Denatured protein from cell lysates was treated o/n at 37°C with Endo H to cleave off immature *N*-glycans (faster-migrating band) in β2. (C, D) Lysates were treated o/n at 37°C with NA to cleave off all terminal sialic acids. The upper band displays a slight increase in mobility in WT and single and double mutants not including the N42Q mutation (red fonts). Blots for actin are included in A and C as loading controls. (E) Blots of unprocessed lysates used in B and D show comparable amounts of actin, serving as loading controls. Note that β2 levels are slightly variable due to differences in transient expression. The division line in C separates different blots (taken from the same exposure) conveniently put together for clear display. Molecular weight markers are in kDa.

5.1.3 *N*-glycosylation is required for efficient cell surface localization of β2

Since glycosylation is a well-known mechanism for many proteins to efficiently reach the PM [164], we tested by protein biotinylation whether partially or fully unglycosylated β2 properly localizes to the cell surface. Only the triple mutant displayed a substantial defect, and band quantitation showed that it reaches the surface at a rate of ~ 1/3rd in comparison with the WT (Figure 18A and B). Moreover, the portion of unglycosylated mutant at the surface was only ~ 8% over total cellular β2 protein, contrasting with 25-30% by the WT and single or double mutants. A comparable defect was found in fully polarized cells. In these, the rate by which unglycosylated β2 reached the apical surface was also ~ 1/3rd relative to β2 WT or the partial mutants (Figure 18C and 18D). To note, all variants of β2 remained nearly undetected at the basolateral surface, or at least clearly de-enriched comparing with lysates, excluding a role of *N*-glycosylation in determining polarized distribution of β2 (Figure 18E).

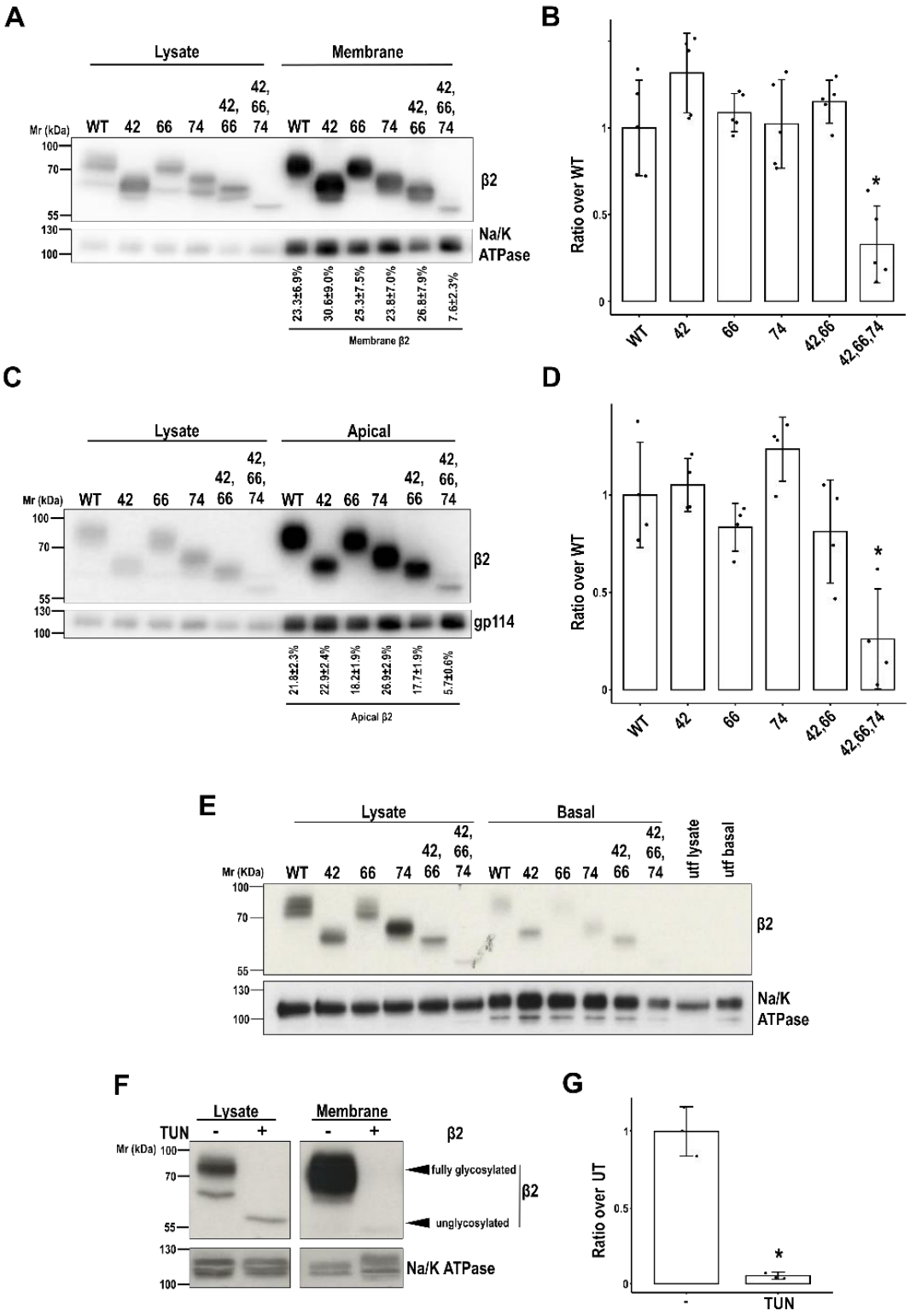

Figure 18. N-glycosylation is required for efficient cell surface localization of β2. MDCK cells were transiently transfected with the *SCN2B*-yfp vector to express WT, partially or fully unglycosylated β2. Cells were grown for 2 days in wells (A, B) or polarized in TWs (C, D, E) and surface biotinylated at 4ºC. Representative western blots (A, C, E) and band quantitation (B, D) show that levels of fully unglycosylated β2 were reduced compared with the WT and partially glycosylated mutants in biotin-NeutrAvidin pulldowns,

both in subconfluent and in polarized cells. One-way ANOVA with Tukey's HSD post hoc test highlighted these differences (B, *, $p < 0.001$; D, *, $p < 0.05$). Values underneath blots show the percentage of each β2 variant at the surface over total cellular β2 protein (A, C). (E) Representative western blot showing negligible levels of all variants of β2 (WT and mutants) in biotin-NeutrAvidin pulldowns of the basolateral (Basal) surface (utf, untransfected cells). (F, G) Cells were treated with TUN to block *N*-glycosylation, grown for 1 day in wells, and surface biotinylated at 4ºC (UT, untreated cells). (F) Representative western blots and (G) band quantitation show absence of unglycosylated β2 in pulldowns (two-tailed Student's *t* test show significant differences; *, $p = 0.009$). The same amount of protein was used to process each lysate (~ 130 µg), and the corresponding portion (9/10th) was subjected to overnight pulldown. Na/K-ATPase (A, E, F) or gp114 (C) were blotted as surface markers to correct for quantitations in pulldowns. All data are mean ± SD (error bars) ($n \geq 3$). Molecular weight markers are in kDa. The division line in F separates different parts of the same blot (taken from the same exposure) conveniently put together for clear display.

To determine the magnitude of glycosylation loss in trafficking deficiency of β2 over time, we analyzed its surface levels along various days from transfection. Indeed, the defect was maintained throughout time. Therefore, these data show that total lack of glycosylation significantly prevents β2 localization to the surface (Figure 19). While a single glycosylation site appeared sufficient for proper surface localization of β2, TUN treatment further confirmed that unglycosylated β2 virtually does not reach the PM in cells (Figure 18F and 18G).

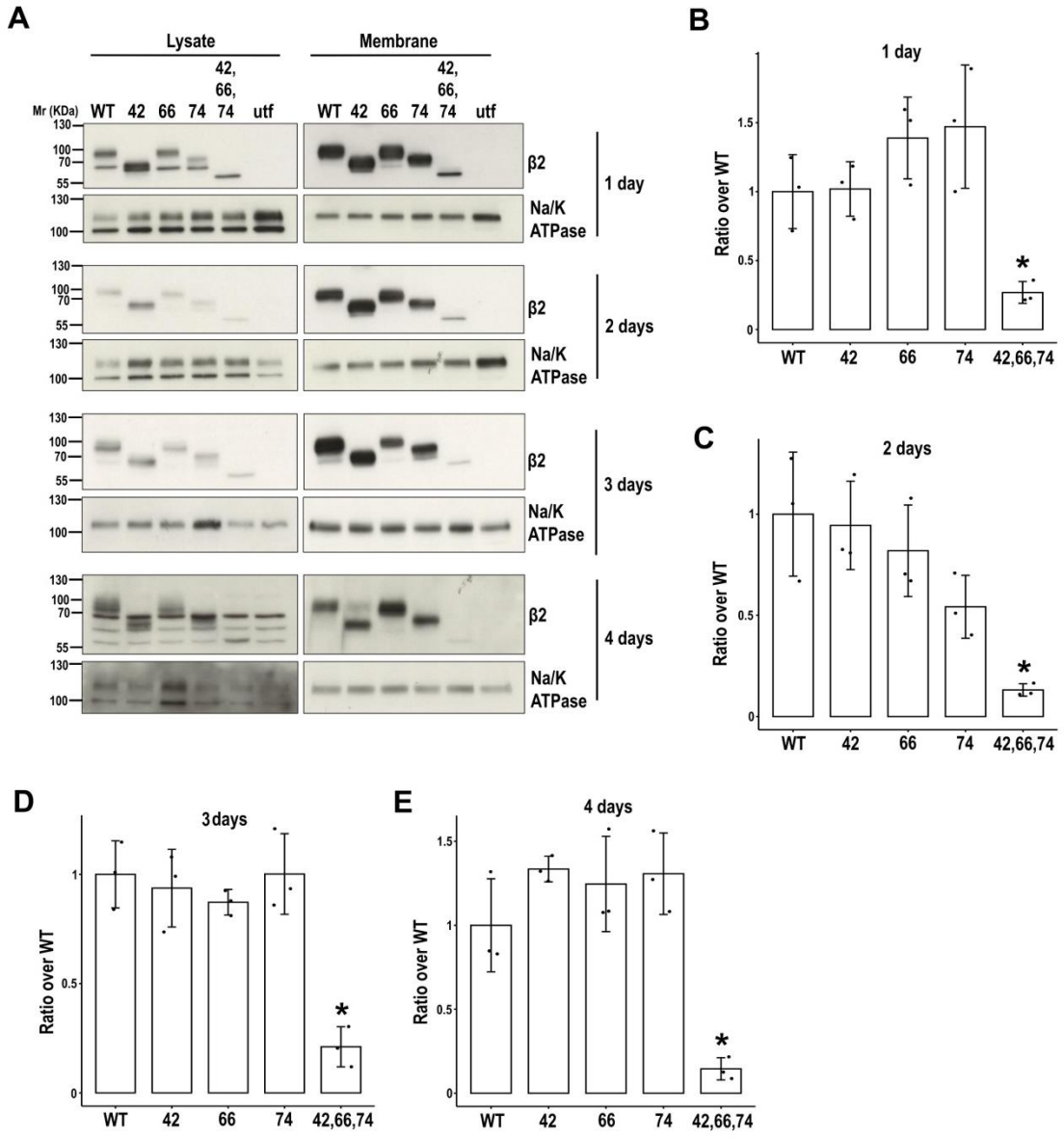

Figure 19. Defect over time in β2 surface localization due to lack of *N*-glycosylation. MDCK cells were transiently transfected with the *SCN2B-yfp* vector to express WT, partially or fully unglycosylated (UNG) β2. Cells were grown in wells for the indicated number of days and surface biotinylated at 4ºC. (A) Representative western blots and band quantitation (B-E) show that levels of fully unglycosylated β2 were reduced in comparison with the WT and partially glycosylated mutants in biotin-NeutrAvidin pulldowns (Membrane). Note that due to gradual loss of β2 transient expression, band intensity in lysates has decreased after 4 days, becoming then manifested non-specific (irrelevant) bands that migrate at similar molecular weight. One-way ANOVA with Tukey's HSD post hoc test highlighted the differences, with a few exceptions (B, all $p < 0.05$, except 42 vs. UNG ($p = 0.054$); C, all $p < 0.05$ except 42 vs. UNG ($p = 0.052$) and 74 vs. UNG ($p = 0.189$); D, $p < 0.002$; E, $p < 0.005$). The same amount of protein was used to process each

lysate (~130 µg), and the corresponding portion (9/10th) was subjected to overnight pulldown. Na/K-ATPase was blotted as surface marker to correct for quantitations in pulldowns. Data are mean ± SD (error bars) (n ≥ 3). Molecular weight markers are in kDa.

We next determined in which subcellular compartment β2 trafficking becomes interrupted. To do so, cells were immunostained for detection of various subcellular markers of the endocytic and exocytic pathways. These included the EE marker EEA1, the late endosomal lysobisphosphatidic acid (LBPA), the lysosome-associated membrane protein LAMP2, the cis-Golgi marker Golgi matrix protein of 130 kDa (GM130), and the TGN marker TGN46. None of them overlapped markedly with unglycosylated β2 (Figure 20). However, an apparent overlap found with the ER chaperone calnexin indicates that a large portion of the triple mutant is retained at the ER membranes. Moreover, its pattern was highly comparable with that of β2 WT in cells treated with TUN (Figure 21A). Indeed, the Manders' coefficient, to indicate the fraction of β2 overlapping to compartments labeled with calnexin, was ~ 0.7 in cells expressing unglycosylated β2 and in TUN-treated cells, in contrast with negligible overlap in untreated cells expressing β2 WT (Figure 21B). In the latter, β2 outlined the cell end, displaying an obvious dotted pattern, which likely corresponds to β2 getting positioned at the developing apical surface, i.e. its final location in polarized cells. Because of its predominant surface localization, no manifested overlap was observed between β2 WT and any of the markers tested (Figure 20). Altogether, these data indicate that unglycosylated β2 becomes retained in the ER.

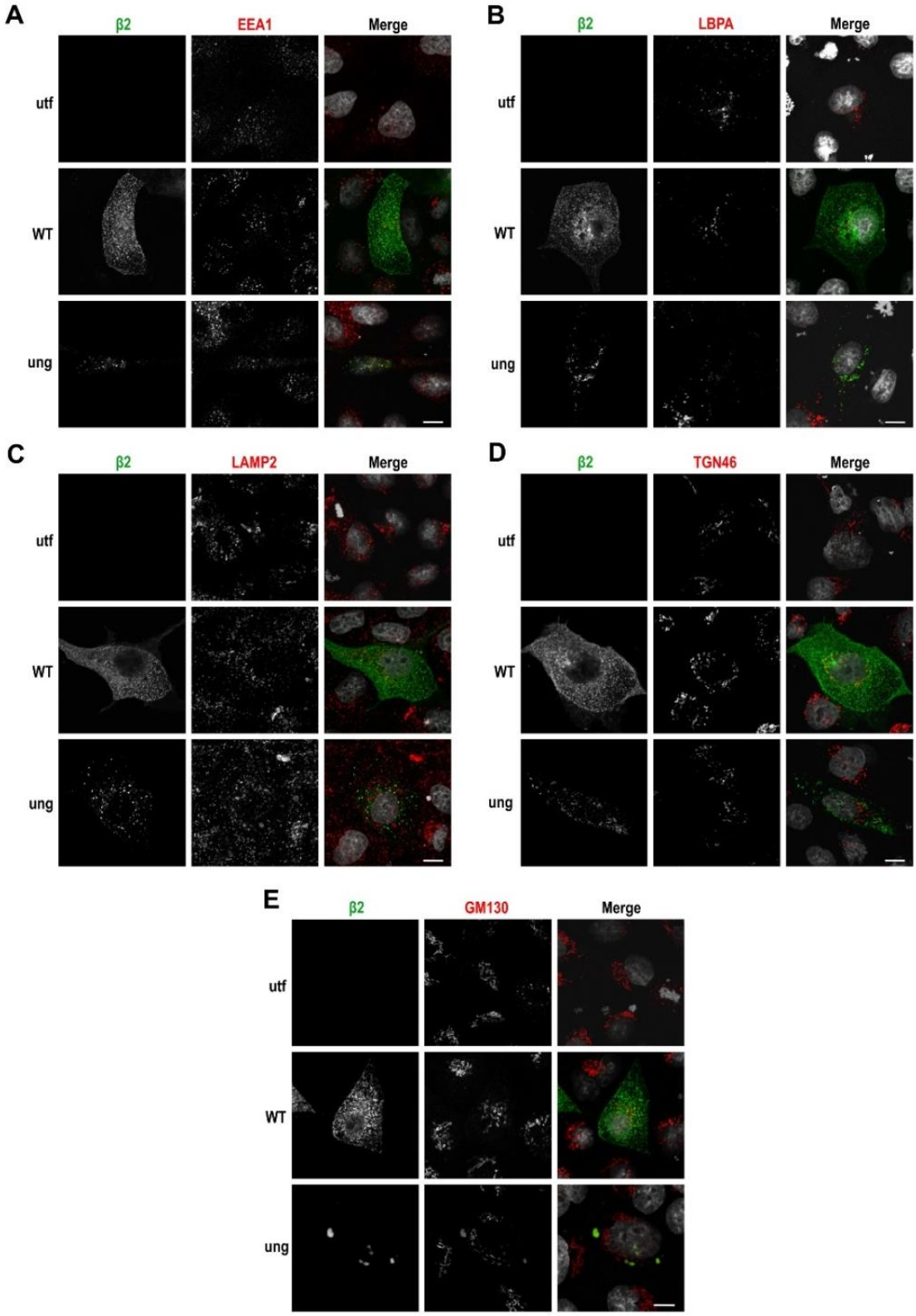

Figure 20. WT or unglycosylated β2 do not overlap with various subcellular markers of the endocytic and exocytic pathways. MDCK cells were transiently transfected with

the *SCN2B*-yfp vector to express WT or fully unglycosylated β2 (ung), or left untransfected (utf), and grown for 1 day in wells. Cells were fixed and immunostained with an antibody against each of the subcellular markers tested (red). Images were obtained by confocal microscopy. In merged images, the YFP-emitted fluorescence is in green and DAPI is in grey. Representative XY sections (taken at the level where β2 is mainly found in each case) show peripheral and scattered staining of β2 WT, contrasting with the intracellular distribution of the unglycosylated mutant. In all cases, the pattern differs with that of the marker compared, not displaying any visible overlap. Scale bars are 10 µm.

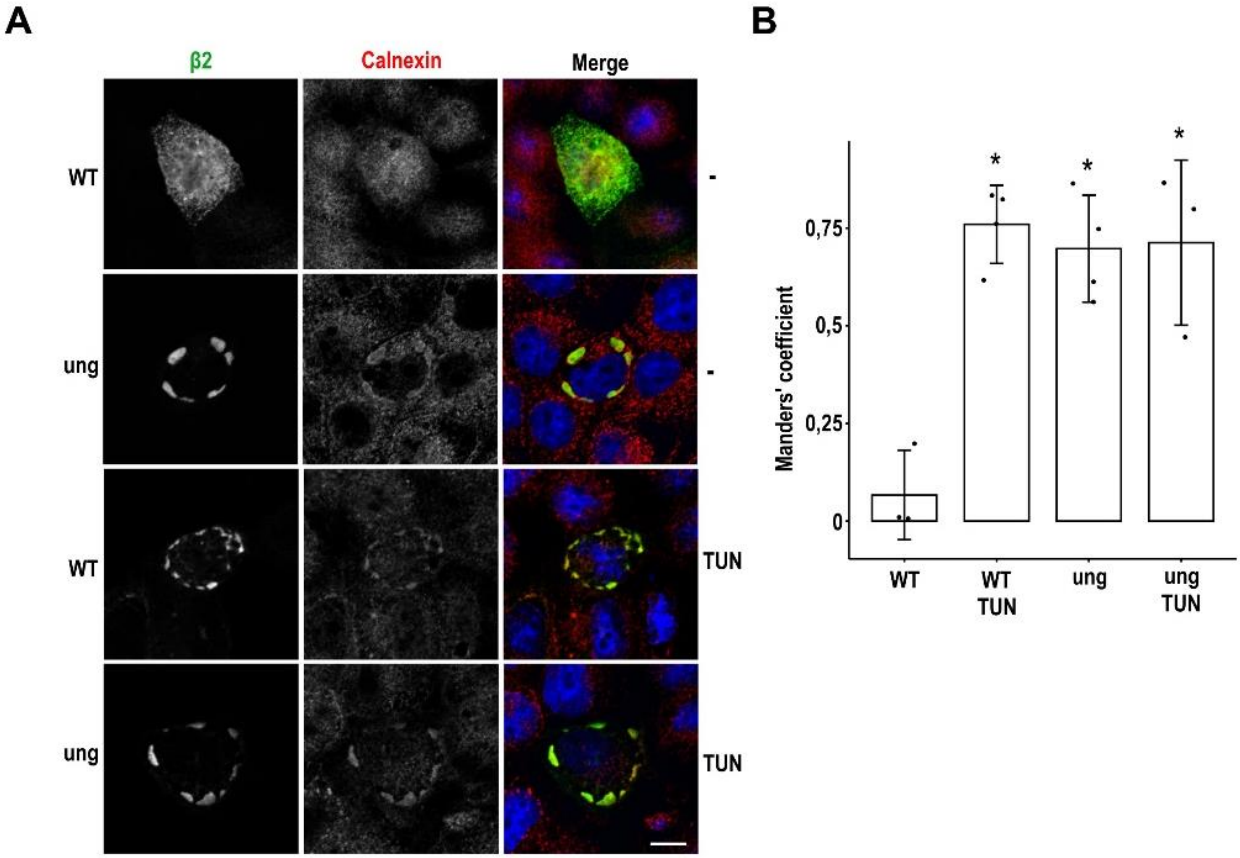

Figure 21. Unglycosylated β2 is retained in the ER. MDCK cells were transiently transfected with the *SCN2B-yfp* vector to express WT or fully unglycosylated β2 (ung), and grown for 1 day in wells. Cells were treated with TUN ~ 2 h after transfection, or left untreated (-), fixed, and immunostained with a rabbit polyclonal antibody against calnexin (red). (A) Representative XY sections show that unglycosylated β2 (green) is intracellular and overlaps with calnexin, as does the WT in TUN-treated cells. This contrasts with the localization of β2 WT at the cell end in untreated cells, also displaying a scattered pattern. To focus more accurately where β2 is found in each condition, sections were taken right above the nucleus (WT -) or at the nuclear level (for the rest). Nuclear staining by DAPI is

in blue. Scale bar is 10 µm. (B) Line chart showing Manders' coefficients calculated along the cell *z*-axis and indicating the fraction of β2 overlapping to compartments labeled with calnexin. The high overlap in TUN-treated cells and in those expressing unglycosylated β2 contrasts with negligible overlap in untreated cells expressing β2 WT. One-way ANOVA with Tukey's HSD post hoc test revealed differences among means (*, $p < 0.0005$). Data are mean ± SD (n ≥ 3).

5.1.4 Unglycosylated β2 can reach the cell surface by bypassing the Golgi compartment

Even though unglycosylated β2 was retained in the ER, a small fraction reached the cell surface and, in polarized MDCK cells, even properly localized to the apical domain. We therefore tested whether blocking the ER-to-Golgi pathway with BFA would prevent arrival of immature β2 to the PM in a similar manner. Here, transfected cells were treated o/n with BFA and both lysates and pulldowns were then deglycosylated with Endo H. As expected, mature, fully glycosylated β2 WT was not visible in cells treated with BFA, confirming lack of processing by Golgi enzymes (Figure 22A). Upon Endo H treatment, the faster-migrating band (immature β2) increased its mobility, coinciding with unglycosylated β2 (Figure 22A; see Figure 16A for comparison). Remarkably, this immature form was the only constituent of pulldowns from BFA-treated cells, indicating that it can reach the PM by bypassing Golgi glycosylation. Subsequently, pulldowns were also treated with Endo H, which again shifted a small fraction of immature β2 to the position of (faster-moving) unglycosylated (fully deglycosylated) β2 (Figure 22A).

Albeit to a lesser extent, β2 WT was still enriched in pulldowns of BFA-treated cells. However, quantitation of western blots indicated that, similarly to unglycosylated β2, the ratio by which immature β2 reached the cell surface in BFA-treated cells was only ~ 1/3rd as compared with untreated cells (Figure 22B). Proper validation that the drug produced accumulation of β2 in the ER was seen by its considerable overlap with calnexin (Figure 22D), whose pattern clearly differed from that of the cis-Golgi marker GM130, which became more tubulated and dispersed in the presence of BFA (see also Figure 23A). Thus, a large portion of β2 WT now appeared accumulated in enlarged calnexin-positive structures, often undistinguishable from unglycosylated β2 accumulations (arrowheads in Figure 22D). Moreover, in untreated cells expressing low levels of unglycosylated β2, the mutated protein largely overlapped with calnexin, further confirming its retention in the ER (Figure 23B).

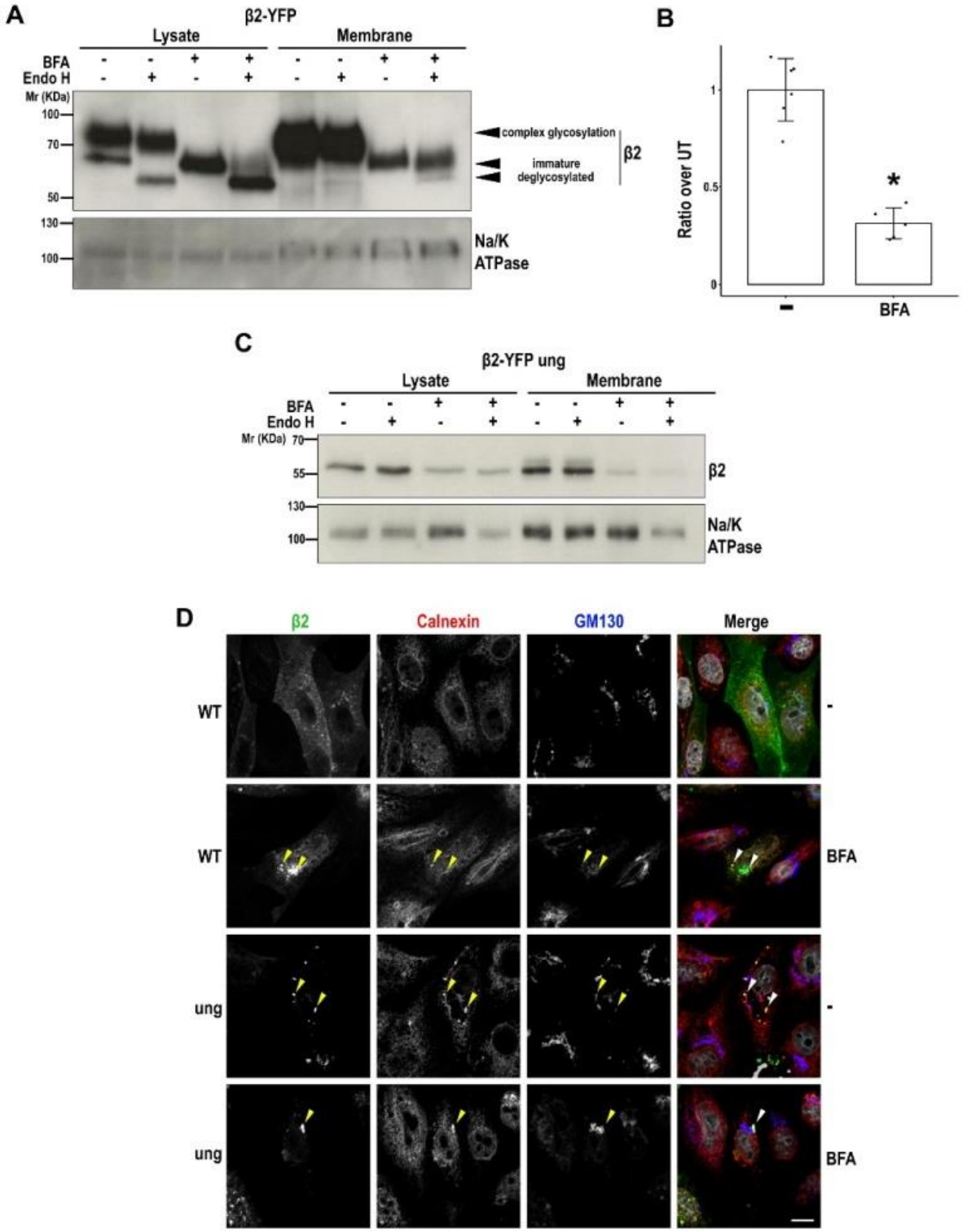

Figure 22. Brefeldin A (BFA) prevents complex glycosylation of β2, a fraction of which can reach the cell surface. MDCK cells were transiently transfected with the *SCN2B-yfp* vector to express WT or fully unglycosylated β2 (ung), then treated 2 h later with BFA (+), or left untreated (-), and grown o/n in wells. (A, C) Cells were surface

biotinylated at 4ºC. The same amount of protein was used to process each lysate (~ 100 µg) and the corresponding portion (9/10th) was subjected to overnight pulldown. Denatured protein from cell lysates and pulldowns was treated o/n at 37°C with Endo H to cleave off immature *N*-glycans, or left untreated (-). Representative western blots show that the (lower) faster-migrating band of β2 WT is the only one visible in cells treated with BFA and increases its mobility with Endo-H; upon Endo-H treatment, this band (fully deglycosylated β2) coincides with unglycosylated β2 (C; compare with Figure 16A). Note that Endo-H digestion in pulldowns is only partial, either due to saturation of the enzyme or to suboptimal conditions for enzyme action. Blots for Na/K-ATPase are included as loading controls. Molecular weight markers are in kilodaltons (kDa). (*B*) band quantitation shows reduced levels of immature β2 in biotin-NeutrAvidin pulldowns (*Membrane*) of BFA-treated cells. Two-tailed Student's *t* test shows significant difference (*, $p < 0.05$). Data are mean ± S.D. (*error bars*) ($n \geq 3$). (D) Cells were fixed and immunostained with a rabbit polyclonal antibody against calnexin (red) and a mouse monoclonal to GM130 (blue). Representative XY sections show that β2 WT displays an intracellular accumulation in BFA-treated cells comparable to that of mutated β2 (green), grossly overlapping with calnexin in enlarged structures (arrowheads). This contrasts with its apparent PM localization in untreated cells, displaying also a scattered pattern that does not overlap with calnexin (sections were taken at the cell level where β2 is mainly found in each case). Nuclear staining by DAPI is in grey. Scale bar is 10 µm.

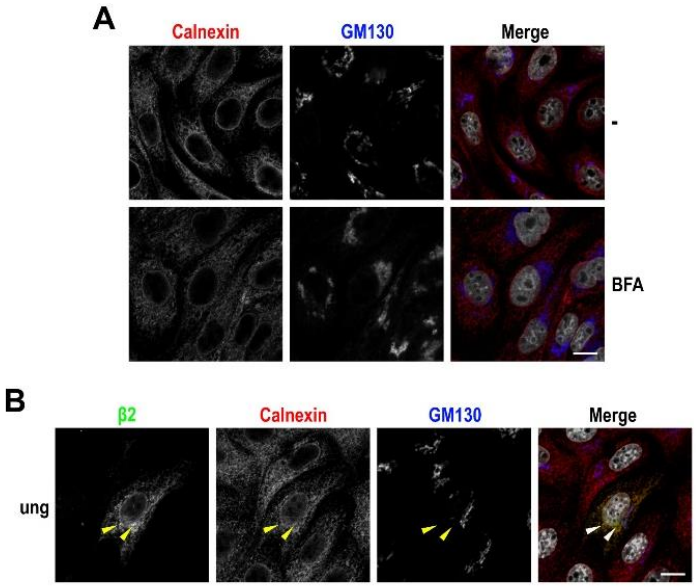

Figure 23. Unglycosylated β2 is largely retained in the ER. MDCK cells were transiently transfected with the *SCN2B*-yfp vector to express fully unglycosylated β2 (ung), and grown o/n in wells (B); alternatively, cells were left untransfected and treated o/n with BFA 2 h after plating, or left untreated (-) (A). Cells were fixed and immunostained with a rabbit polyclonal antibody against calnexin (red), co-staining with a mouse monoclonal to GM130 (blue). (A) Representative XY sections (taken at the level where GM130 is mainly found) show that these markers do not overlap even in BFA-treated cells, although the GM130 pattern becomes more tubulated and disperse. (B) Representative XY sections

(taken at the level where β2 is mainly found) of untreated cells expressing low levels of unglycosylated β2 show its overlap with calnexin (arrowheads), confirming retention in the ER. Nuclear staining by DAPI is in grey. Scale bar is 10 μm.

5.1.5 Dynamics of β2 in the plane of the membrane is not influenced by *N*-glycosylation

The data above provide strong evidence that *N*-glycosylation is required for β2 to reach the PM. It is plausible to contemplate that *N*-glycans ensure β2 oligomerization and correct folding to exit the ER properly. In addition, glycosylation may favor β2 clustering at the TGN, which may in turn increase affinity to lipid rafts, for subsequent inclusion into apical transport carriers [167]. Thus, we hypothesized that β2 dynamics in the plane of the membrane may be influenced by its glycosylation, which could have important functional implications. Movement of fluorescently tagged β2 was monitored by FRAP. The MF, that is, the portion of molecules undergoing diffusion, differed depending on the cell's location where the measurement was taken. Hence, we chose three representative regions for analysis, i.e. at the cell end, mostly representing cell surface β2 (Figure 24A); within the cytoplasm matrix, likely including the dispersed ER network as well as clusters of β2 near the surface (Figure 24B); and in vesicular structures of unknown nature, which may represent large perinuclear ER elements with β2 in transit to the cell surface (Figure 24C). At the cell end, ~ 60% of β2 WT molecules underwent diffusion 4-5 min after bleaching. MF at the cell end was slightly increased for unglycosylated β2, yet differences were not significant (Figure 24A and Table 1). Similar data were found for cytoplasmic β2 (Figure 24B). However, when β2 found in large vesicles was bleached, fluorescence never recovered above 10% of the total initial signal (Figure 24C). These MF differences suggest that the molecular environment of these large vesicles where β2 accumulates differs from that of the other cellular areas analyzed.

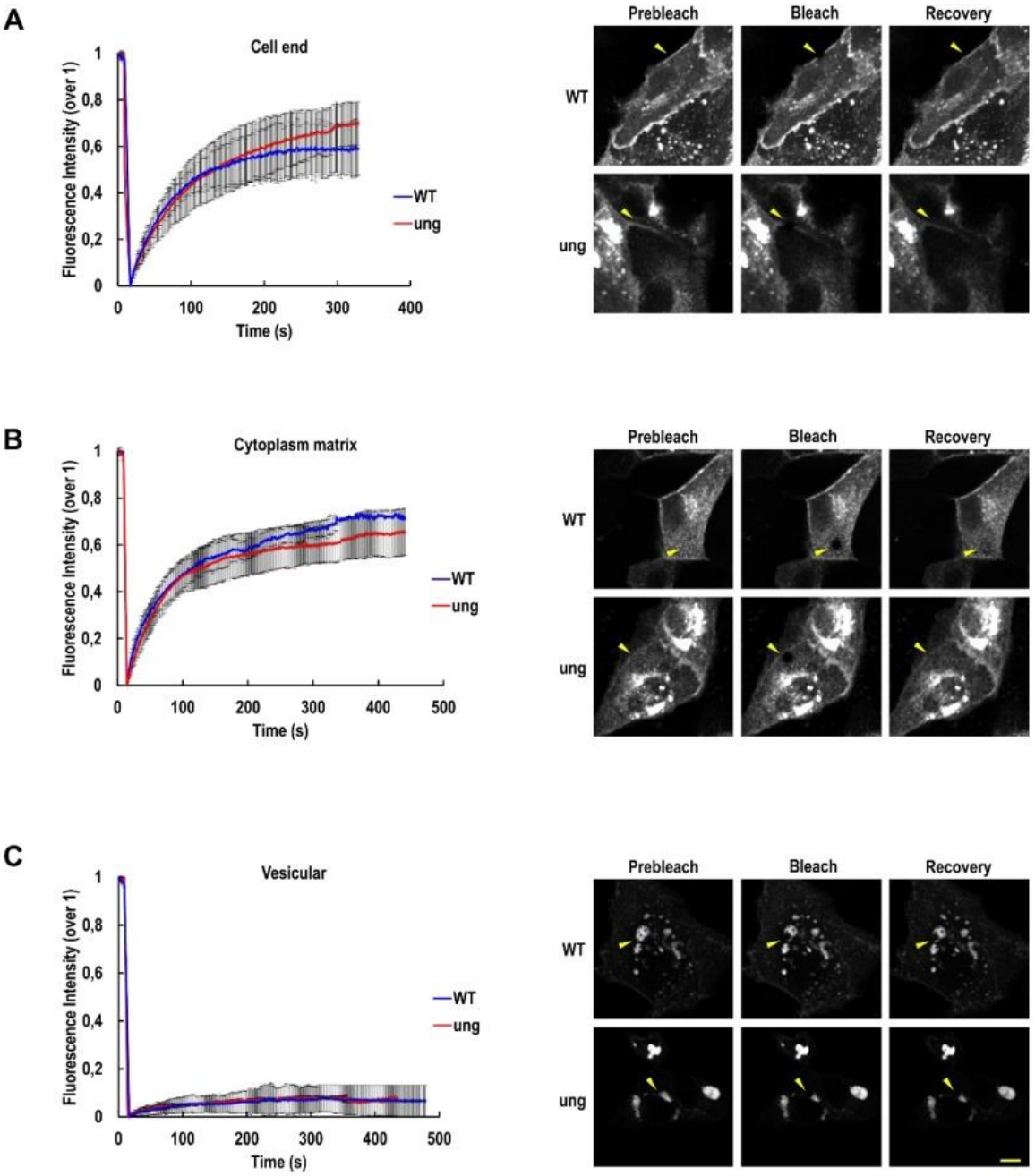

Figure 24. Dynamics of β2 is not influenced by *N*-glycosylation. MDCK cells were transiently transfected with the *SCN2B*-yfp vector to express WT or fully unglycosylated (ung) β2, and grown for 2 days on glass supports. Mobility of β2-YFP at three different cellular locations was monitored by FRAP with a confocal microscope. Line charts of fluorescence intensity (mean ± SD) of ≥ 3 representative experiments show comparable mobile fraction between β2 WT (blue line) and mutant (red line) at the three regions analyzed, i.e. (A) the cell end, (B) the cytoplasm matrix, and (C) in large vesicular structures. For each, images on the right show a representative cell pre-bleached, right

after bleaching, and after fluorescence recovery (yellow arrowheads mark the bleached area). Scale bars are 10 µm. See the complete FRAP data in Table 1.

Table 1. FRAP data for WT and unglycosylated β2 indicate no differences in dynamics in the plane of the membrane.

		cell end	cytoplasm matrix	vesicular
MF (%)	**WT**	60 ± 10	68 ± 4	7 ± 6
	ung	68 ± 9	63 ± 8	8 ± 1
	***p* value**	0.12	0.29	0.77
$\tau_{1/2}$ (s)	**WT**	57.9 ± 12.8	55.8 ± 5.9	57.0 ± 15.8
	ung	74.4 ± 18.2	58.8 ± 10.7	68.4 ± 21.9
	***p* value**	0.06	0.60	0.51
***D* (µm^2/s)**	**WT**	0.018 ± 0.004	0.018 ± 0.002	0.005 ± 0.001
	ung	0.014 ± 0.003	0.018 ± 0.004	0.004 ± 0.001
	***p* value**	0.07	0.78	0.51

Each value is the mean ± SD of ≥ 3 experiments. Mobile fraction (MF), half-time of recovery ($\tau_{1/2}$), and diffusion coefficient (D). *P* values compare unglycosylated β2 over WT.

The FRAP data also showed that the mobility rate of WT and unglycosylated β2 is comparable, with only a slight tendency of the mutant to move slower. Regardless of the location, $\tau_{1/2}$ (the time-point of half fluorescence recovery) was ~ 1 min in both β2 variants (Table 1). Consequently, a D ~ 0.02 µm^2/s was found in general, although β2 in large vesicles moved even slower, i.e. at ~ 1/4th of this speed (see Materials and methods).

5.2 *S*-palmitoylation and cellular cholesterol ensure β2 partition to plasma membrane subdomains

We have found that *N*-glycosylation is required for efficient trafficking and localization of β2 to the PM. In polarized MDCK cells, exogenously expressed β2 localizes to the apical domain. Since palmitoylation could increase protein affinity for glycosphingolipid/cholesterol-rich raft domains [168], it is plausible to consider that this post-translational modification may influence the preferential apical targeting of β2 [169]. Therefore, we hypothesized that β2 can be palmitoylated.

5.2.1 β2 is palmitoylated

We aimed to detect β2 palmitoylation in MDCK cells by an ABE assay. To ensure that β2 would reach its steady state localization, we used stable cell lines. YFP-tagged β2 was first immunoprecipitated using a rabbit polyclonal antibody to GFP. A band at ~ 80 KDa, corresponding to the molecular weight of fully glycosylated β2-YFP (see section 5.1), was effectively detected by anti-biotin blot in immunoprecipitates after BMCC-Biotin labeling under treatment with HAM; HAM exposes thiol groups that can then be biotinylated. Evidence of specificity was confirmed by absence of biotinylated β2 in immunoprecipitates using an irrelevant polyclonal antibody – specifically, against Vps26, a major endosomal protein [140] – and similarly in native MDCK cells (Figure 25A).

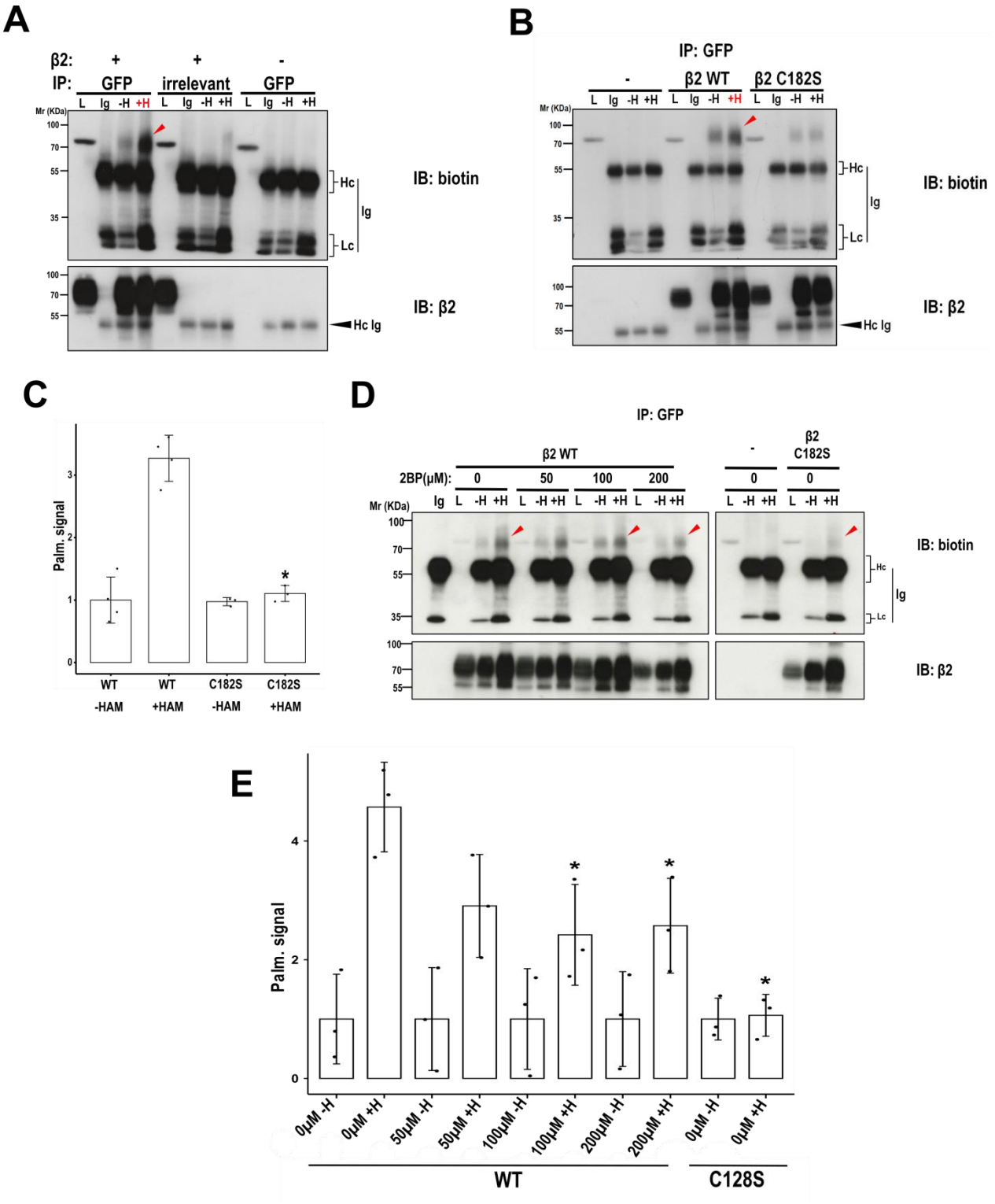

Figure 25. β2 is palmitoylated at Cys-182. MDCK cells, parental (-) or stably expressing β2-YFP, WT (+) or C182S, were grown in wells until confluence and subjected to an ABE assay. The same amount of protein was used to process each lysate (~ 300 μg), and 9/10th was subjected to overnight immunoprecipitation (IP) in the presence of NEM; L, 1/10th of the lysate. An antibody to GFP was used to immunoprecipitate β2 and an irrelevant antibody was used as a control. The pulled-down beads were then split and one-

half of each treated with (+H) or without (-H) HAM. An equivalent amount of antibody alone (Ig) was processed in parallel in the presence of HAM. After BMCC-Biotin labeling, proteins were analyzed by western blot (IB) to detect acylated (biotin) and total β2 (serving to adjust and obtain relative levels in band quantitation). Representative western blots (A, B) and (C) band quantitation show that β2 WT (red arrowhead), but not C182S, is palmitoylated. (D) Prior to the experiment, cells were grown for 1 h in 2% serum, then 2-BP was added at the indicated concentration and left for 1 h more; 0, an equivalent volume of solvent was added instead. Hc and Lc indicate heavy and light chain immunoglobulins (Ig), respectively. In western blots anti-biotin, note the presence of a non-specific band in lysates migrating as, but unrelated to, β2-YFP. Molecular weight markers are in kilodaltons (kDa). (C, E) Data, expressed as normalized palmitoylation (Palm.) signal, are mean ± SD (error bars; n ≥ 3). Differences were highlighted by two-tailed Student's *t*-test (C, $*p$ = 0.0013, compared with WT +HAM), and by one-way ANOVA with Dunnett's post-hoc test (E, WT, 0 µM vs. 100 µM, $*p$ = 0.0183; vs. 200 µM, $*p$ = 0.0268; and vs. C182S, at 0 µM, $*p$ = 0.0007; in all cases, + HAM).

This experiment suggests that β2 is palmitoylated, a PTM that may regulate its trafficking and subcellular localization. In its C-terminal ICD, β2 has a single Cys residue, i.e. Cys-182, which is conserved [80] and corresponds to the second residue after its predicted TMD [129]; see UniProtKB – O60939. We therefore mutated Cys-182 to Ser (C182S), which is expected to prevent β2 palmitoylation. By ABE, no manifested band was observed in immunoprecipitates from β2 C182S-expressing cells treated with HAM as compared to untreated samples (Figure 25B-E). Evidence that NEM effectively blocked free Cys residues during the immunoprecipitation was seen by the presence, when NEM was omitted, of several non-specific bands, resulting from free thiol groups susceptible of cleavage by HAM, and later biotinylated, which were absent when NEM was included (empty arrowheads in Figure 26). Moreover, the reaction was inhibited under increasing concentrations of the palmitate analog 2-BP, which acts as a palmitoylation inhibitor in live cells (Figure 25D and E). These data provide biochemical evidence that β2 is palmitoylated at Cys-182.

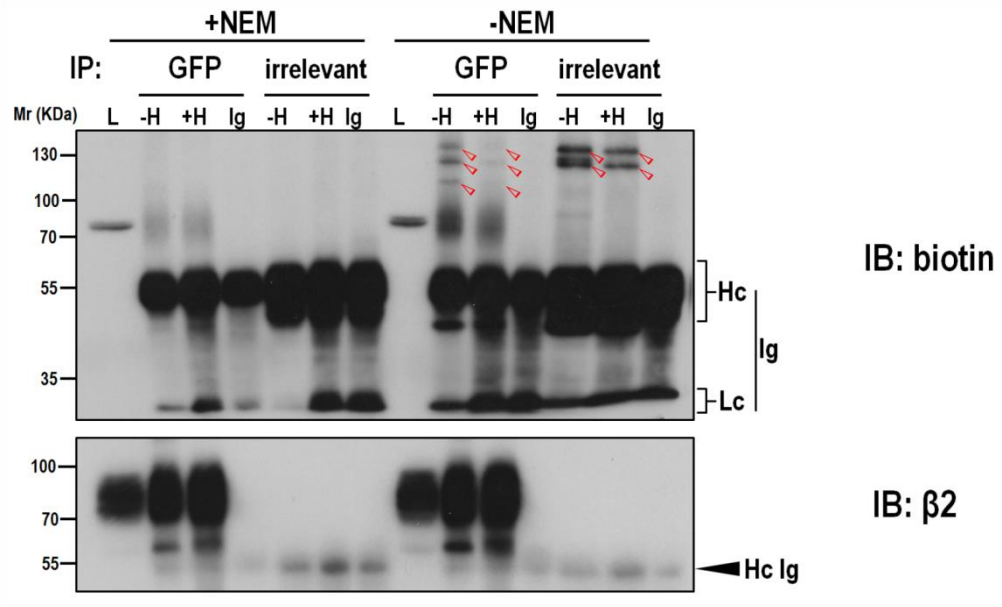

Figure 26. Acyl-biotin exchange assay in the absence of NEM indicates specificity. MDCK cells stably expressing β2-YFP WT, were grown in wells until confluence and subjected to an ABE assay. The same amount of protein was used to process each lysate (~ 300 µg), and 9/10th was subjected to overnight immunoprecipitation (IP) with or without NEM; L, 1/10th of the lysate. An antibody to GFP was used to immunoprecipitate β2 and an irrelevant antibody as a control. The pulled-down beads were then split and one-half of each treated with (+H) or without HAM (-H). An equivalent amount of antibody alone (Ig) was processed in parallel in the presence of HAM. After BMCC-Biotin labeling, proteins were analyzed by western blot (IB) to detect acylated (biotin) and total β2. Representative western blots show that in the absence of NEM (-) several non-specific bands appear as a result of the presence of free thiol groups which were later biotinylated (empty arrowheads); these bands are absent when NEM was included (+). Hc and Lc indicate heavy and light chain immunoglobulins (Ig), respectively. In western blots anti-biotin, note the presence of a non-specific band in lysates migrating as, but unrelated to, β2-YFP. Molecular weight markers are in kilodaltons (kDa).

5.2.2 β2 association to detergent-resistant membranes (DRM) is dependent on palmitoylation

We hypothesized that β2 palmitoylation may influence its subcellular localization, including perhaps its apical delivery [170]. We took a biochemical approach to address the potential association of β2 to PM subdomains that may be representative of lipid rafts, defined as the Lo phase of the membrane [171]. To this end, we isolated DRMs by solubilizing cell extracts with a non-ionic detergent at 4ºC and following previously published procedures [147]. As previously described, albeit not as apparent [88], β2 WT was partially recovered in the upper 2-3 fractions

of the sucrose gradient, in which both flotillin-1 and caveolin-1 concentrate. On the contrary, β2 C182S was not detected in these DRM fractions, similarly to non-raft Na/K-ATPase, both found exclusively in the bottom half of the gradient, and therefore are completely Triton X-100-soluble (Figure 27). These data suggest that palmitoylation in Cys-182 is required for the presence of β2 in DRMs and may be implicated in its association to the membrane Lo phase.

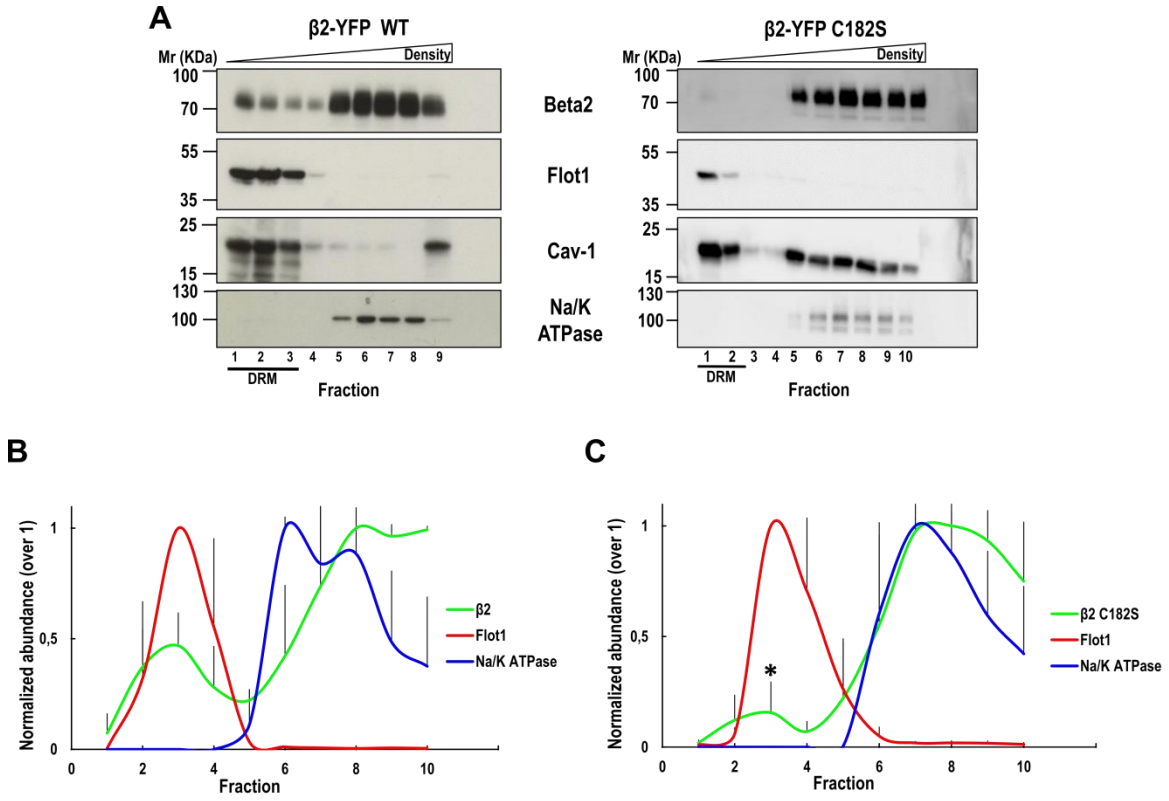

Figure 27. Palmitoylated β2 partitions into DRMs. MDCK cells stably expressing β2-YFP, WT or C182S, were grown in dishes until confluence and lysed in 1% Triton X-100 at 4ºC. Membranes were pelleted, overlaid with a sucrose density gradient and spun overnight. Approx. 10 fractions were collected (1 ml each) and analyzed by western blot after TCA precipitation. (A) Representative western blots, and (B, C) band quantitations, show a portion of β2 WT, but not C182S, floating in DRMs enriched with flotillin-1 (Flot1), as well as caveolin-1 (Cav-1). Blots for Na/K-ATPase indicate the distribution of this non-raft protein in the bottom half of the gradient. The same amount of protein from each fraction was loaded into each lane. Molecular weight markers are in kilodaltons (kDa). Data are mean ± S.D. (error bars; n = 3). Two-tailed Student's *t*-test shows significant differences for fraction 3 (*p = 0.046).

5.2.3 The polarized localization of β2 is dependent on cholesterol

Previous evidence from our laboratory indicate that β2 localization at the apical surface of polarized MDCK is dependent on cholesterol, as acute cholesterol depletion mislocalized the protein to the basolateral domain. We confirmed this observation (Figure 28A). To better understand β2 polarized delivery, we treated polarized MDCK cells with U18666A and lovastatin for an extended period of time, i.e. 24 h; U18666A blocks intracellular cholesterol transport [144] and lovastatin inhibits its synthesis [145]. Interestingly, while β2 was observed, as expected, exclusively at the apical surface in untreated cells (Figure 28B), it redistributed partially to the basal region under the treatment (Figure 28C). Evidence that the effect is specific on β2 was seen by proper basolateral localization of Na/K-ATPase and the tight junction marker ZO-1 (Figure 28B and C). Quantitation of fluorescence along apical-to-basal *z*-stacks further highlighted β2 mislocalization under the treatment, as the β2 curve peak extended towards more nuclear (basal) sections in treated cells. Thus, the relative fluorescence intensity in the basolateral region, as measured by CTCF, changed upon treatment from 20-30% of the maximum fluorescence recorded (at the most apical section) to 60-80% (Figure 28D and E).

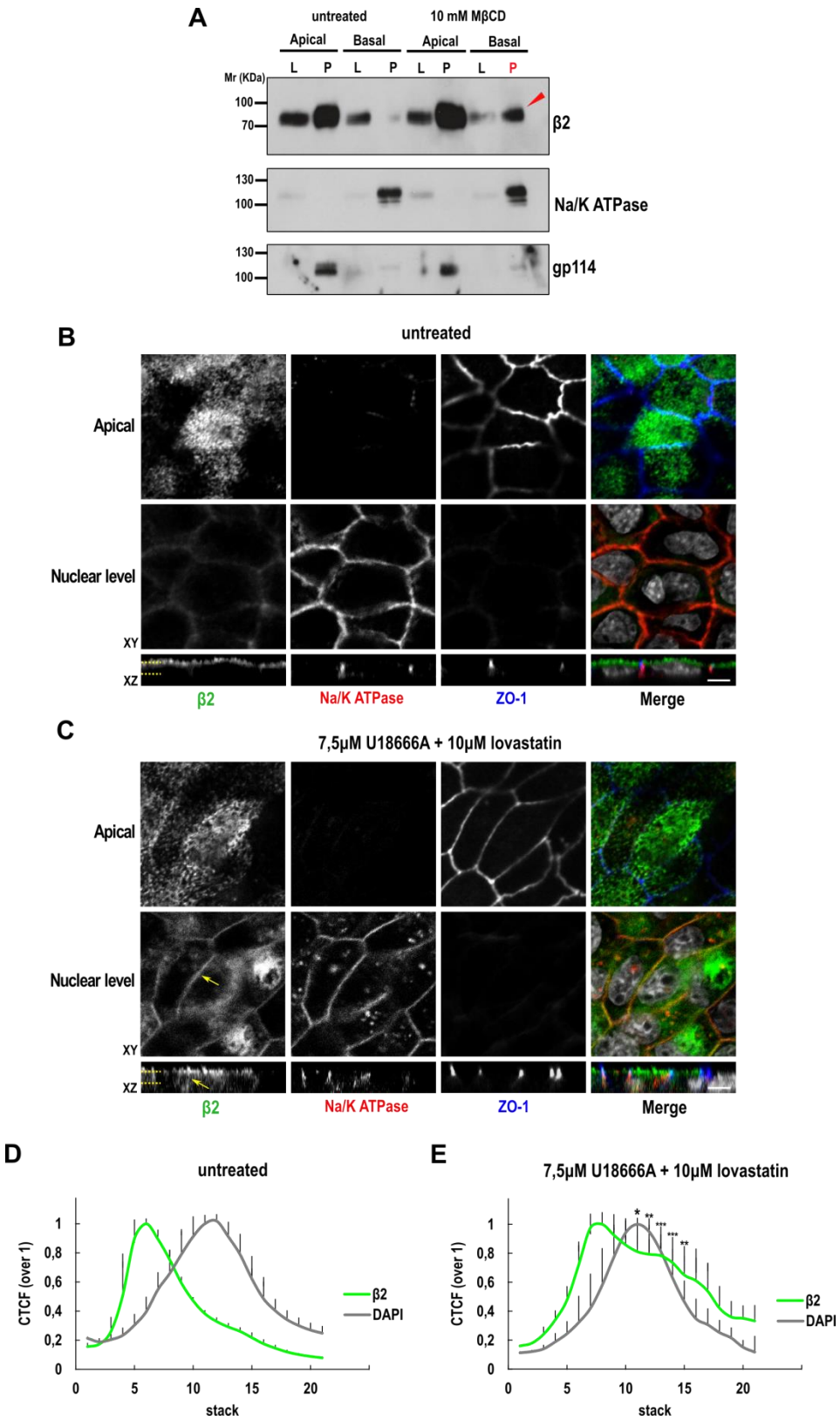

Figure 28. β2 is mislocalized to the basolateral surface when depleting cellular cholesterol or by blocking intracellular cholesterol transport. MDCK cells stably

expressing β2-YFP WT were grown polarized in Transwells. Cells were treated for 1h with 10mM MβCD or left untreated (A). Cells were surface biotinylated at 4ºC, either at the apical or basolateral (Basal) surface. The same amount of protein was used to process each lysate (~ 200 µg), and 9/10th were subjected to overnight NeutrAvidin pulldown (P); L, 1/10th of the lysate. Representative western blots show redistribution of β2 to the basolateral surface in the presence of MβCD (red arrowhead), while the polarity markers gp114 and Na/K-ATPase remain at their apical and basolateral domains, respectively (A). Molecular weight (Mr) markers are in kilodaltons (kDa). Cells were treated for 24 h with 7.5 µM U18666A and 10 µM lovastatin (C), or left untreated (B). Cells were fixed and immunostained for β2 (green), Na/K-ATPase (red), and ZO-1 (blue). Images were obtained by confocal microscopy. In merged images, nuclear staining by DAPI is in grey. Representative XY sections, and corresponding *z*-axis reconstructions, show that β2 is also present at the basolateral membrane upon the treatment (yellow arrows), while Na/K-ATPase and ZO-1 remain unaffected, (the two parallel yellow dashed lines in XZ mark the sections shown by XY, either apical or nuclear). Scale bars are 5 µm. (D, E) Line charts displaying the CTCF (mean percentage ± SD; error bars) along an apical-to-basal *z*-stack (section 1: most apical; 0.5 µm optical slice thickness) show the β2 curve with its peak located apically (D). In contrast, β2 is displaced into basal sections in treated cells, in part overlapping with DAPI (E), included as reference for the nuclear level (10 cells were analyzed per condition). Two-tailed Student's *t*-test shows significant difference in stacks 11-15 (*$p < 0.05$; **$p < 0.01$; ***$p < 0.001$).

Intriguingly, the non-palmitoylable β2 C182S maintained apical polarity, displaying clear enrichment at the apical surface, similarly as β2 WT (Figure 29). This indistinguishable behavior indicates that Cys-182 is not required for the steady state apical localization of β2, although it may serve for partitioning apically localized β2 into surface domains potentially relevant for its function.

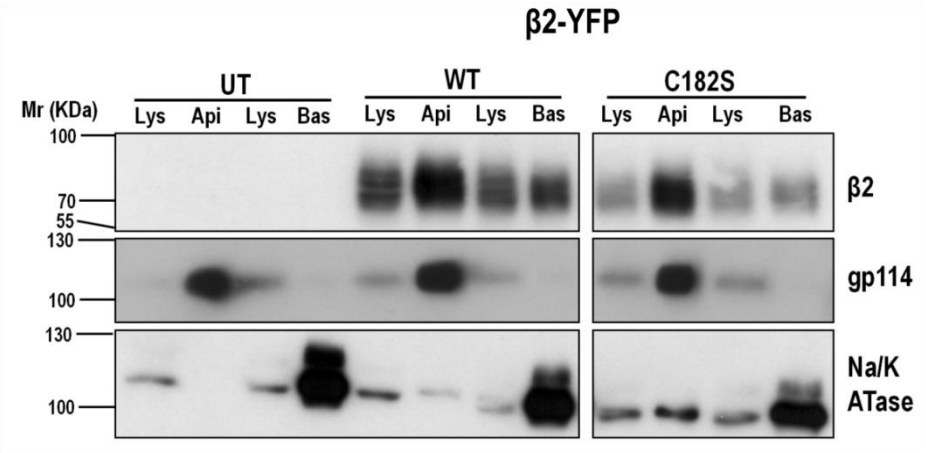

Figure 29. β2-YFP C182S localizes to the apical surface. MDCK cells were transiently transfected with the *SCN2B-cfp* vector to express β2, WT or C182S, or left untransfected (UT), and grown polarized in Transwells. Cells were surface biotinylated at 4ºC, either at

the apical (Api) or basolateral (Bas) surface. The same amount of protein was used to process each lysate (~ 200 µg), and 9/10th were subjected to overnight NeutrAvidin pulldown; Lys, 1/10th of the lysate. Representative western blots show comparable enrichment of both WT and C182S β2 only at the apical surface, with much reduced levels at the basolateral domain. Distribution of polarity markers gp114 and Na/K-ATPase, for apical and basolateral domains, respectively, is shown to ensure that cells were fully polarized. Molecular weight markers are in kilodaltons (kDa).

5.2.4 Lack of endocytosis and limited membrane diffusion of β2

These results so far suggest that β2 dynamics within the membrane may be influenced by cholesterol content as a result of its Cys residue susceptible to palmitoylation. Potential alterations in dynamics of Na_V β subunits may influence the functionality of the α subunit. Therefore, we examined first whether β2 is internalized. To this end, we biotinylated the apical cell surface and examined β2 endocytosis upon glutathione cleavage of surface-exposed biotinylated protein, which leaves intracellular biotin moieties protected. The label from biotinylated β2 was effectively gone after glutathione cleavage, performed at time zero. However, even after 60 min at 37ºC, β2 was not detected in pulldowns, similarly as gp114, known to display very little endocytosis in MDCK cells [172], and cytoplasmic Vps26, not accessible to the biotin reagent (Figure 30A). To have a positive control, we performed the assay also in cells transiently expressing BACE1, which localizes to the apical surface and undergoes endocytosis [140]. As expected, its effective endocytosis was recorded at 15 min, remaining undetected at a later time point because biotinylated BACE1 had been already recycled, degraded, or transported by transcytosis to the basolateral surface [140], and its biotin moiety therefore been cleaved by glutathione (Figure 30B).

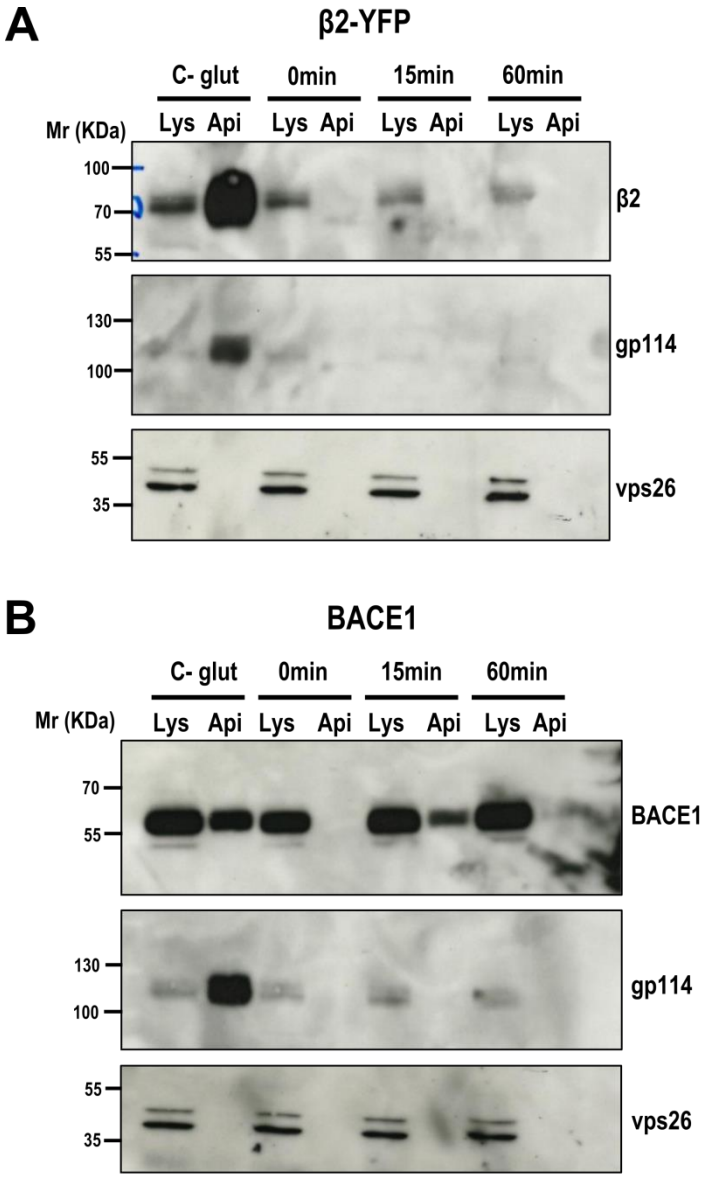

Figure 30. β2 does not undergo endocytosis. MDCK cells were transiently transfected with the *SCN2B-yfp* vector to express β2 WT (A), or with a vector to express human BACE1 (B), and grown polarized in Transwells. Cells were biotinylated at the apical (Api) surface at 4ºC. Biotinylated proteins were allowed to internalize for various time periods at 37°C, after which the surface biotin tag was stripped off with reduced glutathione (glut) at 4°C, remaining protected the endocytosed biotinylated proteins. The same amount of protein was used to process each lysate (~ 200 µg), and 9/10th were subjected to overnight NeutrAvidin pulldown; Lys, 1/10th of the lysate. Representative western blots show increased cellular levels of BACE1 in pulldowns after 15 min (B), denoting apical endocytosis, but not of β2 at any time point analyzed (A). As controls, note total absence of biotinylated protein in pulldowns of cells treated with glutathione immediately after

labeling (0 min). In addition, apical gp114 does not get endocytosed and Vps26 is a cytoplasmic protein not accessible to the biotin reagent. Molecular weight markers are in kilodaltons (kDa).

Since cholesterol depletion caused β2 mislocalization to the basolateral surface, we reasoned that movement of β2 in the plane of the membrane monitored by FRAP in live cells would be affected upon this treatment. As we have seen previously, β2 generally shows partial fluorescence recovery, obtaining an even smaller MF if increasing the bleached area (Figure 31A), as often expected [173]. We therefore performed the analyses using the minimum possible r_n of 2 μm in our set up. Acute cholesterol depletion, with increasing doses of MβCD, dramatically decreased the MF of β2, as measured at the cell end between two adjacent cells (Figure 31B). However, neither $\tau_{1/2}$ nor *D* were affected (Table 2), indicating that the portion of molecules that can undergo diffusion diminished whereas the rate of diffusion, or speed at which molecules move, did not change.

We next addressed potential differences in membrane dynamics between β2 WT and C182S. Interestingly, the MF of β2 C182S at the cell surface was slightly, yet significantly, decreased compared with that of the WT (Figure 31C). Likewise, $\tau_{1/2}$ displayed a tendency to increase in the mutant, indicative of an overall reduced mobility (Table 2).

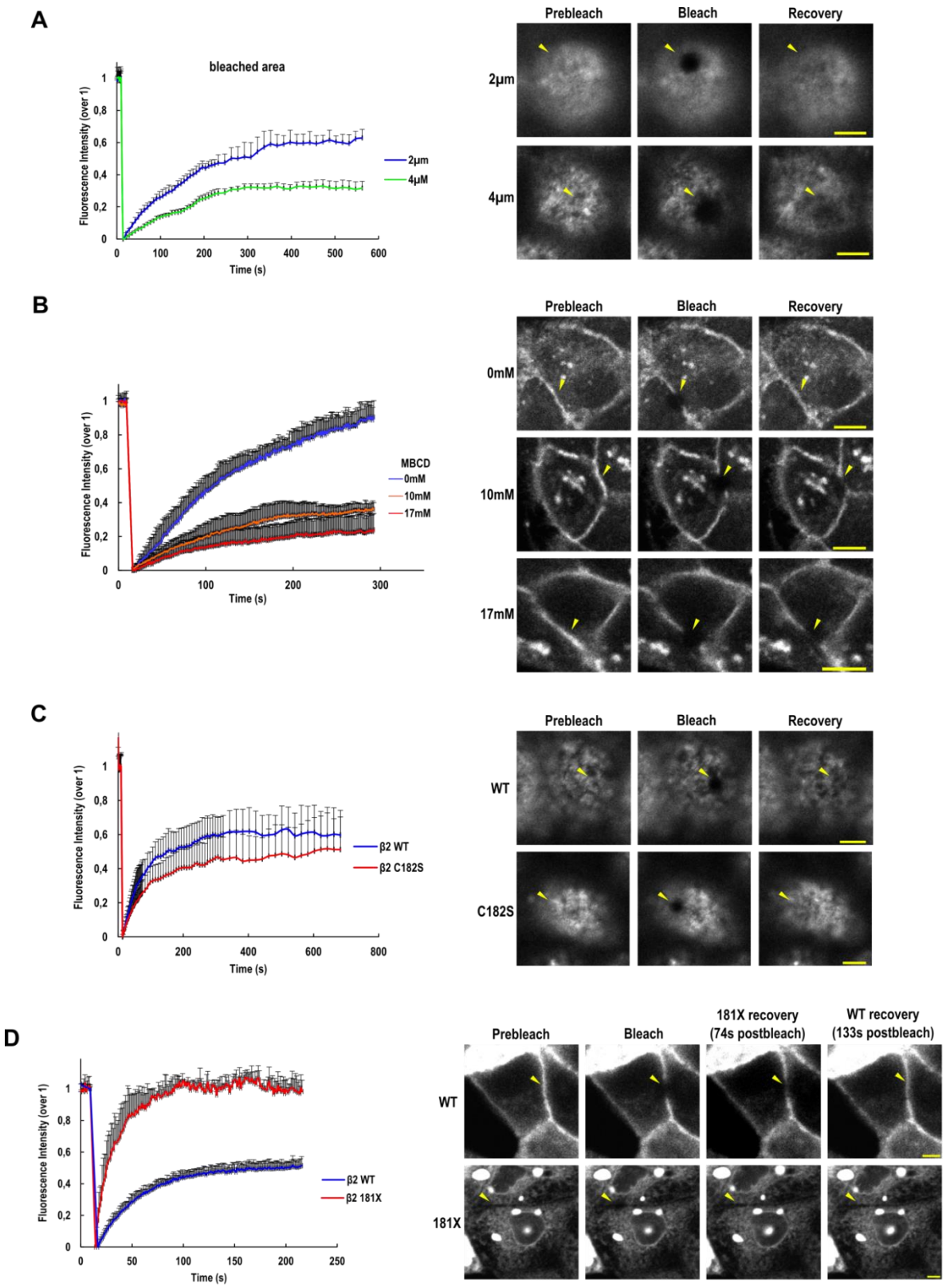

Figure 31. Cholesterol depletion and the C182S mutation cause a decrease in the MF of β2, whereas removal of its ICD causes a dramatic increase. MDCK cells stably

expressing β2-YFP, WT or C182S (A, B, C), or transiently transfected with the *SCN2B-yfp* vector to express β2 WT or lacking its ICD (181X) (D), were grown and kept subconfluent in a μ-slide with glass bottom for 1 (B) or 2 days (A, C, D). Mobility of cell surface β2-YFP was monitored by FRAP with a confocal microscope; bleaching was performed at the upper cell level, which includes the PM as seen by an XY section (A, C) or, in a nuclear section, at the cell end between two adjacent cells (B, D). Line charts of fluorescence intensity show MF of β2 (mean ± SD; error bars) of at least three representative experiments. (A) MF is reduced by increasing the bleached area (from r_n of 2 μm to 4 μm). (B) Increasing concentrations of MβCD dramatically reduce β2 MF. (C) The MF of β2 C182S is slightly decreased compared with that of the WT. (D) β2 181X displays considerable more mobility than the WT. For each graph, images on the right show a representative cell pre-bleached, right after bleaching, and after fluorescence recovery (yellow arrowheads mark the bleached point). To highlight the apparent differences in MF between β2 WT and 181X, pictures of two time points are shown (D). Scale bars are 5 μm (A, C, D) or 10 μm (B). See the complete FRAP data in Table 2.

The slow dynamics of β2 also suggests that its mobility may be limited by anchoring to the cytoskeleton. Thus, we tested the mobility of β2 lacking its ICD (181X). Strikingly, β2 181X displayed complete fluorescence recovery (Figure 31D) and a comparatively faster mobility than the WT (Table 2). This experiment also substantiates the evidence that a fraction of β2 associates with Lo membrane domains, which cluster around TM proteins acting as anchors to the cytoskeleton [174,175].

Table 2. FRAP data indicate that cholesterol depletion and the C182S mutation cause a decrease in the MF of β2, whereas removal of its ICD causes a dramatic increase.

bleached area (r_n, μm)	n	MF (%)	$\tau_{1/2}$ (s)	D (μm^2/s)
2	3	65 ± 2	138.0 ± 14.4	0.002 ± 0.000
4	3	35 ± 2	140.7 ± 10.7	0.007 ± 0.001
***p* value**		< 0.001	0.810	0.002
MβCD (mM) treatment				
0	5	89 ± 7	94.8 ± 21.4	0.003 ± 0.001
20	5	39 ± 2	106.2 ± 39.2	0.003 ± 0.001
35	5	23 ± 8	93.0 ± 47.2	0.003 ± 0.001
***p* value**		< 0.000 (0 vs. 20 mM) < 0.000 (0 vs. 35 mM) 0.004 (20 vs. 35 mM)	0.850	0.760
WT and C182S				
WT	17	63 ± 8	62.8 ± 16.5	0.004 ± 0.001
C182S	26	52 ± 11	79.4 ± 24.4	0.003 ± 0.001
***p* value**		< 0.001	0.011	0.028
WT and 181X				
WT	3	49 ± 3	45.5 ± 6.61	0.006 ± 0.001
181X	3	100 ± 0	25.5 ± 2.83	0.010 ± 0.001
***p* value**		< 0.001	0.007	0.060

Each value is the mean ± SD of ≥ 3 experiments (n, total number of cells analyzed); *p* values indicate differences by two-tailed Student's *t*-test in all cases, except for the treatment with MβCD, analyzed by one-way ANOVA ($\tau_{1/2}$ and *D*) or one-way ANOVA with Tukey's honest significant difference post-hoc test (MF).

5.2.5 A fraction of β2 co-localizes with lipid rafts

To support our finding that a fraction of β2 is indeed present in Lo membrane domains, we labeled polarized live cells with CTX, whose B subunit (CTB) binds to lipid raft-associated GM1 [158], detecting by subsequent incubation with an anti-CTB antibody. CTX labeling was seen most predominantly apical, with some lateral staining as well (Figure 32B); absence of labeling without CTX confirmed specificity of the antibody (Figure 32A). Interestingly, β2 overlapped considerably with CTX (Figure 32C). This was verified by calculation of their CTCF along *z*-stacks, showing maximum fluorescence peaks overlapping at the apical sections (Figure 32D). The Manders' coefficient, defined here as the fraction of β2 present in CTX-positive compartments, indicated an approx. 40% overlap at the apical region.

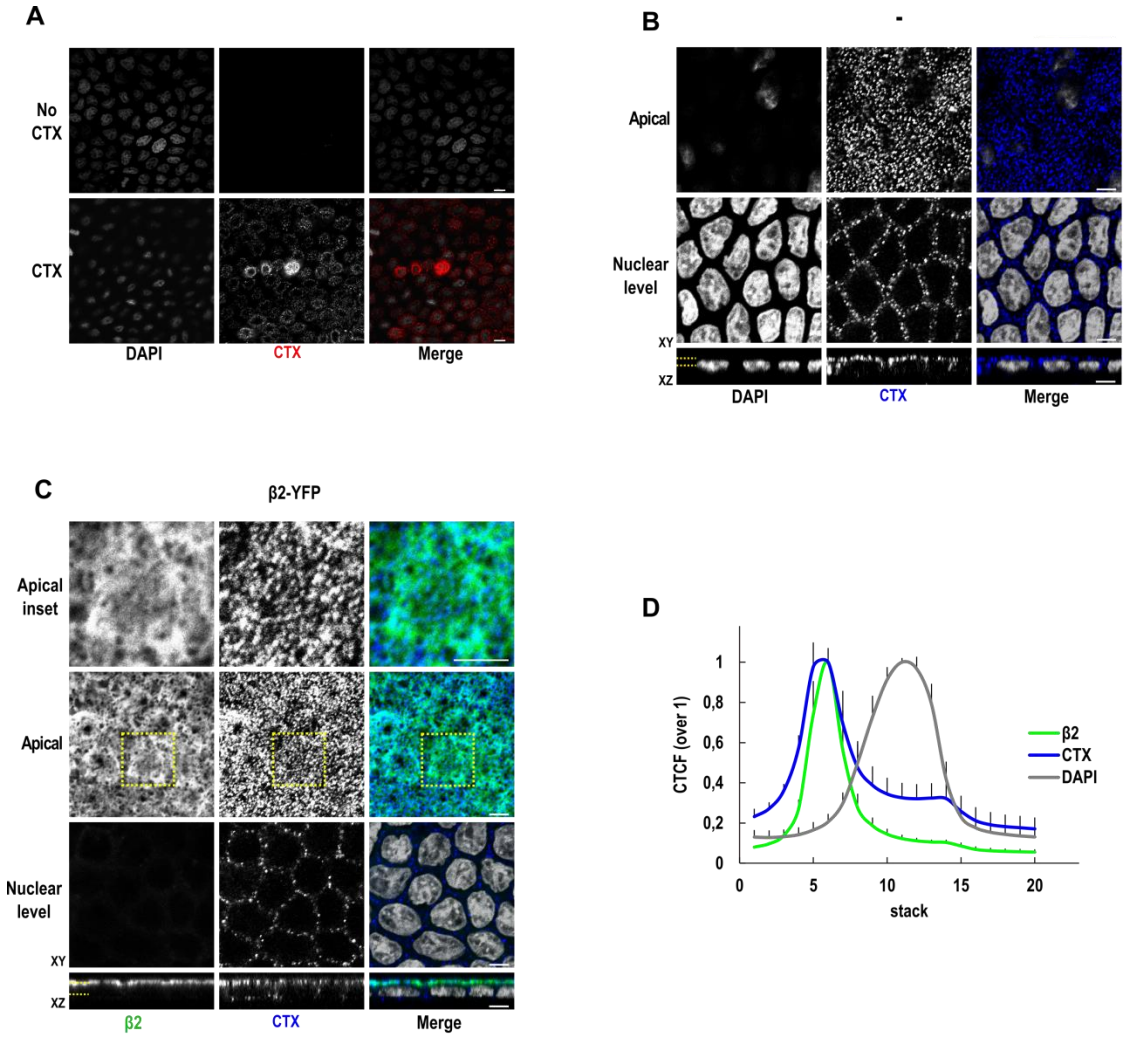

Figure 32. Partial overlap of β2 with CTX-labeled raft domains. MDCK cells, parental (A, B), or stably expressing β2-YFP WT (C), were grown polarized in Transwells. Live cells

were incubated with CTX for 10 min, and bound CTB was clustered with an anti-CTB antibody for 15 min. Cells were fixed and immunostained with an Alexa-conjugated secondary antibody (A, red; B and C, blue). Images were obtained by confocal microscopy. In merged images, the YFP-emitted fluorescence is in green and DAPI is in grey. Representative XY sections and corresponding *z*-axis reconstructions are shown (the yellow dashed square in XY indicates the inset in C, and the two parallel yellow dashed lines in XZ mark the section shown by XY, either apical or nuclear). (A) Nuclear view showing no labeling without CTX, ensuring specificity of the antibodies; note some heterogeneous labeling intensity among cells in the presence of CTX. (B) CTX labeling is most predominantly apical, although also present in the basolateral region. (C) Partial overlap of β2 with CTX is mainly at the apical domain (inset), with a Manders' coefficient of 0.41 ± 0.14 (mean ± SD; error bars; n = 8 images). Scale bars are 10 μm (A) and 5 μm (B, C). (D) Line chart displaying the CTCF (mean percentage ± SD; error bars) along an apical-to-basal *z*-stack (section 1: most apical; 0.5 μm optical slice thickness) shows the β2 curve peak coinciding with that of apical CTX, well above the nuclear level, as defined by DAPI (10 cells were analyzed).

Altogether, these data show that a fraction of β2 is associated with Lo membrane regions, which can be considered as lipid raft domains. Our results indicate that palmitoylation is contributing to the distribution of β2 within these membrane domains. Moreover, since a fraction of β2, i.e. palmitoylated β2, partitions into CTX-positive lipid rafts, our data suggest that palmitoylation contributes to establishing the apical localization of β2, and therefore its polarized distribution at the cell surface.

5.3 β2 promotes $Na_V1.5$ plasma membrane localization

It has been shown that the major function of β2 *in vivo* is to chaperone α subunits to the PM, both in the heart ventricle [176] and in neurons [97]. Moreover, previous evidence has shown that the BrS-associated mutant D211G causes a 40% decrease in I_{Na}; it was proposed that such defect was due to affected surface localization of $Na_V1.5$ [3]. Based on that work, we hypothesized that some β2 mutations may become pathogenic by negatively affecting PM localization of $Na_V1.5$. Here, we addressed the potential influence of β2 in the subcellular localization of $Na_V1.5$ in MCDK cells.

5.3.1 $Na_V1.5$ localizes to the ER in polarized MDCK cells

Transient transfection of *SCN5A* cDNA in MDCK cells turned into limited expression, often insufficient for biochemical or functional assays. Therefore, we stably expressed FLAG-tagged $Na_V1.5$. A three-dimensional (3D) reconstruction of *z*-stacks throughout the entire cell showed most of $Na_V1.5$ staining largely cytosolic, with very little, if any, co-labeling with the apical marker gp114 (Figure 33A). Likewise, it did not overlap with Na/K-ATPase (Figure 33B), indicating absence also in the basolateral surface. Surface protein biotinylation confirmed lack of $Na_V1.5$ at the PM, remaining undetected in pulldowns from apical and basolateral surface-labeled proteins, indicating that virtually all $Na_V1.5$ remains intracellular; Na/K-ATPase was blotted as a control for proper cell polarity, localizing exclusively at the basolateral membrane (Figure 33I).

The apparently vesicular pattern of $Na_V1.5$ did not overlap either with the EE marker EEA1 (Figure 33C) or with sorting nexin (SNX) 2, a subunit of the retromer complex (Figure 33D). The same applied to the TGN marker TGN46 (Figure 33E), altogether indicating absence in endosomes and at the endosome/Golgi boundary. It has been proposed that the ER may serve as a reservoir for cardiac Na_V [134]. Therefore, we probed potential overlap with the ER chaperone calnexin, whose pattern turned out to be comparable to that of $Na_V1.5$. Indeed, $Na_V1.5$ accumulated in enlarged calnexin-positive structures (arrowheads in Figure 33F), indicating that most of it also resides in the ER of MDCK cells. To get an approximation of the fraction of $Na_V1.5$ present in compartments positive for calnexin, we estimated their overlap in the *z*-axis by calculating the Manders' coefficient, which reached values of ~ 0.7 at the levels above the nucleus, indicating considerable presence of $Na_V1.5$ in the ER (Figure 33G and H).

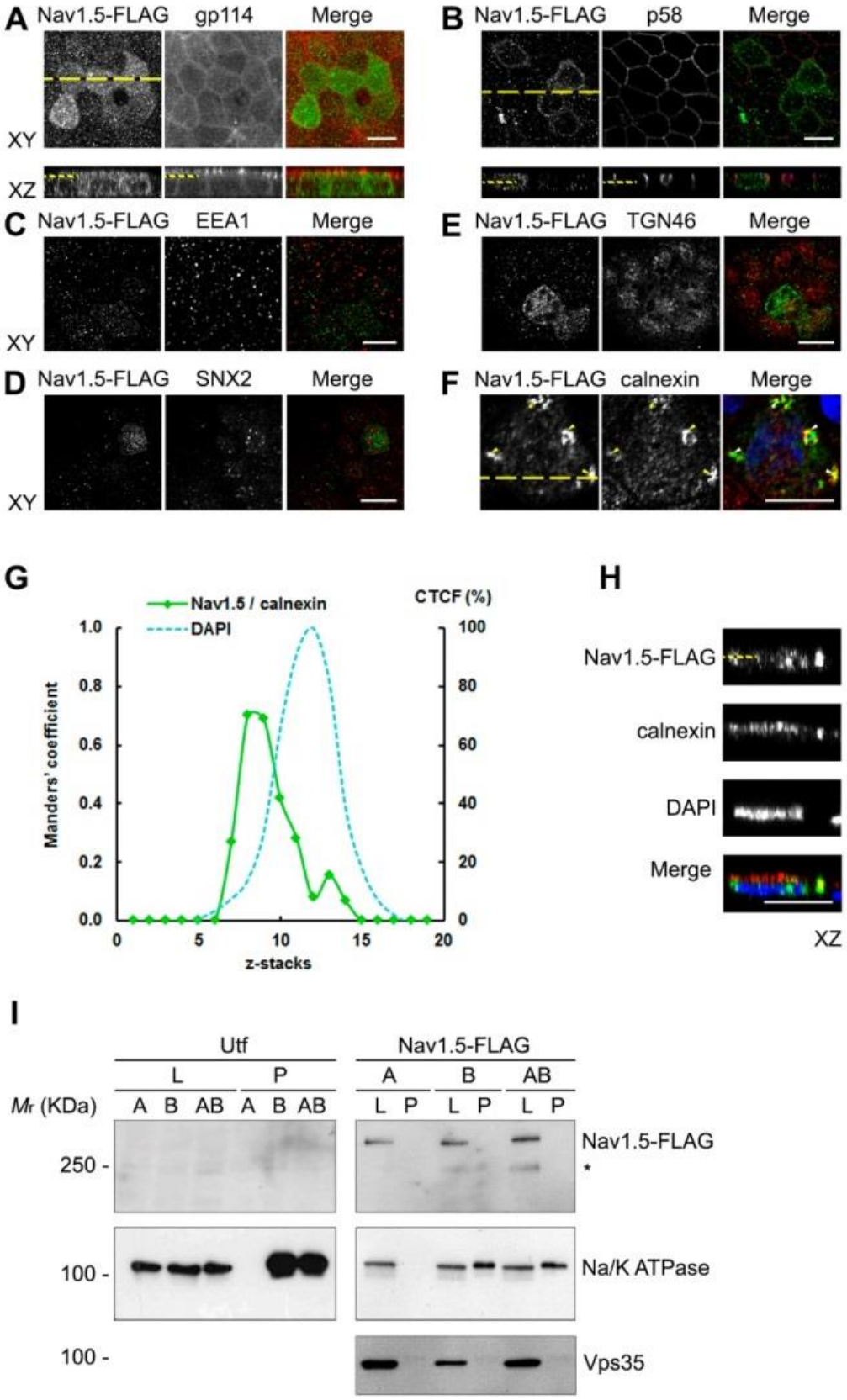

Figure 33. $Na_V1.5$-FLAG localizes to the endoplasmic reticulum in polarized MDCK

cells. MDCK cells stably expressing $Na_V1.5$-FLAG were grown polarized in Transwells, fixed and immunostained with a rabbit polyclonal antibody against $Na_V1.5$ (green) and for subcellular markers using mouse monoclonal antibodies (red) (A-E). Alternatively, $Na_V1.5$ was detected with the anti-FLAG M2 monoclonal antibody (green) and the ER marker calnexin with a rabbit polyclonal antibody (red; F). Images were obtained by confocal microscopy. Representative XY sections taken at the subapical (A) or nuclear (B) level, and z-axis reconstructions (reciprocal XZ and XY sections are marked by a yellow dashed line), show lack of $Na_V1.5$ overlap with apical gp114 (A) and basolateral Na/K-ATPase β subunit (p58, B). XY sections taken above the nucleus show that $Na_V1.5$ does not overlap with endosome/TGN markers EEA1 (C), SNX2 (D), or TGN46 (E). (F-H) Instead, $Na_V1.5$ often accumulates in enlarged calnexin-positive structures (arrowheads in F); sections were taken at the cell level where $Na_V1.5$ is mainly found in each case. (G) Line chart of a representative experiment with Manders' coefficients along apical-to-basal *z*-stacks (stack 1: most apical; 0.5 µm optical slice thickness) displaying the fraction of $Na_V1.5$ overlapping to compartments labeled with calnexin, which is maximum above the nuclear level, outlined with the CTCF of DAPI staining (in %). Experiments performed, n = 3 (7 cells analyzed). (H) XZ reconstruction displaying $Na_V1.5$/calnexin overlap above the nucleus (yellow dashed line) marks correspondence with the XY image shown in F. (Note that non-specific puncta in $Na_V1.5$-negative cells do not affect the conclusion from this figure.) Scale bars are 10 µm. (I) MDCK cells stably expressing $Na_V1.5$-FLAG and untransfected parental cells (Utf) were grown polarized in Transwells. Cells were biotinylated at 4ºC at the apical (A) or basolateral (B) surface, or simultaneously at both (AB). Representative western blots show absence of $Na_V1.5$ in biotin-NeutrAvidin pulldowns (P; ~ 200 µg protein) obtained from each surface domain, contrasting with basolateral enrichment of Na/K-ATPase over the lysate (L; 20 µg). Depending on expression levels, protein amount loaded, and solubilization conditions, two bands may show in the blot for $Na_V1.5$, the lower one marked with an asterisk. Evidence that the biotin reagent did not reach intracellular proteins is included by showing absence of endosomal Vps35 in pulldowns. Molecular weight markers are shown in kilodaltons (kDa). N ≥ 3 experiments performed.

5.3.2 $Na_V1.5$ interacts with β2

β2 interacts with $Na_V1.5$ in cardiac cells [177]. We also obtained evidence of specific β2/$Na_V1.5$ association in MDCK cells. To ensure functional significance, the interaction was analyzed in MDCK cells stably expressing β2-CFP in moderate levels, and maintaining cell morphology and polarity unaffected. Nonetheless, we transiently transfected these cells with considerable amounts of plasmid vector to allow $Na_V1.5$ detection even in cell lysates. Only then, β2 specifically co-immunoprecipitated with $Na_V1.5$. Evidence that the conditions were specific was provided by absence in immunoprecipitates of Vps35, not expected to associate with $Na_V1.5$ (Figure 34). Thus, we confirmed that $Na_V1.5$ and β2 can interact also in MDCK cells.

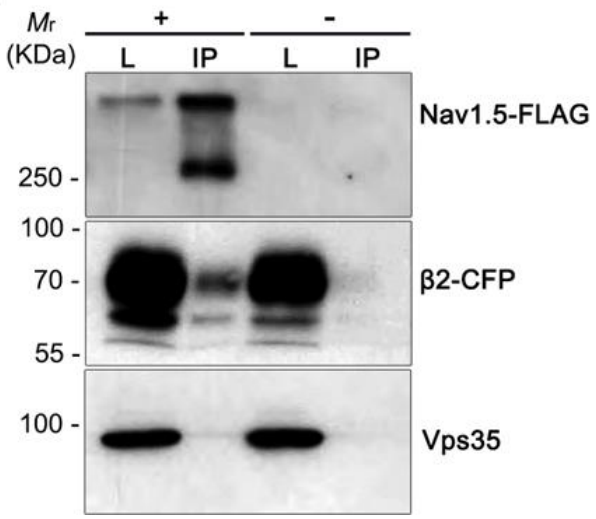

Figure 34. β2-CFP interacts with Na_V1.5-FLAG in MDCK cells. MDCK cells stably expressing β2-CFP were transiently transfected with the *SCN5A*-FLAG vector (+), or left untransfected (-), and grown until confluence on 35 mm wells. Cells were processed for Na_V1.5 immunoprecipitation (IP; ~ 200 µg protein) from cell lysates (L; 20 µg) with the anti-FLAG M2 antibody. Representative western blot shows that β2-CFP is only brought down in cells expressing Na_V1.5-FLAG. Depending on expression levels, protein amount loaded, and solubilization conditions, two bands may show in the blot for Na_V1.5. An overexposed blot against Vps35 shows that immunoprecipitates are sufficiently clean. Molecular weight markers are shown in kilodaltons (kDa). The experiment was performed a minimum of 3 times.

5.3.3 Localization of Na_V1.5 to the apical surface of MDCK cells is promoted by β2 WT but not by the BrS-associated mutant D211G

We have seen, by confocal microscopy and cell surface biotinylation that transiently transfected CFP-tagged β2 localizes to the apical surface in polarized MDCK cells (Figure 15). To ensure that the fluorescent protein tag is not influencing β2 localization, these experiments were also performed in cells expressing untagged β2, which – as expected – also localized apically (Figure 35 and Figure 36B).

As previously reported [178], we also found that the subcellular localization of Na_V1.5 in our model system poorly correlates with its expected presence at the CM sarcolemma; lack of cell surface localization hampers studying Na_V1.5 trafficking. We thus addressed whether β2 co-expression could promote surface localization of Na_V1.5.

Previous work in our laboratory has shown that the BrS-associated mutant β2 D211G causes a decrease of ~40% in the I_{Na} peak, proposed to be as a result of reduced surface $Na_V1.5$ localization [3]. Thus, we also analyzed by cell surface biotinylation and confocal microscopy the location of β2 D211G, which localized identically to the WT (Figures 35 and 36C).

In MDCK cells, while β2 is essentially at the apical surface, the major pool of $Na_V1.5$ is mostly intracellular, particularly in the ER. Yet, we tested their potential co-localization in polarized cells stably expressing YFP-tagged $Na_V1.5$ and transiently transfected with β2-CFP. Strikingly, upon β2 WT expression, $Na_V1.5$ also localized to the apical surface, thus patches of $Na_V1.5$, β2 and gp114 overlapped (Figure 36A). In addition, untagged β2 WT similarly brought $Na_V1.5$ to the apical surface, at least partially, indicating that the effect is not caused by the fluorescent tag (Figure 36B). In contrast, untagged β2 D211G did not modify the localization of $Na_V1.5$, which remained intracellular (Figures 36C).

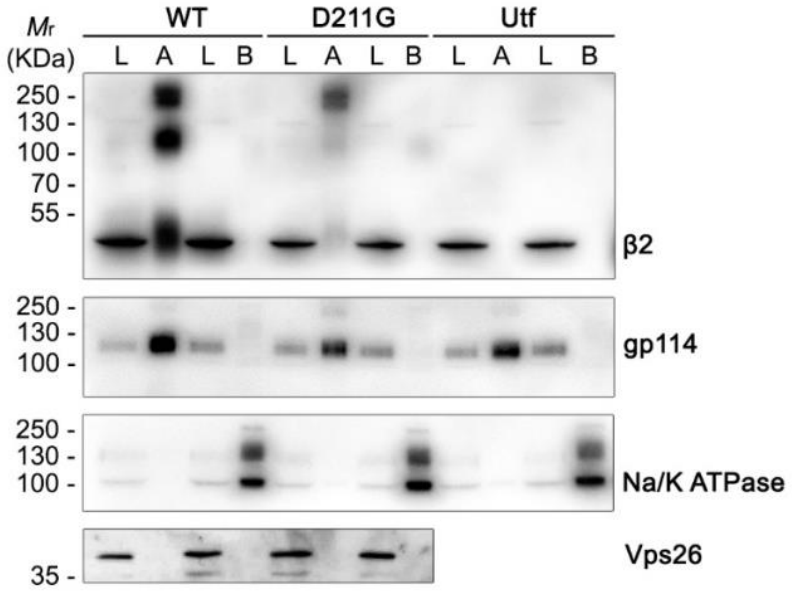

Figure 35. Untagged β2 WT and the BrS-associated D211G mutant are similarly localized to the MDCK apical surface. MDCK cells were transiently transfected with the *SCN2B* vector to express WT or D211G β2, or left untransfected (Utf), and grown polarized in Transwells. Cells were biotinylated at 4ºC at the apical (A) or basolateral (B) surface. Representative western blots (of experiments performed a minimum of 3 times) show apical localization of both WT and D211G β2. Na/K-ATPase and gp114 were blotted as markers for basolateral (B) and apical (A) localization, respectively. An overexposed blot against endosomal Vps26 provides evidence that the biotin reagent did not reach intracellular proteins, appearing only in lysates (L; 20 µg), and not in biotin-NeutrAvidin pulldowns (~ 200 µg protein). Molecular weight markers are shown in kilodaltons (kDa). Note that D211G β2 levels appear lower than WT β2 (including a likely oligomer running at high molecular weight). This phenomenon may be due to reduced immunoreactivity of the antibody used, which epitope encompasses this mutation. N ≥ 3 experiments performed.

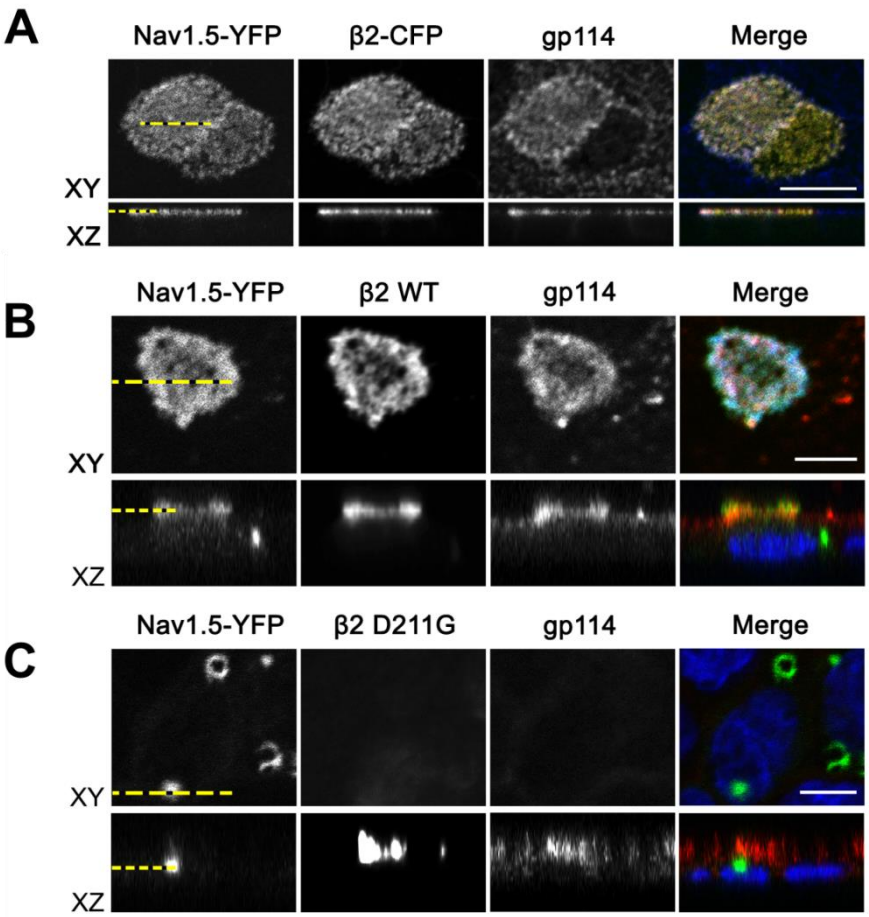

Figure 36. Apical localization of Na_V1.5-YFP with WT but not D211G β2. MDCK cells stably expressing Na_V1.5-YFP were transiently transfected with the vector to express β2-CFP (A) or with the bicistronic *SCN2B*:gfp vector, to express untagged WT (B) or D211G (C) β2, and grown polarized. Cells were fixed and immunostained with a rabbit polyclonal antibody against β2 (red), and for gp114, using a mouse monoclonal antibody. Images were obtained by confocal microscopy. Representative XY sections taken at the apical level (A, B), or right above the nucleus (C), and corresponding *z*-axis reconstruction (location of the XZ section marked by a yellow dashed line) show apical localization of Na_V1.5 only with β2 WT (A, B). Na_V1.5 is retained intracellularly with β2 D211G (C); all sections were taken at the cell level where Na_V1.5 is mainly found in each case. In the merged images, the YFP-emitted fluorescence is in green, DAPI is in dark blue (not shown in A) and gp114 is in cyan Images shown are representative of experiments performed a minimum of 3 times. Scale bars are 10 µm.

These data show that β2 WT shifts localization of stably expressed $Na_V1.5$ from the ER to the apical surface and that this effect is abolished by a single amino acid change in the ICD of β2. To exclude that apical delivery of transiently overexpressed WT β2 was not artificially affecting $Na_V1.5$ trafficking, we asked whether the reciprocal would also apply. We thus tested whether localization of transiently transfected $Na_V1.5$-FLAG could be modulated by stably expressed β2-YFP; this strategy allowed us to use moderate levels of β2. In parental cells, Manders' coefficient for $Na_V1.5$/gp114 always remained ≤ 0.1, indicating absence of $Na_V1.5$ at the apical PM. Although some points of overlap were apparent, Manders' coefficient for $Na_V1.5$/β2 WT was still ≤ 0.2 in β2 stable cells transiently expressing $Na_V1.5$. Nevertheless, $Na_V1.5$ labeling was consistently stronger in the most apical sections of *z*-axis reconstructions in the presence of β2 WT (Figure 37A), while it predominated toward the basal region or throughout the cell without β2 (Figure 37G).

To compare the MFI of $Na_V1.5$ with that of β2 and gp114 along the *z*-axis, we calculated their CTCF. At the peak for gp114, corresponding to the apical PM, the CTCF for $Na_V1.5$ was ~ ⅔ of its maximum fluorescence level in all sections (Figure 37G). On the contrary, in the presence of β2 the $Na_V1.5$ CTCF peak coincided completely with the peak for β2-YFP and gp114, which mark the apical surface (Figure 37H). To exclude the potential influence of the YFP tag in β2, the assay was performed in cells stably expressing untagged β2, co-expressed with GFP in a bicistronic vector to allow visualization of the β2-expressing cells. Similarly, $Na_V1.5$ and gp114 CTCF peaks coincided (Figure 37C). Therefore, the presence of β2 caused a shift of the CTCF peak for $Na_V1.5$ to the apical surface.

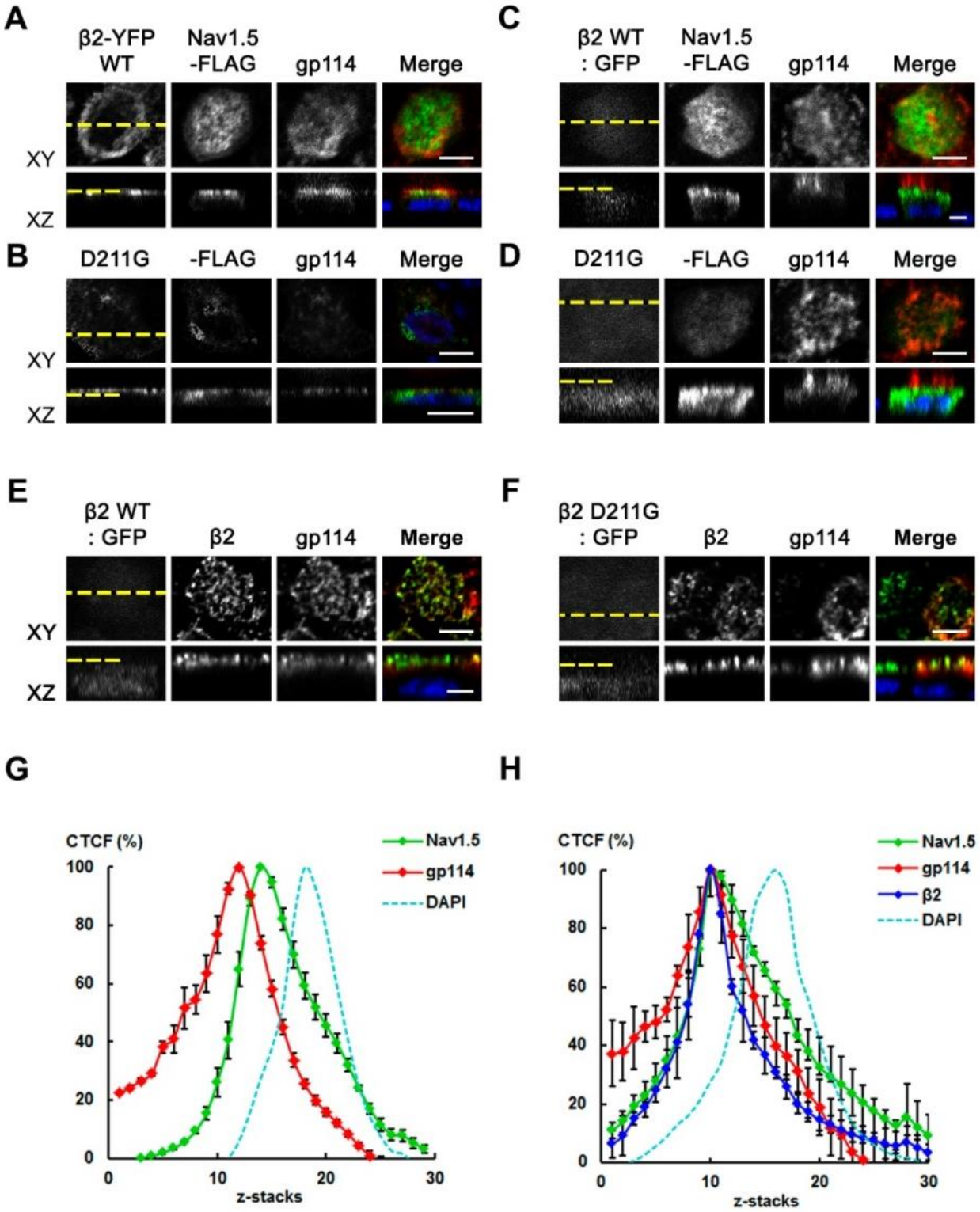

Figure 37. Increase of $Na_V1.5$-FLAG at the apical surface with WT but not D211G β2. MDCK cells stably expressing WT (A) or D211G (B) β2-YFP were transiently transfected with the *SCN5A*-FLAG vector and grown polarized in Transwells. Cells were fixed and immunostained with a rabbit polyclonal antibody against the corresponding β subunit, and

for gp114, using a mouse monoclonal antibody. In the merged images, $Na_V1.5$-FLAG is in green, gp114 in red, and DAPI in blue. Images were obtained by confocal microscopy. Representative XY sections taken at the apical level (A), or right above the nucleus (B), and *z*-axis reconstructions (reciprocal XZ and XY sections are marked by a yellow dashed line), show presence of $Na_V1.5$ at the apical surface well manifested only with β2 WT, appearing more widely distributed throughout the cytoplasm with β2 D211G (B). MDCK cells stably expressing untagged WT (C) or D211G (D) β2, co-expressed with GFP in a bicistronic vector, were transiently transfected with the *SCN5A*-FLAG vector and processed as above. Similarly, $Na_V1.5$ (green) appears more diffusely distributed in the cytoplasm with β2 D211G (D). Both untagged WT (E) and D211G (F) β2 (green) are localized apical, along with gp114 (red); all sections were taken at the cell level where $Na_V1.5$ is mainly found in each case. The nuclei are stained with DAPI (blue). YFP or GFP-derived fluorescence is shown in the grey channel only. Scale bars are 5 μm except in B, 10 μm. (G, H) Line charts of the CTCF (mean percentage ± SEM) along apical-to-basal *z*-stacks (stack 1: most apical; 0.5 μm optical slice thickness) show the $Na_V1.5$ curve (65.0 ± 5.9% at gp114 peak) mostly within intracellular stacks compared to the gp114 peak that marks the apical surface (G). This contrasts with displacement of $Na_V1.5$ (99.4 ± 1.1% at gp114 peak) to the apical surface in the presence of β2-YFP, converging with both gp114 and β2 (H, p = 0.02, comparing $Na_V1.5$ with and without β2-YFP; n = 5 cells). Similar values were obtained for cells expressing $Na_V1.5$ and untagged β2 (Nav1.5 CTCF was 91.4 ± 7.9% at gp114 peak, n = 3 cells). The curve for DAPI is shown as reference of nuclear/basal cell sections. Images shown are representative of a minimum of three experiments performed, and similar results were obtained.

Since the resolution achieved by confocal microscopy does not allow to ensure that $Na_V1.5$ is effectively inserted at the apical surface with β2 WT, we performed surface biotinylation of $Na_V1.5$-YFP expressing cells in subconfluence, i.e. when these appear to have a widespread $Na_V1.5$ expression. These cells allowed us to estimate more accurately the level of defect caused by D211G β2 in the cell extract. Indeed, $Na_V1.5$-YFP could be detected in pulldowns by cell surface biotinylation of cells transfected with β2-YFP WT (Figure 38A). Band quantitation showed ~ two-fold more $Na_V1.5$ amount in pulldowns of cells with WT β2-YFP compared to those of untransfected cells, or with D211G β2-YFP. A similar effect was found in cells transiently expressing untagged β2 WT in comparison to β2 D211G (Figure 38B).

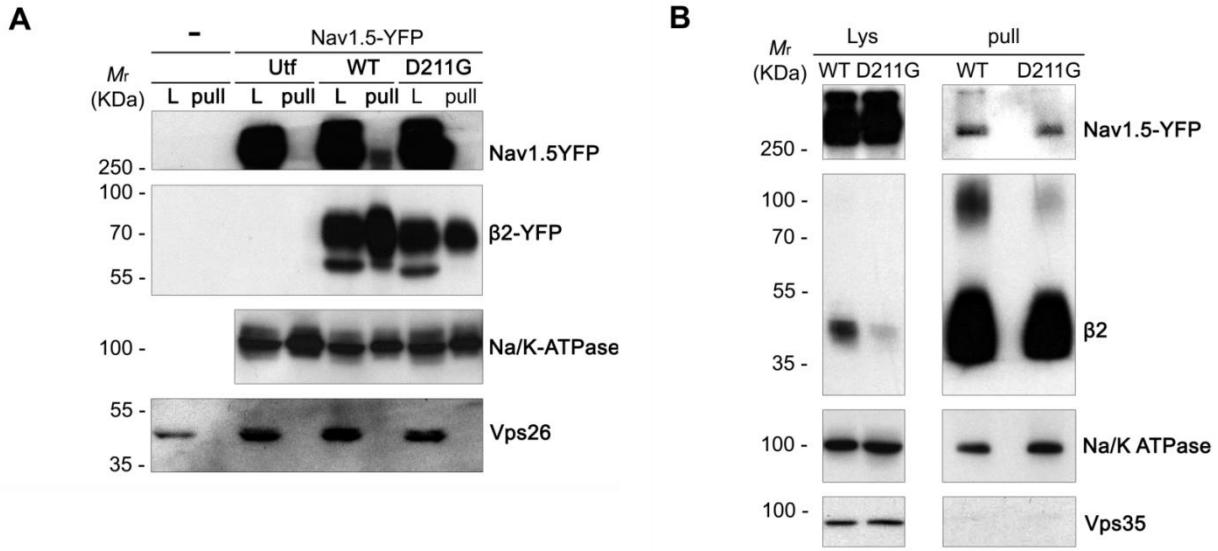

Figure 38. Biochemical detection of $Na_V1.5$-YFP at the cell surface with WT but not D211G β2. (A) MDCK cells stably expressing $Na_V1.5$-YFP were transiently transfected with the *SCN2B-yfp* vector to express WT or D211G β2-YFP, or left untransfected (Utf), and grown for 1 day in 35 mm wells. Cells were surface biotinylated at 4ºC. Representative western blots (of experiments performed 5 times) show the presence of $Na_V1.5$-YFP essentially in biotin-NeutrAvidin pulldowns from cells expressing WT β2; parental MDCK cells (-) are included to indicate that the bands shown correspond to the transfected subunits. Band quantitation indicated x 1.9 ± 0.2 (mean ± SEM; n=5) increase in PM $Na_V1.5$. (B) MDCK cells stably expressing $Na_V1.5$-YFP were transiently transfected with the bicistronic *SCN2B*:gfp vector to express WT or D211G β2, grown and processed as above. While detected with either WT or D211G β2, $Na_V1.5$-YFP levels in pulldowns are higher in the presence of WT β2. Na/K-ATPase was blotted as surface marker. Evidence that the biotin reagent did not reach intracellular proteins is included by showing that endosomal Vps26 and Vps35 (clearly visible in lysates; L or Lys, 20 µg) remain undetected in pulldowns (pull; ~ 200 µg protein). Molecular weight markers are shown in kilodaltons (kDa). Division lines separate different parts of the same blot conveniently put together for clear display.

5.3.4 Unglycosylated β2 is defective in promoting surface localization of $Na_V1.5$

Given the importance of glycosylation in β2 trafficking to the PM, we hypothesized that it could also be implicated in its effect on the α subunit. Thus, we tested whether unglycosylated β2 was defective in promoting surface localization of $Na_V1.5$ in MDCK cells. To this end, we used stably expressing WT or unglycosylated β2-YFP cells transiently transfected with $Na_V1.5$-FLAG. A fraction of $Na_V1.5$ co-localized with β2 and the apical marker gp114 (Figure 39A). Even though some $Na_V1.5$ staining could be seen throughout the cell, calculation of the CTCF along *z*-stacks showed its maximum fluorescence peak nearly overlapping with those of gp114 and β2, corresponding to the apical PM (Figure 39C). However, in the presence of unglycosylated β2, $Na_V1.5$ distribution was broader, mostly abounding at the nuclear level and right above the nucleus (Figure 39B and D). Moreover, a large portion of $Na_V1.5$ co-localized with intracellular accumulations of mutated β2 (arrowhead in Figure 39B).

We also biotinylated surface proteins to detect $Na_V1.5$ in pulldowns, whose levels were visibly reduced in cells expressing fully unglycosylated β2 (Figure 39E and F), supporting the data obtained by immunofluorescence.

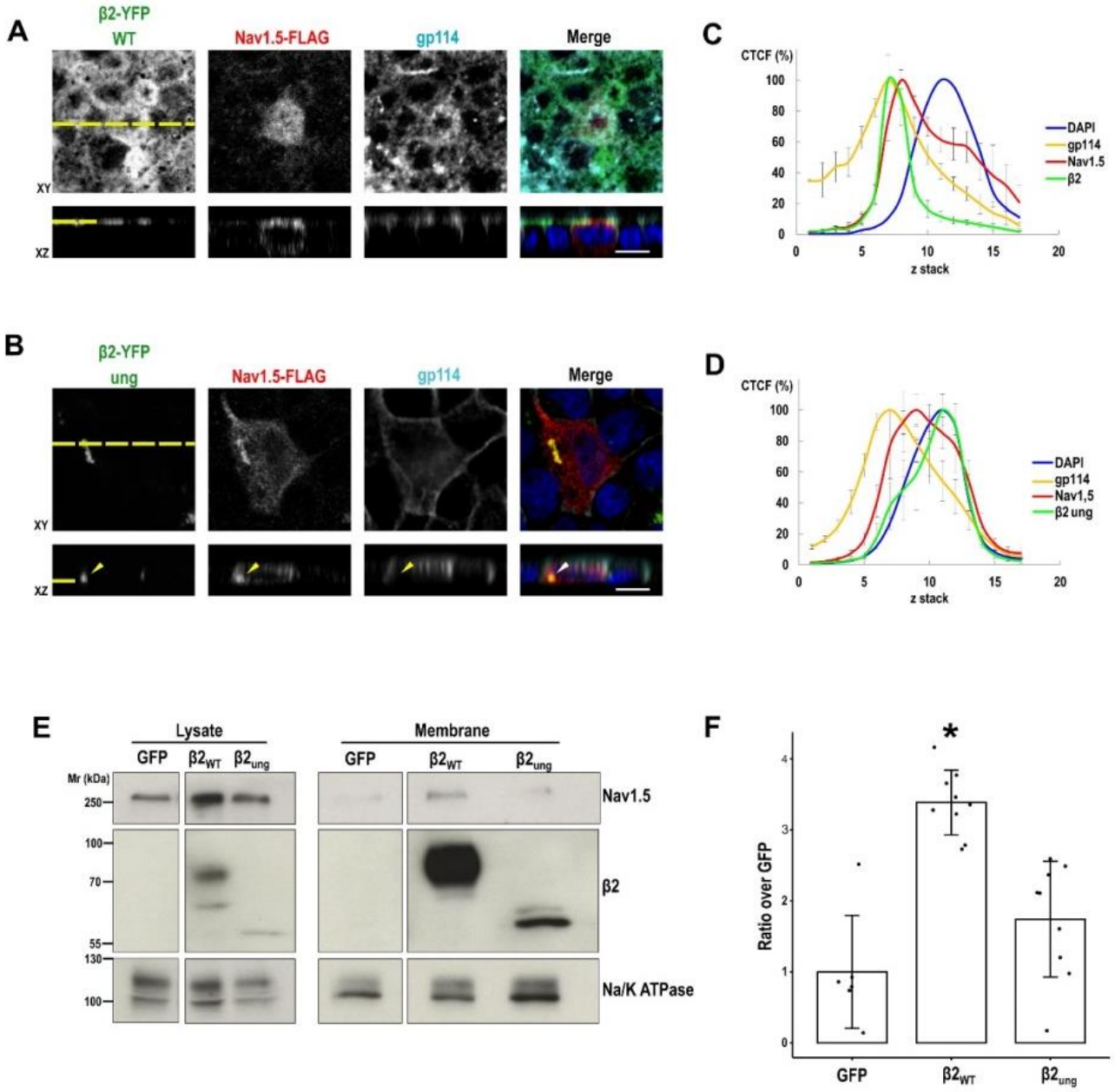

Figure 39. Surface localization of $Na_V1.5$ is reduced with unglycosylated β2. (A, B) MDCK cells stably expressing WT or fully unglycosylated (ung) β2-YFP were transiently transfected with the vector *SCN5A*-FLAG and grown polarized in Transwells. Cells were fixed and immunostained with a rabbit polyclonal antibody against $Na_V1.5$ (red), and with a mouse monoclonal antibody to gp114 (cyan). Images were obtained by confocal microscopy. In merged images, the YFP-emitted fluorescence is in green and DAPI is in blue. Representative XY sections taken at the apical (A), or nuclear (B) levels (sections taken at the cell level where $Na_V1.5$ is mainly found in each case), and corresponding *z*-axis reconstruction (reciprocal XZ and XY sections are marked by a yellow dashed line), show improved apical localization of $Na_V1.5$ with β2 WT (A), whereas $Na_V1.5$ remains mostly intracellular in the presence of unglycosylated β2 (B); note the intracellular $Na_V1.5$

accumulation with mutated β2 (arrowhead). Scale bars are 10 μm. (C, D) Line charts displaying the CTCF (mean percentage ± SD) along an apical-to-basal *z*-stack (section 1: most apical; 0.5 μm optical slice thickness) show the $Na_V1.5$ curve peak nearly overlapping with those of apical gp114 and β2 WT (C). In contrast, $Na_V1.5$ is displaced toward nuclear sections with mutated β2, which overlays with DAPI (D), included as reference for the nuclear level (≥ 6 cells were analyzed per condition). (E) MDCK cells stably expressing $Na_V1.5$-YFP were transiently cotransfected with the *SCN2B-yfp* vector to express β2, WT or fully unglycosylated (ung), plus additional *SCN5A*-FLAG vector to ensure extensive $Na_V1.5$ overexpression, and grown o/n in wells; the pEGFP-N1 vector was used as a control. Cells were surface biotinylated at 4ºC. The same amount of protein was used to process each lysate (~ 600 μg), 97% of which was subjected to overnight NeutrAvidin pulldown. Representative western blots and (F) band quantitation show reduced levels of $Na_V1.5$ in biotin-NeutrAvidin pulldowns (Membrane) in the presence of unglycosylated β2, or without β2 (GFP), when comparing with the WT. One-way ANOVA with Tukey's HSD post hoc test showed significant differences (*, $p < 0.002$). The percentage of $Na_V1.5$ at the cell surface over total cellular $Na_V1.5$ protein varied from 1.42 ± 0.98 in the WT to 0.73 ± 0.50% with unglycosylated β2. Data are mean ± SD (n ≥ 6). Na/K-ATPase was blotted as surface marker to correct for quantitations in pulldowns. Molecular weight markers are in kilodaltons (kDa). For clear display, the blot in E shows lysates and pulldowns separated by division lines, indicating different exposure between lysates and pulldowns but equal exposure within each group.

We then asked whether this deficiency in β2 function persisted over time. Thus, we first analyzed the effect of β2 on promoting $Na_V1.5$ arrival to the surface early from transfection. To this end, we performed the analysis in cells growing non-polarized in wells. Here, we took advantage of our approach to quantify relative fluorescence levels, i.e., MFI, along a segment drawn from the cell end perpendicularly into the cytoplasm; by means of confocal microscopy, the cell end taken is a close approximation of the PM region. As expected, localization of $Na_V1.5$ to the PM was not promoted by unglycosylated β2 throughout time, and the bulk of $Na_V1.5$ label remained intracellular (Figure 40C and D), similarly as in cells not expressing β2 (Figure 40E and F). In contrast, the MFI of $Na_V1.5$ was concentrated at the cell end in the presence of β2 WT, also in parallel with Na/K-ATPase, especially at day 1, displaying a more widespread distribution at days 2 and 3 (Figure 40A and B); a general defect in promoting surface localization of $Na_V1.5$ at late time points was also verified by cell surface biotinylation, by which all β2 variants were ineffective, including the WT (Figure 41).

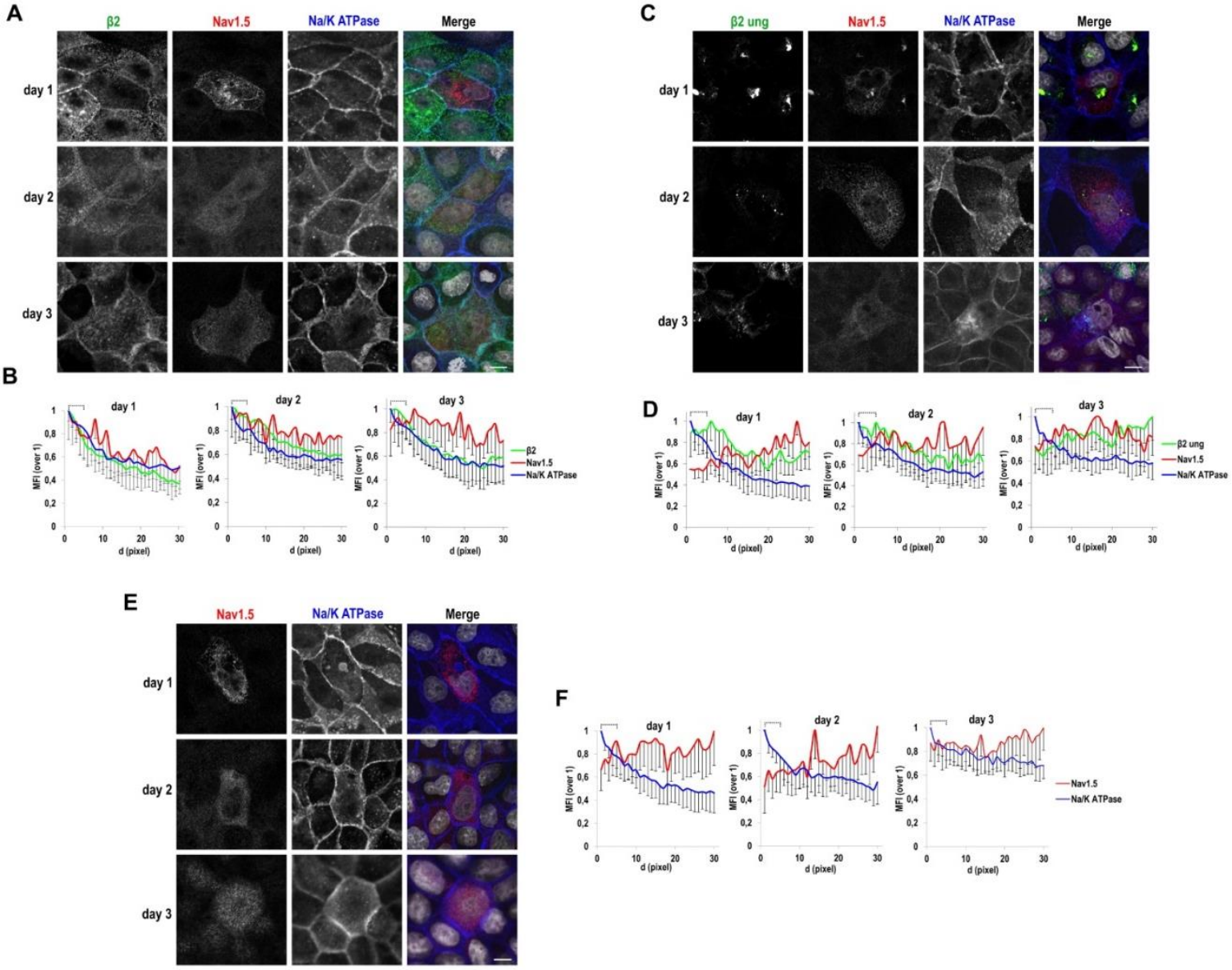

Figure 40. Defect over time of unglycosylated β2 in promoting surface localization of $Na_V1.5$. MDCK cells stably expressing WT (A), fully unglycosylated (ung) β2-YFP (C), or untransfected (parental) cells (E), were transiently transfected with the vector *SCN5A*-FLAG and grown in wells for the indicated number of days. Cells were fixed and immunostained with a rabbit polyclonal antibody against $Na_V1.5$ (red), and with a mouse monoclonal antibody to Na/K-ATPase (blue). Images were obtained by confocal microscopy. In merged images, the YFP-emitted fluorescence is in green and DAPI in grey. (A, C, E) Representative XY sections (sections taken at the cell level where $Na_V1.5$ is mainly found in each case) show a general diffuse $Na_V1.5$ pattern, intracellular and often perinuclear, except for a noticeable overlap with PM Na/K-ATPase, particularly at day 1, seen only in the presence of β2 WT. Scale bars are 10 µm. Confocal images were analyzed by calculating the MFI along linear segments of 30 pixels in length (d, distance; 0.1 µm/pixel) drawn from the cell end perpendicularly into the cytoplasm. (B, D, F) Line charts show MFIs with the first 5 pixels of the segments, equivalent to the PM region (cell

end), marked with a square bracket. The highest MFI levels are at the cell end for Na/K-ATPase and for β2 WT, which progressively decrease intracellularly. The profile for $Na_V1.5$ reaches its maximum at the cell end only in the presence of β2 WT, and especially at day 1 (B), but remains low within this region with unglycosylated β2 (D) or in the absence of β2 (F). Data are mean ± SD (number of cells analyzed ≥ 3; 4 segments / cell).

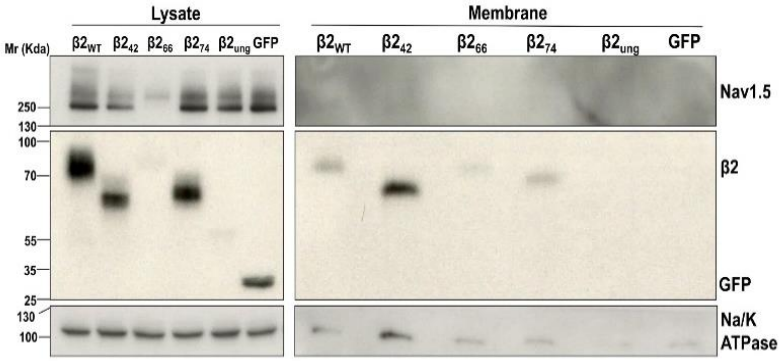

Figure 41. All β2 variants are defective at later time points in promoting surface localization of $Na_V1.5$. MDCK cells stably expressing $Na_V1.5$-YFP were transiently cotransfected with the *SCN2B-yfp* vector to express β2, WT, single or fully unglycosylated (ung), as indicated, plus additional *SCN5A*-FLAG vector to ensure extensive $Na_V1.5$ overexpression, and grown for 3 days in wells; the pEGFP-N1 vector was used as a control. Cells were surface biotinylated at 4ºC. The same amount of protein was used to process each lysate (~ 600 µg), 97% of which was subjected to overnight NeutrAvidin pulldown. Representative western blots show absence of $Na_V1.5$ in biotin-NeutrAvidin pulldowns (Membrane) in the presence of any variant of β2. Na/K-ATPase is included as loading control. Molecular weight markers are in kilodaltons (kDa). For clear display, blots are separated by division lines, indicating different exposure between lysates and pulldowns.

We have shown that a single glycosylation in β2 is sufficient for its proper surface localization (see Figures 18 and 19). Now, we asked whether incomplete glycosylation would affect β2 in promoting surface localization of $Na_V1.5$. Interestingly, partial loss of glycosylation still allowed a positive effect, namely, only fully unglycosylated β2 is clearly defective in promoting surface localization of $Na_V1.5$. Thus, we found that single β2 mutants maintain effectiveness at day 1 from transfection (Figure 42), which we also verified by cell surface biotinylation (Figure 43 G-H). By biochemical means, we also observed a comparable behavior in double mutants, appearing similarly effective as the WT in promoting surface localization of $Na_V1.5$ (Figure 43I-J). Moreover, single mutants were also effective

to promote apical localization of $Na_V1.5$ in cells growing polarized in Transwells, (Figure 43A-F; compare with Figure 39A-D).

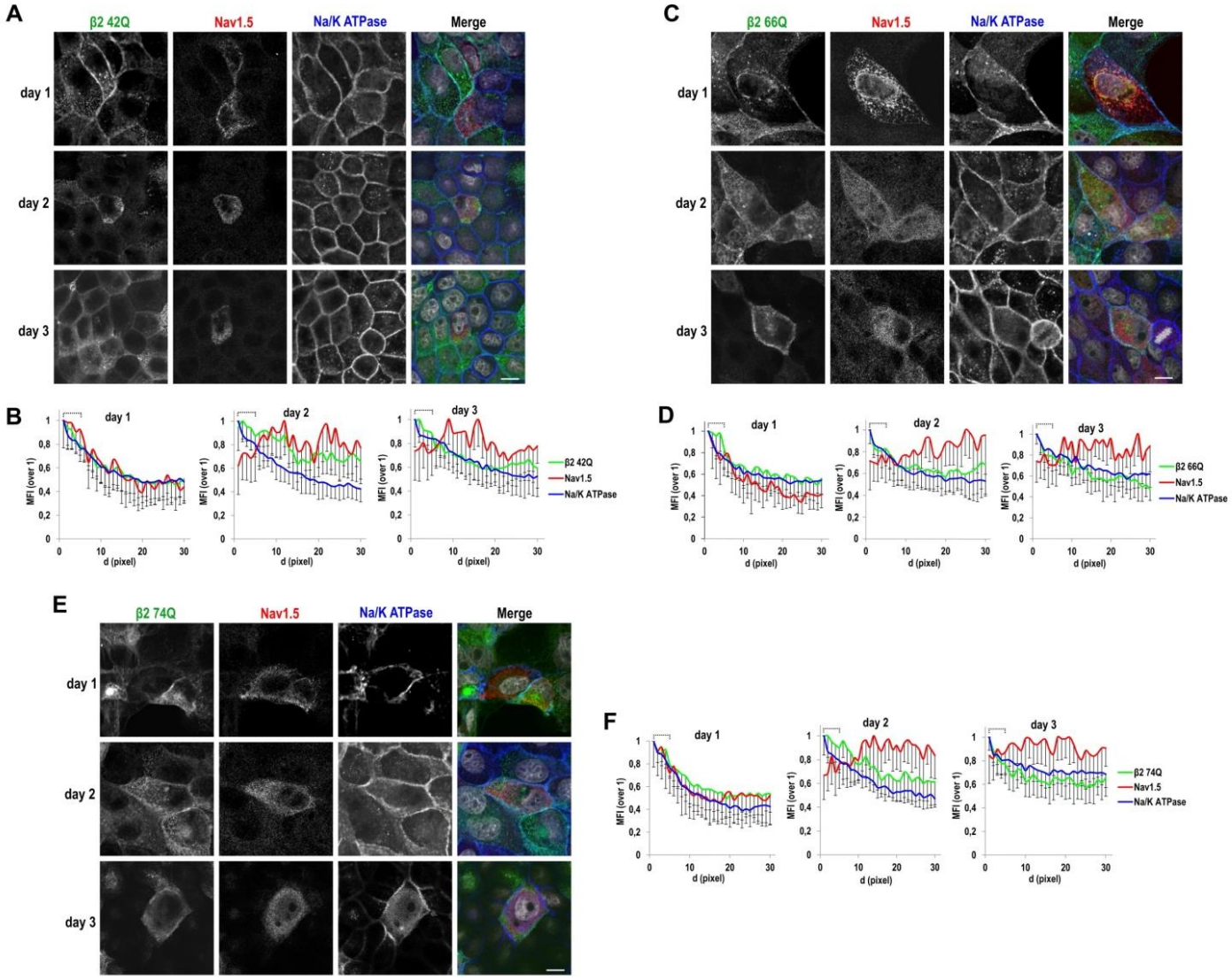

Figure 42. Single β2 glycosylation mutants can promote surface localization of $Na_V1.5$ – analysis over time. MDCK cells stably expressing the indicated single mutants for β2-YFP glycosylation were transiently transfected with the vector *SCN5A*-FLAG and grown in wells for the specified number of days. Cells were fixed and immunostained with a rabbit polyclonal antibody against $Na_V1.5$ (red), and with a mouse monoclonal antibody to Na/K-ATPase (blue). Images were obtained by confocal microscopy. In merged images, the YFP-emitted fluorescence is in green and DAPI in grey. (A, C, E) Representative XY sections (taken at the level where $Na_V1.5$ is mainly found in each case) show some areas

of overlap of $Na_V1.5$ with Na/K-ATPase at the cell end, particularly at day 1, in the presence of any of the mutants, while remaining mostly disperse throughout the cells at later time points. Scale bars are 10 μm. Confocal images were analyzed by calculating the MFI along linear segments of 30 pixels in length (d, distance; 0.1 μm/pixel) drawn from the cell end perpendicularly into the cytoplasm. (B, D, F) Line charts show MFIs with the first 5 pixels of the segments, equivalent to the PM region (cell end), marked with a square bracket. The highest MFI levels are at the cell end for Na/K-ATPase and for the different β2 single mutants, all of them progressively decreasing intracellularly. The profile for $Na_V1.5$ increases at the cell end at day 1 in all cases, remaining low within this region at later time points. Data are mean ± SD (number of cells analyzed ≥ 3; 4 segments / cell).

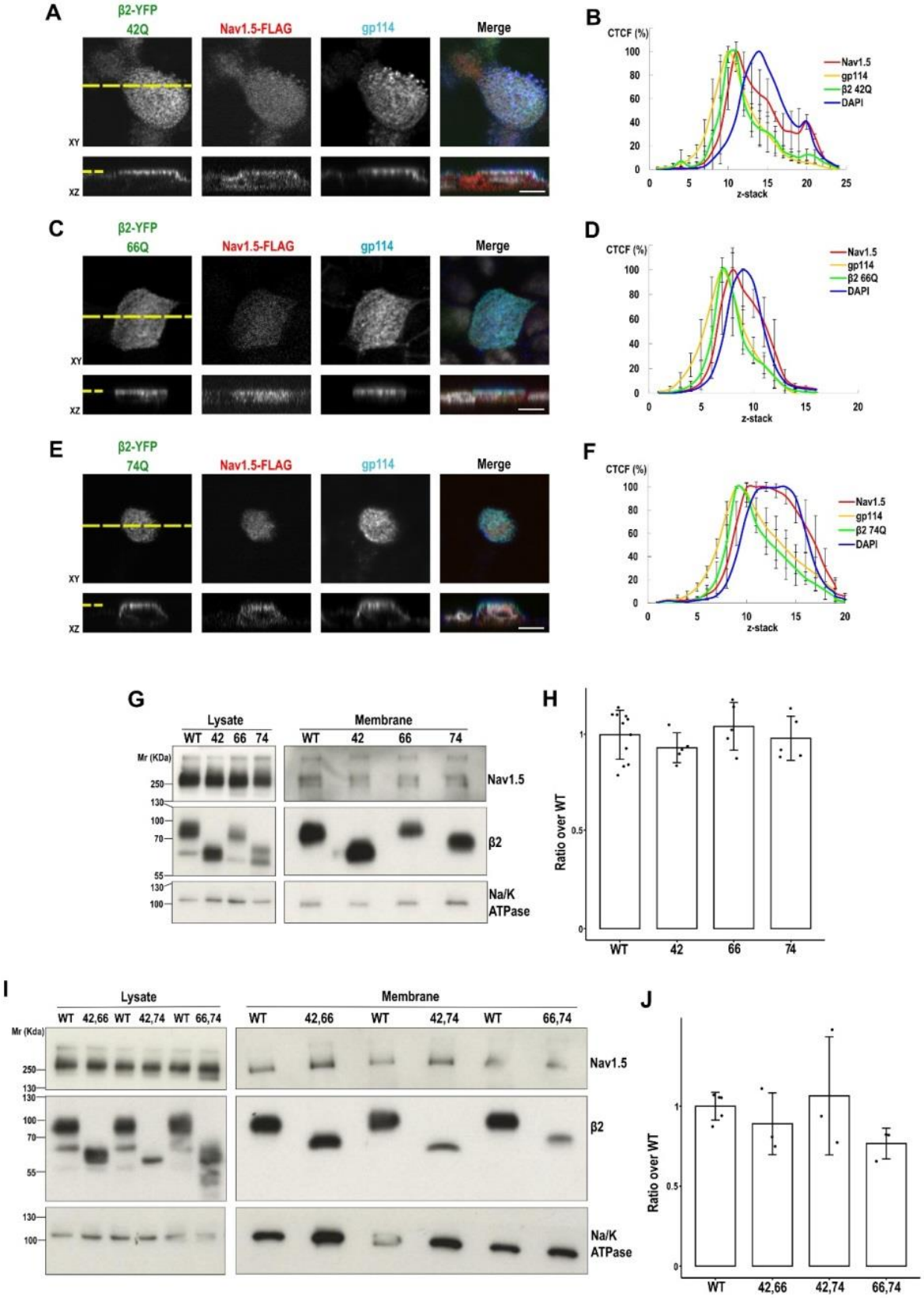

Figure 43. Single and double glycosylation mutants of β2 can promote surface localization of $Na_V1.5$. MDCK cells (A, C, E) stably expressing the indicated single

mutants for β2-YFP glycosylation were transiently transfected with the vector *SCN5A*-FLAG and grown polarized in Transwells. Cells were fixed and immunostained with a rabbit polyclonal antibody against $Na_V1.5$ (red), and with a mouse monoclonal antibody to gp114 (cyan). Images were obtained by confocal microscopy. In merged images, the YFP-emitted fluorescence is in green and DAPI in gray. Representative XY sections taken at the apical level (section level chosen to assess the presence of $Na_V1.5$ at the apical surface), and corresponding *z*-axis reconstruction (reciprocal XZ and XY sections are marked by a yellow dashed line), show noticeable apical localization of $Na_V1.5$ with the different β2 variants. Scale bars are 10 µm. (B, D, F) Line charts displaying the CTCF (mean percentage ± SD) along an apical-to-basal *z*-stack (section 1: most apical; 0.5 µm optical slice thickness) show the $Na_V1.5$ curve peak in close proximity to those of apical gp114 and any of the β2 mutants. DAPI is included as reference for the nuclear level (≥ 6 cells were analyzed per condition). (G, I) MDCK cells stably expressing $Na_V1.5$-YFP were transiently cotransfected with the *SCN2B*-yfp vector to express β2-YFP, WT or any of the indicated single (G) or double (I) mutants, plus additional *SCN5A*-FLAG vector to ensure extensive $Na_V1.5$ overexpression, and grown o/n in wells. Cells were surface biotinylated at 4ºC. The same amount of protein was used to process each lysate (~ 600 µg), 97% of which was subjected to overnight NeutrAvidin pulldown. (G, I) Representative western blots and (H, J) band quantitation show comparable levels of $Na_V1.5$ in biotin-NeutrAvidin pulldowns (Membrane) in the presence of all mutant variants of β2 as with the WT. Data are mean ± SD (n ≥ 3). Na/K-ATPase was blotted as surface marker to correct for quantitations in pulldowns. Molecular weight markers are in kilodaltons (kDa). For clear display, the blots in G and I show lysates and pulldowns separated by division lines, indicating different exposure between lysates and pulldowns.

Overall, these data indicate that β2 increases $Na_V1.5$ localization to the apical surface in polarized MDCK cells, even though co-localization between these proteins throughout the cell remains low. Lack of glycosylation and the D211G mutation in β2 abolish this effect on $Na_V1.5$.

6.DISCUSSION

6. Discussion

In this work, we have extensively explored the biology of the Na_V β2 subunit and how its topology and PTMs regulate its intracellular trafficking, localization and membrane dynamics. Most importantly, we have assessed the effect of β2 on $Na_V1.5$ subcellular localization, to date, the main function of β2, with reported physiological consequences when affected [3,139].

We planned the present research project with the rationale that β2 architecture and biochemical properties define its behavior in the context of the cell. After careful analysis of its amino acid sequence, several features stand out: two intramolecular disulfide bonds, two putative phosphorylation sites, a free cysteine to link with the alpha subunit on the extracellular face, a free cysteine in the cytosolic face that may be palmitoylated and, most prominently, glycosylation [129]. Representing over a third of the relative molecular weight of β2, glycosylation promised to be very influential in its trafficking and thus became the early focus of our research.

6.1 Glycosylation in β2 trafficking

We have assessed the role of *N*-glycosylation in regulating β2 trafficking to the PM. We show that β2 is *N*-glycosylated at residues 42, 66 and 74; remarkably, it is only sialylated at Asn-42. β2 *N*-glycosylation is required for efficient trafficking to the PM, but interestingly, the fully unglycosylated mutant can still reach the cell surface by bypassing the Golgi compartment albeit at a rate of one third to that of the WT.

A minor portion of unglycosylated β2, estimated to be less than 10%, was detected at the cell surface, in comparison with 25-30% of the WT. This rate of reduction was similar when analyzing specifically at the apical domain of polarized cells. No mistargeting to the basolateral domain was detected, implying that the polarized distribution of β2 in MDCK cells is not dependent on its glycosylation state. This agrees with the general tendency of apical trafficking to rely on less apparent lipid-based sorting mechanisms [25]. Nonetheless, the bulk of unglycosylated β2 remained stuck in enlarged ER structures. This is indicative of a trafficking problem rather than a problem of settling (localizing) β2 at the PM. This would explain why cells transiently transfected with unglycosylated β2, either still non-polarized or once polarized in Transwells, maintain throughout time a stable albeit comparatively small amount of unglycosylated protein at the PM.

Curiously, despite the dramatic phenotype of the fully unglycosylated mutant, preservation of a single glycosylation site, no matter which one, was sufficient to maintain normal β2 localization. In fact, all combinations of mutants, either single or double mutants, displayed comparable subcellular localization. Even the versions including the mutation N42Q, which removes the only sialylated *N*-glycan of the protein, behaved indistinguishably from the WT.

Given that β2 glycosylation is exclusively found on its Ig-like loop, and the fact that just a fraction of its original glycosylation is actually required for its efficient localization, we propose that β2 glycosylation plays additional roles, unrelated to its biosynthesis and trafficking. Such alternative roles could be related to binding to lectins and to other elements of the extracellular matrix, protection of β2 and the α subunit from proteases, and regulation of the α subunit biophysical properties. For instance, in sialylation-deficient cells, β2 failed to modulate the gating properties of $Na_V1.5$ [92]. In the case of the related β1 subunit, total lack of sialylation abolished any gating effects on $Na_V1.2$, $Na_V1.5$ and $Na_V1.7$ [91].

Despite the importance of *N*-glycans for β2 arrival to the PM, by blocking ER-to-Golgi transport with the fungal drug BFA, we showed that even immature WT β2, i.e. lacking complex *N*-glycosylation (that takes place in the Golgi), could be detected at the cell surface. Based on this observation, the most likely explanation for the small fraction of unglycosylated (triply-mutated) β2 that is detected at the cell surface is that it can bypass the Golgi apparatus. In the case of the α subunit, there is evidence that immature $Na_V1.5$ can also follow this Golgi-independent, secretory pathway. The role of this alternative anterograde pathway is not clear for $Na_V1.5$, but a potential advantage would be preventing and relieving of ER stress [179]. In fact, it has been shown that a fraction of $Na_V1.5$ remains sensitive to Endo H and associates with Kir2.1 early in their biosynthetic pathway [180]. In this regard, it has been hypothesized that $Na_V1.5$ mutants associated with BrS and retained in the ER may still be delivered to the PM via an unconventional pathway [181]. For clinically relevant $Na_V1.5$ mutants, this mechanism may thus potentially allow a reciprocal regulation with other channels, or with associated subunits, for their effective transport to the surface, preventing dominant-negative effects seen in mutants that can reach the Golgi and thus cannot take this alternative route.

6.2 Membrane cholesterol and palmitoylation underlie β2 polarized localization

We have shown the essential role of *N*-glycosylation in the trafficking to the PM of β2; despite this, modification of glycosylation and even its complete lack does not

affect the polarized distribution of cell surface β2. These data point to a different mechanism regulating the exclusive localization of β2 at the apical domain of polarized MDCK cells.

Here, by ABE, we found that β2 is *S*-acylated at its conserved Cys-182 [80]. Indeed, by treating β2-expressing cells with 2BP, a competitive palmitoylation inhibitor, we significantly reduced β2 *S*-acylation, as detected by ABE. Therefore, it is safe to assume that most of β2 *S*-acylation is in fact *S*-palmitoylation, which is the most common form of *S*-acylation. This PTM is often implicated in protein targeting to lipid rafts [168]. Despite this, there are a few examples of palmitoylated proteins not associating with lipid rafts [48]. Here, we found that the C182S mutation abrogates palmitoylation of the single available cysteine in the β2 ICD. More interestingly, C182S β2 does not localize to DRMs, in contrast to WT β2, a fraction of which is found in DRMs isolated from MDCK cells. Although this mutant properly localizes to the apical PM in a manner indistinguishable from the WT, its absence in DRMs is highly interesting. Therefore, palmitoylation of β2 appears to be the first structural feature determining β2 submembrane localization.

While finding a molecule in DRMs does not provide conclusive evidence of its localization in rafts, DRMs are enriched in sphingolipids and cholesterol, as described for lipid rafts, and are considered a useful tool for studying membrane biology [30]. To further investigate the possibility that a fraction of β2 is indeed associated with lipid raft domains, we labeled polarized live cells with CTX, whose B subunit binds to lipid raft-associated GM1 [158]. Effectively, here we observed partial overlap of β2 with CTX. This data, combined with the presence of β2 WT in DRMs and its apical localization, provide solid evidence to think that indeed a fraction of β2 resides in lipid raft domains in MDCK cells. These results agree with the previous observation in which all four β subunits were found enriched in DRMs from primary cortical neurons. However, the portion of β2 residing in lipid rafts is likely cell type specific, since we have seen here a rather smaller detergent-insoluble fraction of β2 than that previously reported in neurons [88].

A well-accepted role of β2 in the heart is its implication in ensuring surface localization of $Na_V1.5$ [182], likely to specific subdomains of the sarcolemma. It is still unknown if the influence of β2 on $Na_V1.5$ localization occurs already at the PM or perhaps, as we suggest, early in the secretory pathway. However, from our results in polarized MDCK cells, and the published evidence in animal models [85,96,100] and in human atria [98], it is accepted that β2 displays a differential distribution in the surface of polarized cells, thus its effect on $Na_V1.5$ once at the PM is dependent on the close proximity of both proteins. As a result, β2 palmitoylation that we report here must be important for its localization and function in the CMs sarcolemma.

Since palmitoylation is a reversible modification, and our data suggest that only a fraction of β2 expressed in MDCK cells is palmitoylated, it represents a regulatory element that establishes two distinct pools of the protein, probably with a different functionality [47]. Recent evidence describes the *S*-acylation of the related β1 subunit in an analogous juxtamembrane free cysteine, i.e. Cys-181. In the case of β1, the effects of *S*-acylation are somehow more noticeable, as the protein requires this PTM to efficiently localize at the PM. Yet, inhibition of clathrin-mediated endocytosis restores PM localization of the non-palmitoylable mutant. This suggests a stabilizing role on β1 at the PM by *S*-acylation. In addition, *S*-acylation enhances β1 cleavage by BACE1 and γ-secretase; however, the acylation-deficient mutant associates to DRMs in a manner indistinguishable from the WT. As the authors suggest, this could be because the *S*-acylation site is close to the γ-secretase cleavage site, becoming a proteolysis regulator. Regarding β1 effect on $Na_V1.5$, lack of *S*-acylation does not affect I_{Na} modulation [131]. Given the relative similarity of β1 and β2, it is tempting to compare the effects of their *S*-acylation. Nonetheless, caution must prevail. Thus, we have seen that non-palmitoylated β2 localizes also in a polarized fashion, i.e. at the apical domain, as the WT form.

We did not detect endocytosis of apically located β2. We have not explored endocytosis of C182S β2; however, we believe that it is safe to assume that it will not undergo substantial endocytosis. We can think of at least three reasons: the mutant displays similar mobility at the PM, as measured by FRAP; they have identical subcellular localization; and only a small fraction of WT β2 seems to get palmitoylated and partitioned to DRMs, which suggests that should this fraction be more susceptible to endocytosis, we might have not been able to detect it. Localization of β1 has also been analyzed in various cell models. In MDCK [139] and HEK cells [134] (and our unpublished observations), β1 is partially intracellular, localizing throughout the cytoplasm, but mostly above the nucleus. Similarly, in Chinese Hamster Lung cells, β1 is mostly intracellular and the portion localizing to the PM is greatly dependent on being *S*-acylated, thus avoiding rapid clathrin-mediated endocytosis [131].

Relating protease processing, both β1 and β2 undergo sequential cleavage by proteases [88]. Yet, β1 cleavage has been more thoroughly investigated compared to that in the other β subunits, and the results are exciting, as they suggest additional regulatory mechanisms for their functions: as described for β2 [89], it has recently been reported that the β1 ICD modulates gene transcription [131]. This finding opens the door to investigate further related aspects of β2 and of the rest of the subunits. In particular, it would be interesting to study their cleavage, the downstream effects of the released fragments and how PTMs such as palmitoylation regulate this process. Educated guesses for how palmitoylation may regulate proteolysis include

modification of the cleavage site, either by hiding or further exposing the region, and also its potential influence on the subcellular localization of the protein, i.e. to raft domains rich in proteases, such as BACE1 [183].

Understanding the mechanisms governing polarized trafficking is of great importance, since alterations in polarity turn into serious diseases. Polarized trafficking is believed to be controlled by a molecular network responsible of organizing vesicle transport in order to achieve proper polarized distribution of PM proteins [184]. Protein targeting to the apical surface has been subject of intense study. This is the case, for instance, of GPI-anchored proteins, which are mainly sorted to the apical surface in epithelia by partitioning into lipid raft domains. Indeed, lipid rafts have been proposed as a sorting mechanism for apical delivery from the TGN [185]. Another mechanism implicated in apical sorting is recognition of the glycosylated luminal domain of proteins by sugar-binding lectins [186]. Neither of these two mechanisms by themselves appears to be responsible for β2 apical localization. Despite that, acute cholesterol depletion with MβCD or disruption of intracellular cholesterol transport for an extended period with U18666A, missorted β2 to the basolateral domain. While these pharmacological approaches have been used as a tool to assess the potential influence of cholesterol-rich domains in protein localization and trafficking, they have some downsides. For MβCD, non-specific effects may arise when used at high concentrations and/or for an extended period of time. Under such circumstances, it has been reported that the drug removes cholesterol not only from raft regions within the PM, but also from inside the cell, which may disturb important cell functions [143]. To avoid non-specific effects, we thus limited the dose and incubation time of MβCD to the minimum by which β2 localization effectively changed, while polarity markers and tight junctions remained unaffected. The doses of U18666A and lovastatin were analogously adjusted. Therefore, our results clearly indicate that the polarized distribution of β2 in MDCK cells is dependent on the cholesterol content of the PM and the intact intracellular transport of cholesterol.

Another aspect that may be influenced by membrane cholesterol and palmitoylation is endocytosis. Lack of measurable apical endocytosis of β2 reveals the surprisingly stable localization of β2. This is a puzzling finding. Clathrin-coated pits can be formed at the apical surface and internalized; in addition, they are soluble in cold detergent [187]. If the bulk of β2 were excluded from rafts, as we see when isolating the DRMs, one would expect certain endocytosis. However, no internalization could be detected even after one hour. This suggests that the fraction of β2 that we recovered in DRM fractions may be underestimated. Potential apical β2 endocytosis, and similarly as described previously for the non-raft sialoglycoprotein gp114 in MDCK cells [172,188], may be negatively influenced by

its *N*-glycosylation and sialylation. These results also suggest that the mislocalization of β2 that we observed upon cholesterol depletion is due to actual missorting to the basolateral membrane, rather than to enhanced endocytosis and subsequent delivery to this surface domain.

In summary, we have shown that glycosylation and palmitoylation, along with the influence of membrane cholesterol content, have an effect in β2 trafficking. It would be interesting to address in the future whether the cell takes advantage of these two PTMs to ensure the polarized targeting of β2 to the cell surface. Undoubtedly, this is an important aspect that deserves further investigation in particular achieving a better understanding of β2 role, either within the Na_V or independently.

6.3 Dynamics of β2 at the PM

By FRAP, we monitored the membrane dynamics of fluorescently tagged β2. FRAP curves provide information on how β2 moves and interacts with other membrane proteins. We analyzed the potential effect of cholesterol depletion, interaction of β2 with the cytoskeleton, abolishing palmitoylation, and preventing *N*-glycosylation, on its dynamics at the membrane.

Curves for β2 were flat and dependent on the bleaching area. This behavior is indicative of a complex, diffusion-coupled dynamics, likely consequence of the sum of multiple subpopulations. The protein probably undergoes transient, albeit persistent, interactions with other molecules as it diffuses across the membrane [189]. Such diffusion is remarkably slow, especially in fully polarized MDCK cells, where β2 remains rather immobile, although we have seen a tendency to acquire faster mobility in cells grown on glass [190]. Despite this, the calculated *D* always remains relatively small. Therefore, the rate of β2 diffusion depends on the degree of cell polarization. Moreover, membrane properties and associated structures can influence or even impede its mobility. Thus, when *D* is below 0.001 $\mu m^2/s$, proteins are considered to be immobilized with cytoskeletal elements [191]. According to these criterion it seems likely that a considerable fraction of β2 remains associated with the cytoskeleton: this agrees with the idea that β subunits serve as adaptors linking the cytoskeleton, along with signaling and adhesion molecules, to ion channel macromolecular complexes [192]. In support of this model, we provide the data of β2 lacking its ICD (181X). β2 181X displayed considerably faster mobility and complete fluorescence recovery than the WT, most likely due to its defective interaction with the submembrane cytoskeleton. With the relative low *D* of β2 WT ($\leq 0.02\ \mu m^2/s$), it is also conceivable to consider that β2 diffuses inside lipid rafts, fitting with the reported $\leq 0.05\ \mu m^2/s$ in these instances [193].

The mobility of β2 was also greatly reduced upon acute (short-term) cholesterol depletion. This decrease in mobility is consistent with the idea that cholesterol depletion affects raft-associated proteins, as seen in previous studies [194,195]. It has been reported that MβCD can also reduce diffusion of non-raft membrane proteins, suggesting that it may also cause some effects independent of the membrane cholesterol content [196]. Nevertheless, the distribution of polarity markers was not affected, indicating that the conditions employed affected specifically β2. In addition, the palmitoylation-deficient mutant also displayed reduced mobility in control conditions, although the decrease in MF was not dramatic. We propose that this relatively small portion of mutant with reduced mobility corresponds to the fraction of the WT susceptible to palmitoylation. This would also agree with the modest presence of β2 WT that we found in DRMs.

The effect of β2 glycosylation was also assessed by FRAP. Lack of glycosylation probably disturbs the conformation of the extracellular domain, nullifying the potential adhesion function of the Ig loop, and in turn its kinetic properties. Despite that, the mobility of the small fraction of total unglycosylated β2 that localizes at the PM was indistinguishable from that of the WT. In addition, we measured the mobility of β2, both with and without glycosylation, in intracellular membranes. First, we tested β2 mobility in what we called the “cytoplasm matrix”, i.e. a network of β2 positive structures probably derived from the ER and possibly including patches of β2 already at PM. There, β2 behaved surprisingly similar to PM β2. Deeper in the cell, though, in the bright perinuclear ER structures, which appear short after protein expression and persist in the case of unglycosylated β2, mobility was dramatically reduced. We suggest that, even in the case of WT β2, in this early stage of protein synthesis, the ER structures positive for β2 are overwhelmingly abundant because of the large production of β2 protein, which we have seen has a tendency to form dimers and tetramers. In the case of unglycosylated β2, the majority of the protein likely remains misfolded and aggregated, unable of exit the ER. This would be the reason for the very limited mobility of β2 in these structures.

From our observations, we propose that three populations of WT β2 contribute to its overall mobility at the PM. First of all, there is the immobile fraction - which we estimate is equivalent to ~ 40% of total β2 at the PM. That fraction would be represented by cytoskeleton-bound β2, as 181X displays faster and complete mobility. Since the immobile fraction changes according to the cell monolayer confluence and tends to increase with the degree of cell polarity, the ability of the PM to allocate cytoskeleton-bound β2 would be limited and increase along with cell polarity. Secondly, we have mobile β2, which would be represented by β2 undergoing short-term interactions with other membrane elements. This fraction

would be composed of a minor population of palmitoylated β2, occupying lipid rafts, and the bulk of mobile β2, residing outside lipid rafts. At some point, immobile β2 molecules may detach from the cytoskeleton to become mobile, establishing a dynamic equilibrium among these fractions.

6.4 β2 effect on $Na_V1.5$ localization

$Na_V1.5$ is often mislocalized in inherited channelopathies, triggering cardiac arrhythmias. Trafficking defects are often responsible [197], although defective interaction with other interacting partners to stabilize $Na_V1.5$ at the PM can also result in channel dysfunction and altered localization [105,198]. Such proteins may include β subunits. For example, in neurons, β2 is important for proper targeting and localization of the α/β2 complex [96,182].

Here, we analyzed regulation of subcellular localization and trafficking of the major cardiac Na_V by the β2 subunit. By cell surface protein biotinylation and confocal microscopy, we observed that β2 shifts the localization of a portion of $Na_V1.5$ from the ER to the PM. We also show that a BrS-associated mutation in β2 ICD, or a glycosylation-deficient mutant, fail to promote proper localization of $Na_V1.5$ to the cell surface. More importantly, this defect on β2 function occurs in different subcellular localizations and, likely, by different means. This led us to propose that the effect of β2 on $Na_V1.5$ localization takes place both at the PM, as the literature suggests [199], and early in the secretory pathway, establishing β2 as a potential chaperone.

Virtually all exogenously expressed $Na_V1.5$ actually remains intracellular in MDCK cells, mostly in the ER. This is in line with the classical idea that the ER may be a reservoir for cardiac [134] and neuronal Na_V, establishing a pool of channels ready to be exported to appropriate surface localizations [199]. Nonetheless, in MDCK cells, β2 can promote $Na_V1.5$ apical PM localization. The role of β subunits in promoting PM localization of the Na_V α subunit has been previously reported [200–202]. In the case of β2, it has long been believed that its covalent assembly with the α subunit takes place right before their arrival to the PM [199], or at least after the two subunits have left the Golgi apparatus [134]. Regardless of the exact location where they begin to interact, there seems to be no question for an important role of β2 in ensuring adequate levels of functional $Na_V1.5$ at the cell surface. In this regard, *scn2b* deletion in mice causes, in ventricular myocytes [176] and in primary hippocampal neuron cultures [97], approximately a 40% reduction of α subunit levels at the cell surface.

The converse effect has also been reported, i.e. alteration of β subunit localization by Na_V alpha subunits. This is the case of the localization of β1 to the PM in HEK cells [134], and β2 localization to neuron nodes of Ranvier and the AIS, the latter, dependent on its disulfide bond with the α subunit [96], and both apparently promoted by α. A similar scenario is seen for β4 [95]. These evidences may lead us to question whether β acts on the α subunit, vice versa, or if the action is two-ways. However, our data is consistent with the first hypothesis and with the notion that β2 plays an important role in ensuring efficient surface localization of $Na_V1.5$.

It has been previously shown that β1 and β2 co-immunoprecipitate with $Na_V1.5$ and co-localize in CM IDs at the level of the sarcomere Z lines, regulating cardiac action potential and channel-cytoskeleton interactions [177]. We also investigated the interaction of $Na_V1.5$ with β2, and found their specific association by co-immunoprecipitation of $Na_V1.5$/β2 in MDCK cells. However, we estimated that only a very small fraction of total β2 actually interacts with $Na_V1.5$, which we propose takes place likely along their export from the ER to the cell surface. This would be consistent with a recent study on Na_V structure [203], in which the authors propose that, compared to the other Na_V isoforms, $Na_V1.5$ lacks the cysteine predicted to establish a disulfide bond with β2 or β4. This would mean that they interact non-covalently, through much weaker interactions. Additionally, α/β interaction in some systems may be indirect or involving a combination of different β isoforms [204], an aspect that we have not explored. This would explain the relatively small portion of β2 interacting with $Na_V1.5$ that we observed. Moreover, it would be in line with their markedly different localization, as β2 localizes to the PM while the bulk of $Na_V1.5$ is retained in the ER at steady state. In fact, even $Na_V1.5$ localizing at the apical domain along with β2 appeared to be in different submembrane domains, further explaining their minimal co-immunoprecipitation.

In fully polarized cells, β2 increased the levels of $Na_V1.5$ at the apical surface. When we analyzed cells over time, i.e. as their polarity progressed, the effect of β2 on $Na_V1.5$ localization was only temporary and restricted to non-polarized cells, up to ~ 24 hours after transfection. After that, cell surface $Na_V1.5$ levels returned to nearly undetectable levels. The fact that it was seen immediately after the onset of β2 expression further indicates that β2 influences $Na_V1.5$ early in the secretory pathway. Since such effect is temporary, we propose a role for β2 more of guidance and chaperoning rather than a long-term regulator of $Na_V1.5$ subcellular localization. This way, in non-polarized cells, after early arrival of $Na_V1.5$ to the PM, the channel may soon internalize because of a lack of membrane anchors. In contrast, polarized MDCK cells may display additional membrane anchors that would allow the portion of $Na_V1.5$ that gradually reaches the (apical) surface to remain and stabilize there for a longer period; this was consistently seen in a

discrete proportion of polarized cells. In an analogous manner, in CMs, after the arrival of β2 and $Na_V1.5$ to the proper sarcolemma subdomain, $Na_V1.5$ would establish long-term interactions with anchors such as ankyrin-G, SAP97 or plakophilin and remain functional in its proper location [69].

We also describe here the importance of β2 glycosylation for $Na_V1.5$ trafficking. Complete lack of *N*-glycosylation cancelled the effect of β2 on PM localization of $Na_V1.5$. Surprisingly, a single glycosylation site in β2 was sufficient to preserve this function. In this way, the ability of β2 to efficiently reach the PM appears important for its effect on $Na_V1.5$ localization.

When we co-expressed $Na_V1.5$ together with the unglycosylated β2 mutant, the bulk of both proteins appeared stuck in the ER. We reasoned that retention of unfolded overexpressed proteins would induce ERAD. Thus, in order to prevent excessive overexpression of β2, in most of these experiments we used cells stably expressing β2-YFP in moderate levels. Subsequently, these were transiently transfected to express $Na_V1.5$-FLAG. Yet, the unglycosylated mutant dragged along a large portion of $Na_V1.5$ into the ER (Figure 44). According to this observation, we propose that unglycosylated β2 causes retention of $Na_V1.5$ early in the secretory pathway in an attempt to chaperone it for proper folding on its way to the PM. In fact, in multiple attempts to corroborate this hypothesis, we carried out co-immunoprecipitation experiments between ER-stuck β2 and $Na_V1.5$. However, either because of multimerization due to lack of *N*-glycosylation, or as a result of treatments with BFA or TUN prior to immunoprecipitation, unglycosylated β2 was non-specifically pulled down along the α subunit (not shown). In addition, unglycosylated β2 often appeared as high molecular weight bands in western blots. These observations, along with the total immobility of the protein in perinuclear structures (mostly corresponding to ER, based on major $Na_V1.5$ overlap with calnexin in the absence of β2), as measured by FRAP, indicate that unglycosylated β2 in the ER is likely unfolded and aggregated. In such state, β2 likely traps $Na_V1.5$ and perhaps other proteins. This way, our results challenge the view that β2 acts on $Na_V1.5$ at a later stage, such as at the cell surface or in a post-Golgi compartment.

Additionally, we analyzed in more detail the defect of a BrS-associated variant of β2 previously reported in our lab. The D211G mutation causes a 40% decrease in I_{Na} without affecting single channel conductance, but reducing $Na_V1.5$ surface levels [3]. Interestingly, in MDCK cells, β2 D211G localization is indistinguishable from the WT, yet the mutant fails to promote localization of $Na_V1.5$ to the PM (Figure 44), regardless of the cells polarization status. Indeed, this defect of β2 D211G on $Na_V1.5$ localization to the cell surface is also apparent in CM-derived

HL-1 cells [139]. The proper localization of D211G β2 implies that it is faulty through a different mechanism to that of unglycosylated β2.

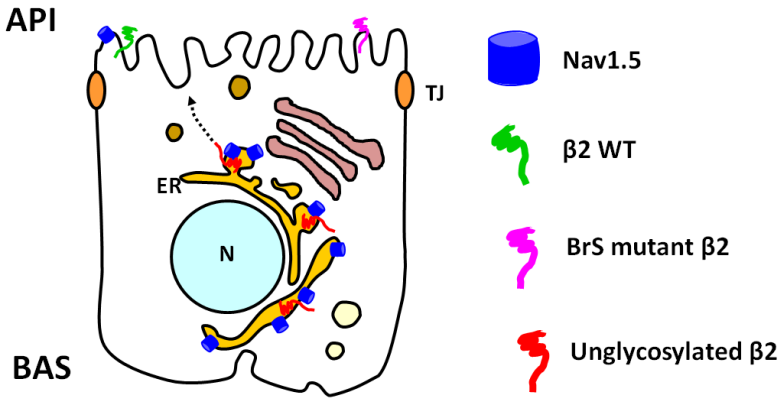

Figure 44. Different variants of β2 fail to promote $Na_V1.5$ cell surface localization in polarized MDCK cells. WT and D211G β2 localize to the apical domain. In contrast, most of unglycosylated β2 and $Na_V1.5$ remain in the ER. WT β2 can rescue a portion of $Na_V1.5$ and take it to the PM. API, apical domain; BAS, basolateral domain; N, nucleus; TJ, tight junctions.

Channel trafficking can be modulated by PTMs, such as phosphorylation [205]. Interestingly, Asp-211 is near two putative phosphorylation sites, i.e. Ser-192 and Thr-204 [129], which are conserved in mammals [80]. Since we do not know how β2 ICD curls, these residues could be in close proximity with Asp-211. Changing Asp for Gly alters charge, and perhaps conformation, of the β2 tail, to such an extent that it may influence potential phosphorylation of nearby residues. Future work should address this possibility. In fact, the β1 Y181E mutation, which mimics phosphorylation, abolishes ankyrin-G recruitment, likely affecting Na_V localization to nodes of Ranvier [206]. Thus, it is also possible that the D211G mutation causes an unstable connection of β2 with ankyrin, or with other submembrane adapters linking TM proteins to the actin cytoskeleton [182]. In consequence, affecting interactions between β2 and other channel-regulatory molecules would interfere with the role of β2 on $Na_V1.5$ localization.

6.5 Cardiomyocytes shadows

CM are highly polarized cells [207] and, like cells of epithelial origin, have specialized PM domains or subregions. Despite analogies in polarity, their surface domains are different [1]. Thus, the co-localization data that we have obtained in MDCK cells do not necessarily represent what we would see in cardiac cells. Nevertheless, our observations are certainly compatible with previous reports, and add on the understanding of the role of β2 in $Na_V1.5$ trafficking and localization. Regarding the β2 subunit, we have dissected its polarized trafficking, describing the topological features that enable it to exit the ER, undergo complex glycosylation, palmitoylation and partitioning to subdomains of the PM. It is reasonable to expect the most elemental requirements ensuring proper membrane trafficking of β subunits, such as glycosylation and palmitoylation, to be conserved in most cell types. However, to fully understand their intracellular pathway in cells displaying complex polarity and a different subset of membrane adaptors, like CMs or neurons, experimental assessment of the subcellular localization of β2 and their variants will be required. Indeed, depending on species and cell type, the subcellular localization of channel subunits may differ [98,208]. This differential localization of channel subunits is important for the electrical properties of the CM and the basis of its conduction anisotropy [117,118].

Given the abundance of regulatory elements in β2 topology, and according to our data, we propose that at least three subpopulations of β2 would coexist in CMs, potentially serving different functions: (i) cytoskeleton-bound, immobile β2; (ii) non-palmitoylated, mobile β2; and (iii) palmitoylated, mobile β2. The latter would associate with lipid rafts and diffuse faster than non-palmitoylated β2. It is plausible to think that phosphorylation determines β2 cytoskeleton binding through ankyrin [209], and thus the presence of the immobile fraction.

Experimental cell models resembling human CMs should be developed, so that interesting and challenging hypothesis can be addressed in a more physiologically relevant context. This way, the data generated could be better understood and translated into the clinical environment.

6.6 Clinical projection of the research on Na_V subunits

Alterations in localization of components of the Na_V are often the cellular basis underlying an increased risk of arrhythmia, and therefore potentially associated with important cardiac pathologies [105]. We have provided evidence at cellular level that supports this premise and, along the way, shed some light on the intricate mechanisms regulating Na_V trafficking. In this regard, it is of utmost importance

that findings in the field lead to a better understanding of how subunits of the Na_V localize. This way, β2, along with the other β subunits, become promising targets to regulate sodium channel density at the PM of excitable cells. However, to this day, potential therapeutic targeting of β subunits remains a mystery. The good news is that the research community in the field is fervent, and an ever-growing knowledge on the matter is providing a better picture of the link between subcellular distribution of Na_V and excitability and electrical coupling in the heart, thereby contributing to a better understanding of how arrhythmias develop. So far, some findings have already been translated into routine clinical practice, most significantly, into genetic testing for channelopathies and sudden death risk management [210].

7.CONCLUSIONS

7. Conclusions

1. β2 undergoes complex *N*-linked glycosylation at residues Asp-42, Asp-66 and Asp-74, from which only Asp-42 is sialylated. Yet, glycosylation of any of these residues is sufficient for proper localization of β2 to the PM and to promote PM localization of $Na_V1.5$

2. Unglycosylated β2 is retained in the ER; however, it can still reach the cell surface through Golgi bypass at a rate of 1/3rd to that of the WT.

3. In polarized MDCK cells, β2 localizes to the apical PM domain. This polarized distribution is dependent on cholesterol levels, implying a requirement of β2 association to cholesterol-rich membrane domains and intact cholesterol transport.

4. β2 is *S*-palmitoylated at Cys-182; this PTM partitions β2 into DRMs, which are enriched in lipid rafts. β2 also co-localizes with lipid rafts at the apical domain of MDCK cells. Altogether, these findings indicate that *S*-palmitoylated β2 associates with cholesterol-rich lipid raft domains.

5. In MDCK cells, three β2 subpopulations in equilibrium coexist at the PM: immobile β2, which is bound to the cytoskeleton through the ICD; non-palmitoylated, mobile β2; and palmitoylated, mobile β2. The two subpopulations comprising mobile β2 undergo slow diffusion. In addition, β2 does not undergo endocytosis. Overall, these results indicate that β2 remains highly stable at the PM.

6. In MDCK cells, β2 promotes the localization of $Na_V1.5$ from the ER to the PM. This effect is dependent on β2 *N*-glycosylation.

7. The BrS-associated D211G mutation, located in the ICD of β2, correctly localizes to the apical domain of MDCK cells; however, it fails to promote $Na_V1.5$ cell surface localization.

8.REFERENCES

8. References

1. Cortada E, Brugada R, Verges M. Trafficking and Function of the Voltage-Gated Sodium Channel β2 Subunit. *Biomolecules*. 2019;9(10):604. doi:10.3390/biom9100604

2. Brackenbury WJ, Isom LL. Na Channel β Subunits: Overachievers of the Ion Channel Family. *Front Pharmacol*. 2011;2(September):53. doi:10.3389/fphar.2011.00053

3. Riuró H, Beltran-Alvarez P, Tarradas A, et al. A Missense Mutation in the Sodium Channel β2 Subunit Reveals SCN2B as a New Candidate Gene for Brugada Syndrome. *Hum Mutat*. 2013;34(7):961-966. doi:10.1002/humu.22328

4. Watanabe H, Darbar D, Kaiser DW, et al. Mutations in Sodium Channel β1- and β2-Subunits Associated With Atrial Fibrillation. *Circ Arrhythmia Electrophysiol*. 2009;2(3):268-275. doi:10.1161/CIRCEP.108.779181

5. Jan CH, Williams CC, Weissman JS. Principles of ER cotranslational translocation revealed by proximity-specific ribosome profiling. *Science*. 2014;346(6210):1257521. doi:10.1126/science.1257521

6. Blobel G. Intracellular protein topogenesis. *Proc Natl Acad Sci U S A*. 1980;77(3):1496-1500. doi:10.1073/pnas.77.3.1496

7. Schwarz DS, Blower MD. The endoplasmic reticulum: Structure, function and response to cellular signaling. *Cell Mol Life Sci*. 2016;73(1):79-94. doi:10.1007/s00018-015-2052-6

8. Aebi M. N-linked protein glycosylation in the ER. *Biochim Biophys Acta - Mol Cell Res*. 2013;1833(11):2430-2437. doi:10.1016/j.bbamcr.2013.04.001

9. Caramelo JJ, Parodi AJ. A sweet code for glycoprotein folding. *FEBS Lett*. 2015;589(22):3379-3387. doi:10.1016/j.febslet.2015.07.021

10. Cui J, Smith T, Robbins PW, Samuelson J. Darwinian selection for sites of Asn-linked glycosylation in phylogenetically disparate eukaryotes and viruses. *Proc Natl Acad Sci*. 2009;106(32):13421-13426. doi:10.1073/pnas.0905818106

11. O'Connor SE, Imperiali B. Modulation of protein structure and function by asparagine-linked glycosylation. *Chem Biol*. 1996;3(10):803-812. doi:10.1016/S1074-5521(96)90064-2

12. Benham AM. Protein Secretion and the Endoplasmic Reticulum. *Cold Spring Harb Perspect Biol*. 2012;4(8):a012872-a012872. doi:10.1101/cshperspect.a012872

13. Schröder M. Endoplasmic reticulum stress responses. *Cell Mol Life Sci*. 2008;65(6):862-894. doi:10.1007/s00018-007-7383-5

14. Ritter C, Helenius A. Recognition of local glycoprotein misfolding by the ER folding sensor UDP-glucose:glycoprotein glucosyltransferase. *Nat Struct Biol*. 2000;7(4):278-280. doi:10.1038/74035

15. Hagiwara M, Maegawa K ichi, Suzuki M, et al. Structural Basis of an ERAD Pathway Mediated by the ER-Resident Protein Disulfide Reductase ERdj5. *Mol Cell*. 2011;41(4):432-444. doi:10.1016/j.molcel.2011.01.021

16. De Matteis MA, Luini A. Exiting the Golgi complex. *Nat Rev Mol Cell Biol*. 2008;9(4):273-284. doi:10.1038/nrm2378

17. Alberts B, Johnson A, Lewis J, et al. Transport from the ER through the Golgi Apparatus. *Mol Biol Cell*. Published online 2002:1-11.

18. Duden R. ER-to-Golgi transport: COP I and COP II function. *Mol Membr Biol*. 2003;20(3):197-207. doi:10.1080/0968768031000122548

19. Glick BS, Nakano A. Membrane Traffic Within the Golgi Apparatus. *Annu Rev Cell Dev Biol*. 2009;25(1):113-132. doi:10.1146/annurev.cellbio.24.110707.175421

20. Cosson P, Perrin J, Bonifacino JS. Anchors aweigh: Protein localization and transport mediated by transmembrane domains. *Trends Cell Biol*. 2013;23(10):511-517. doi:10.1016/j.tcb.2013.05.005

21. Sharpe HJ, Stevens TJ, Munro S. A Comprehensive Comparison of Transmembrane Domains Reveals Organelle-Specific Properties. *Cell*. 2010;142(1):158-169. doi:10.1016/j.cell.2010.05.037

22. Stanley P. Golgi glycosylation. *Cold Spring Harb Perspect Biol*. 2011;3(4):1-13. doi:10.1101/cshperspect.a005199

23. Li J, Hsu HC, Mountz JD, Allen JG. Unmasking Fucosylation: from Cell Adhesion to Immune System Regulation and Diseases. *Cell Chem Biol*. 2018;25(5):499-512. doi:10.1016/j.chembiol.2018.02.005

24. Miyoshi E, Moriwaki K, Nakagawa T. Biological function of fucosylation in cancer biology. *J Biochem*. 2008;143(6):725-729. doi:10.1093/jb/mvn011

25. Stow JL, Murray RZ. Post-Golgi Transport – Cargo, Carriers, and Pathways. In: *Encyclopedia of Cell Biology*. Vol 2. Elsevier; 2016:363-370. doi:10.1016/B978-0-12-394447-4.20035-7

26. Stöckli J, Fazakerley DJ, James DE. GLUT4 exocytosis. *J Cell Sci*. 2011;124(24):4147-4159. doi:10.1242/jcs.097063

27. Spang A. The road not taken: Less traveled roads from the TGN to the

plasma membrane. *Membranes (Basel)*. 2015;5(1):84-98. doi:10.3390/membranes5010084

28. Bard F, Malhotra V. The Formation of TGN-to-Plasma-Membrane Transport Carriers. *Annu Rev Cell Dev Biol*. 2006;22(1):439-455. doi:10.1146/annurev.cellbio.21.012704.133126

29. Pike LJ. The challenge of lipid rafts. *J Lipid Res*. 2009;50(Supplement):S323-8. doi:10.1194/jlr.R800040-JLR200

30. Levental I, Levental KR, Heberle FA. Lipid Rafts: Controversies Resolved, Mysteries Remain. *Trends Cell Biol*. 2020;30(5):341-353. doi:10.1016/j.tcb.2020.01.009

31. Lingwood D, Simons K. Lipid rafts as a membrane-organizing principle. *Science*. 2010;327(5961):46-50. doi:10.1126/science.1174621

32. Stalder D, Gershlick DC. Direct trafficking pathways from the Golgi apparatus to the plasma membrane. *Semin Cell Dev Biol*. 2020;(April):0-1. doi:10.1016/j.semcdb.2020.04.001

33. Grieve AG, Rabouille C. Golgi bypass: Skirting around the heart of classical secretion. *Cold Spring Harb Perspect Biol*. 2011;3(4):1-15. doi:10.1101/cshperspect.a005298

34. Lippincott-Schwartz J, Yuan LC, Bonifacino JS, Klausner RD. Rapid redistribution of Golgi proteins into the ER in cells treated with brefeldin A: Evidence for membrane cycling from Golgi to ER. *Cell*. 1989;56(5):801-813. doi:10.1016/0092-8674(89)90685-5

35. Niu T-K, Pfeifer AC, Lippincott-Schwartz J, Jackson CL. Dynamics of GBF1, a Brefeldin A-Sensitive Arf1 Exchange Factor at the Golgi. *Mol Biol Cell*. 2005;16(3):1213-1222. doi:10.1091/mbc.e04-07-0599

36. Yoo JS, Moyer BD, Bannykh S, Yoo HM, Riordan JR, Balch WE. Non-conventional trafficking of the cystic fibrosis transmembrane conductance regulator through the early secretory pathway. *J Biol Chem*. 2002;277(13):11401-11409. doi:10.1074/jbc.M110263200

37. Gee HY, Noh SH, Tang BL, Kim KH, Lee MG. Rescue of Δf508-CFTR trafficking via a GRASP-dependent unconventional secretion pathway. *Cell*. 2011;146(5):746-760. doi:10.1016/j.cell.2011.07.021

38. Schotman H, Karhinen L, Rabouille C. dGRASP-Mediated Noncanonical Integrin Secretion Is Required for Drosophila Epithelial Remodeling. *Dev Cell*. 2008;14(2):171-182. doi:10.1016/j.devcel.2007.12.006

39. Jung J, Kim J, Roh SH, et al. The HSP70 co-chaperone DNAJC14 targets misfolded pendrin for unconventional protein secretion. *Nat Commun*. 2016;7(1):1-15. doi:10.1038/ncomms11386

40. Lodowski KH, Lee R, Ropelewski P, Nemet I, Tian G, Imanishi Y. Signals governing the trafficking and mistrafficking of a ciliary GPCR, rhodopsin. *J Neurosci*. 2013;33(34):13621-13638. doi:10.1523/JNEUROSCI.1520-13.2013

41. Baldwin TA, Ostergaard HL. The protein-tyrosine phosphatase CD45 reaches the cell surface via Golgi-dependent and -independent pathways. *J Biol Chem*. 2002;277(52):50333-50340. doi:10.1074/jbc.M209075200

42. Hanus C, Ehlers MD. Secretory outposts for the local processing of membrane cargo in neuronal dendrites. *Traffic*. 2008;9(9):1437-1445. doi:10.1111/j.1600-0854.2008.00775.x

43. Rabouille C. Pathways of Unconventional Protein Secretion. *Trends Cell Biol*. 2017;27(3):230-240. doi:10.1016/J.TCB.2016.11.007

44. Rabouille C, Malhotra V, Nickel W. Diversity in unconventional protein secretion. *J Cell Sci*. 2012;125(22):5251-5255. doi:10.1242/jcs.103630

45. Abrami L, Leppla SH, Gisou Van Der Goot F. Receptor palmitoylation and ubiquitination regulate anthrax toxin endocytosis. *J Cell Biol*. 2006;172(2):309-320. doi:10.1083/jcb.200507067

46. Abrami L, Kunz B, Iacovache I, Van Der Goot FG. Palmitoylation and ubiquitination regulate exit of the Wnt signaling protein LRP6 from the endoplasmic reticulum. *Proc Natl Acad Sci U S A*. 2008;105(14):5384-5389. doi:10.1073/pnas.0710389105

47. Charollais J, Van Der Goot FG. Palmitoylation of membrane proteins (Review). *Mol Membr Biol*. 2009;26(1-2):55-66. doi:10.1080/09687680802620369

48. Alvarez E, Girones N, Davis RJ. A point mutation in the cytoplasmic domain of the transferrin receptor inhibits endocytosis. *Biochem J*. 1990;267(1):31-35. doi:10.1042/bj2670031

49. McCormick PJ, Dumaresq-Doiron K, Pluviose A-S, Pichette V, Tosato G, Lefrancois S. Palmitoylation Controls Recycling in Lysosomal Sorting and Trafficking. *Traffic*. 2008;9(11):1984-1997. doi:10.1111/j.1600-0854.2008.00814.x

50. Vergés M. Retromer in Polarized Protein Transport. In: *International Review of Cell and Molecular Biology*. Vol 323. Elsevier Inc.; 2016:129-179. doi:10.1016/bs.ircmb.2015.12.005

51. Hayashi T, Rumbaugh G, Huganir RL. Differential regulation of AMPA receptor subunit trafficking by palmitoylation of two distinct sites. *Neuron*. 2005;47(5):709-723. doi:10.1016/j.neuron.2005.06.035

52. Charrin S, Manié S, Oualid M, Billard M, Boucheix C, Rubinstein E.

Differential stability of tetraspanin/tetraspanin interactions: Role of palmitoylation. *FEBS Lett*. 2002;516(1-3):139-144. doi:10.1016/S0014-5793(02)02522-X

53. Cullen PJ, Steinberg F. To degrade or not to degrade: mechanisms and significance of endocytic recycling. *Nat Rev Mol Cell Biol*. 2018;19(11):679-696. doi:10.1038/s41580-018-0053-7

54. Elkin SR, Lakoduk AM, Schmid SL. Endocytic pathways and endosomal trafficking: a primer. *Wiener Medizinische Wochenschrift*. 2016;166(7-8):196-204. doi:10.1007/s10354-016-0432-7

55. Gruenberg J. The endocytic pathway: A mosaic of domains. *Nat Rev Mol Cell Biol*. 2001;2(10):721-730. doi:10.1038/35096054

56. Harder T, Simons K. Caveolae, DIGs, and the dynamics of sphingolipid-cholesterol microdomains. *Curr Opin Cell Biol*. 1997;9(4):534-542. doi:10.1016/S0955-0674(97)80030-0

57. Murata M, Peränen J, Schreiner R, Wieland F, Kurzchalia T V., Simons K. VIP21/caveolin is a cholesterol-binding protein. *Proc Natl Acad Sci U S A*. 1995;92(22):10339-10343. doi:10.1073/pnas.92.22.10339

58. Parton RG, Del Pozo MA. Caveolae as plasma membrane sensors, protectors and organizers. *Nat Rev Mol Cell Biol*. 2013;14(2):98-112. doi:10.1038/nrm3512

59. Henley JR, Krueger EWA, Oswald BJ, McNiven MA. Dynamin-mediated internalization of caveolae. *J Cell Biol*. 1998;141(1):85-99. doi:10.1083/jcb.141.1.85

60. Mellman I. Endocytosis and molecular sorting. *Annu Rev Cell Dev Biol*. 1996;12(1):575-625. doi:10.1146/annurev.cellbio.12.1.575

61. Zakon HH, Jost MC, Lu Y. Expansion of Voltage-dependent Na+ Channel Gene Family in Early Tetrapods Coincided with the Emergence of Terrestriality and Increased Brain Complexity. *Mol Biol Evol*. 2011;28(4):1415-1424. doi:10.1093/molbev/msq325

62. Peters CH, Ruben PC. Introduction to sodium channels. *Handb Exp Pharmacol*. 2014;221. doi:10.1007/978-3-642-41588-3_1

63. Catterall WA, Goldin AL, Waxman SG. International Union of Pharmacology. XLVII. Nomenclature and structure-function relationships of voltage-gated sodium channels. *Pharmacol Rev*. 2005;57(4):397-409. doi:10.1124/pr.57.4.4

64. Watanabe E, Hiyama TY, Shimizu H, et al. Sodium-level-sensitive sodium channel Na x is expressed in glial laminate processes in the sensory circumventricular organs. *Am J Physiol Integr Comp Physiol*.

2006;290(3):R568-R576. doi:10.1152/ajpregu.00618.2005

65. Lipkind GM, Fozzard HA. Voltage-gated Na Channel Selectivity: The Role of the Conserved Domain III Lysine Residue. *J Gen Physiol*. 2008;131(6):523-529. doi:10.1085/jgp.200809991

66. Favre I, Moczydlowski E, Schild L. On the structural basis for ionic selectivity among Na+, K+, and Ca2+ in the voltage-gated sodium channel. *Biophys J*. 1996;71(6):3110-3125. doi:10.1016/S0006-3495(96)79505-X

67. West JW, Patton DE, Scheuer T, Wang Y, Goldin AL, Catterall WA. A cluster of Hydrophobic amino acid residues required for fast Na+-channel inactivation. *Proc Natl Acad Sci U S A*. 1992;89(22):10910-10914. doi:10.1073/pnas.89.22.10910

68. Bezanilla F. Voltage-gated ion channels. *IEEE Trans Nanobioscience*. 2005;4(1):34-48. doi:10.1109/TNB.2004.842463

69. Abriel H. Microdomain Interactions of Macromolecular Complexes and Regulation of the Sodium Channel Nav1.5. In: *Cardiac Electrophysiology: From Cell to Bedside: Seventh Edition*. Vol 53. Elsevier Inc.; 2018:167-176. doi:10.1016/B978-0-323-44733-1.00018-3

70. Savio-Galimberti E, Gollob MH, Darbar D. Voltage-gated sodium channels : biophysics , pharmacology , and related channelopathies. *Front Pharmacol*. 2012;3(July):1-19. doi:10.3389/fphar.2012.00124

71. Rubart M, Zipes DP. Mechanisms of sudden cardiac death. *J Clin Invest*. 2005;115(9):2305-2315. doi:10.1172/JCI26381

72. Mehra R. Global public health problem of sudden cardiac death. *J Electrocardiol*. 2007;40(6 SUPPL. 1). doi:10.1016/j.jelectrocard.2007.06.023

73. Campuzano O, Beltrán-Álvarez P, Iglesias A, Scornik F, Pérez G, Brugada R. Genetics and cardiac channelopathies. *Genet Med*. 2010;12(5):260-267. doi:10.1097/GIM.0b013e3181d81636

74. Brugada P, Brugada J. Right bundle branch block, persistent ST segment elevation and sudden cardiac death: A distinct clinical and electrocardiographic syndrome. A multicenter report. *J Am Coll Cardiol*. 1992;20(6):1391-1396. doi:10.1016/0735-1097(92)90253-J

75. Bastiaenen R, Behr ER. Sudden death and ion channel disease: Pathophysiology and implications for management. *Heart*. 2011;97(17):1365-1372. doi:10.1136/hrt.2011.223883

76. Giudicessi JR, Wilde AAM, Ackerman MJ. The genetic architecture of long QT syndrome: A critical reappraisal. *Trends Cardiovasc Med*. 2018;28(7):453-464. doi:10.1016/j.tcm.2018.03.003

77. Xu J, Luc JGY, Phan K. Atrial fibrillation: Review of current treatment strategies. *J Thorac Dis*. 2016;8(9):E886-E900. doi:10.21037/jtd.2016.09.13

78. Behere S, Weindling S. Catecholaminergic polymorphic ventricular tachycardia: An exciting new era. *Ann Pediatr Cardiol*. 2016;9(2):137. doi:10.4103/0974-2069.180645

79. Bouza AA, Isom LL. Voltage-gated sodium channel β subunits and their related diseases. In: *Handbook of Experimental Pharmacology*. Vol 246. Springer New York LLC; 2018:423-450. doi:10.1007/164_2017_48

80. Chopra SS, Watanabe H, Zhong TP, Roden DM. Molecular cloning and analysis of zebrafish voltage-gated sodium channel beta subunit genes: Implications for the evolution of electrical signaling in vertebrates. *BMC Evol Biol*. 2007;7:1-24. doi:10.1186/1471-2148-7-113

81. Calhoun JD, Isom LL. The role of non-pore-forming b subunits in physiology and pathophysiology of voltage-gated sodium channels. *Handb Exp Pharmacol*. 2014;221:51-89. doi:10.1007/978-3-642-41588-3_4

82. Isom LL, Scheuer T, Brownstein AB, Ragsdale DS, Murphy BJ, Catterall WA. Functional co-expression of the β1 and type IIA α subunits of sodium channels in a mammalian cell line. *J Biol Chem*. 1995;270(7):3306-3312. doi:10.1074/jbc.270.7.3306

83. Qu Y, Isom LL, Westenbroek RE, et al. Modulation of cardiac Na+ channel expression in Xenopus oocytes by β1 subunits. *J Biol Chem*. 1995;270(43):25696-25701. doi:10.1074/jbc.270.43.25696

84. Nguyen HM, Miyazaki H, Hoshi N, et al. Modulation of voltage-gated K+ channels by the sodium channel β1 subunit. *Proc Natl Acad Sci U S A*. 2012;109(45):18577-18582. doi:10.1073/pnas.1209142109

85. Malhotra JD, Thyagarajan V, Chen C, Isom LL. Tyrosine-phosphorylated and Nonphosphorylated Sodium Channel β1 Subunits Are Differentially Localized in Cardiac Myocytes. *J Biol Chem*. 2004;279(39):40748-40754. doi:10.1074/jbc.M407243200

86. McEwen DP, Isom LL. Heterophilic Interactions of Sodium Channel β1 Subunits with Axonal and Glial Cell Adhesion Molecules. *J Biol Chem*. 2004;279(50):52744-52752. doi:10.1074/jbc.M405990200

87. Chiquet-Ehrismann R. Tenascins. *Int J Biochem Cell Biol*. 2004;36(6):986-990. doi:10.1016/j.biocel.2003.12.002

88. Wong HK, Sakurai T, Oyama F, et al. β subunits of voltage-gated sodium channels are novel substrates of β-site amyloid precursor protein-cleaving enzyme (BACE1) and γ-secretase. *J Biol Chem*. 2005;280(24):23009-23017. doi:10.1074/jbc.M414648200

89. Kim DY, Ingano LAMK, Carey BW, Pettingell WH, Kovacs DM. Presenilin/γ-secretase-mediated cleavage of the voltage-gated sodium channel β2-subunit regulates cell adhesion and migration. *J Biol Chem*. 2005;280(24):23251-23261. doi:10.1074/jbc.M412938200

90. Kim DY, Carey BW, Wang H, et al. BACE1 regulates voltage-gated sodium channels and neuronal activity. *Nat Cell Biol*. 2007;9(7):755-764. doi:10.1038/ncb1602

91. Johnson D, Montpetit ML, Stocker PJ, Bennett ES. The sialic acid component of the β1 subunit modulates voltage-gated sodium channel function. *J Biol Chem*. 2004;279(43):44303-44310. doi:10.1074/jbc.M408900200

92. Johnson D, Bennett ES. Isoform-specific Effects of the β2 Subunit on Voltage-gated Sodium Channel Gating. *J Biol Chem*. 2006;281(36):25875-25881. doi:10.1074/jbc.M605060200

93. Watanabe H, Koopmann TT, Le Scouarnec S, et al. Sodium channel β1 subunit mutations associated with Brugada syndrome and cardiac conduction disease in humans. *J Clin Invest*. 2008;118(6):2260-2268. doi:10.1172/JCI33891

94. Rasband MN. The axon initial segment and the maintenance of neuronal polarity. *Nat Rev Neurosci*. 2010;11(8):552-562. doi:10.1038/nrn2852

95. Buffington SA, Rasband MN. Na+ Channel-Dependent Recruitment of Nav 4 to Axon Initial Segments and Nodes of Ranvier. *J Neurosci*. 2013;33(14):6191-6202. doi:10.1523/JNEUROSCI.4051-12.2013

96. Chen C, Calhoun JD, Zhang Y, et al. Identification of the Cysteine Residue Responsible for Disulfide Linkage of Na + Channel α and β2 Subunits. *J Biol Chem*. 2012;287(46):39061-39069. doi:10.1074/jbc.M112.397646

97. Chen C, Bharucha V, Chen Y, et al. Reduced sodium channel density, altered voltage dependence of inactivation, and increased susceptibility to seizures in mice lacking sodium channel 2-subunits. *Proc Natl Acad Sci*. 2002;99(26):17072-17077. doi:10.1073/pnas.212638099

98. Kaufmann SG, Westenbroek RE, Maass AH, et al. Distribution and function of sodium channel subtypes in human atrial myocardium. *J Mol Cell Cardiol*. 2013;61:133-141. doi:10.1016/j.yjmcc.2013.05.006

99. Veeraraghavan R, Hoeker GS, Alvarez-Laviada A, et al. The adhesion function of the sodium channel beta subunit (β1) contributes to cardiac action potential propagation. *Elife*. 2018;7. doi:10.7554/eLife.37610

100. Maier SKGG, Westenbroek RE, McCormick K a., Curtis R, Scheuer T, Catterall WA. Distinct Subcellular Localization of Different Sodium Channel and Subunits in Single Ventricular Myocytes From Mouse Heart.

Circulation. 2004;109(11):1421-1427. doi:10.1161/01.CIR.0000121421.61896.24

101. Miyazaki H, Oyama F, Inoue R, et al. Singular localization of sodium channel β4 subunit in unmyelinated fibres and its role in the striatum. *Nat Commun*. 2014;5(1):1-15. doi:10.1038/ncomms6525

102. Waxman SG. Axonal conduction and injury in multiple sclerosis: The role of sodium channels. *Nat Rev Neurosci*. 2006;7(12):932-941. doi:10.1038/nrn2023

103. O'Malley HA, Shreiner AB, Chen G-H, Huffnagle GB, Isom LL. Loss of Na+ channel β2 subunits is neuroprotective in a mouse model of multiple sclerosis. *Mol Cell Neurosci*. 2009;40(2):143-155. doi:10.1016/j.mcn.2008.10.001

104. Lopez-Santiago LF, Pertin M, Morisod X, et al. Sodium channel β2 subunits regulate tetrodotoxin-sensitive sodium channels in small dorsal root ganglion neurons and modulate the response to pain. *J Neurosci*. 2006;26(30):7984-7994. doi:10.1523/JNEUROSCI.2211-06.2006

105. Balse E, Boycott HE. Ion Channel Trafficking: Control of Ion Channel Density as a Target for Arrhythmias? *Front Physiol*. 2017;8(OCT):808. doi:10.3389/fphys.2017.00808

106. Lei M, Wu L, Terrar DA, Huang CL-H. Modernized Classification of Cardiac Antiarrhythmic Drugs. *Circulation*. 2018;138(17):1879-1896. doi:10.1161/CIRCULATIONAHA.118.035455

107. Valdivia CR, Tester DJ, Rok BA, et al. A trafficking defective, Brugada syndrome-causing SCN5A mutation rescued by drugs. *Cardiovasc Res*. 2004;62(1):53-62. doi:10.1016/j.cardiores.2004.01.022

108. Schotten U, Verheule S, Kirchhof P, Goette A. Pathophysiological mechanisms of atrial fibrillation: A translational appraisal. *Physiol Rev*. 2011;91(1):265-325. doi:10.1152/physrev.00031.2009

109. Oliver D, Lien CC, Soom M, Baukrowitz T, Jonas P, Fakler B. Functional Conversion between A-Type and Delayed Rectifier K+ Channels by Membrane Lipids. *Science (80-)*. 2004;304(5668):265-270. doi:10.1126/science.1094113

110. Epshtein Y, Chopra AP, Rosenhouse-Dantsker A, Kowalsky GB, Logothetis DE, Levitan I. Identification of a C-terminus domain critical for the sensitivity of Kir2.1 to cholesterol. *Proc Natl Acad Sci U S A*. 2009;106(19):8055-8060. doi:10.1073/pnas.0809847106

111. Steele DF, Eldstrom J, Fedida D. Mechanisms of cardiac potassium channel trafficking. *J Physiol*. 2007;582(1):17-26. doi:10.1113/jphysiol.2007.130245

112. Balse E, El-Haou S, Dillanian G, et al. Cholesterol modulates the recruitment of Kv1.5 channels from Rab11-associated recycling endosome in native atrial myocytes. *Proc Natl Acad Sci U S A*. 2009;106(34):14681-14686. doi:10.1073/pnas.0902809106

113. LeGrice IJ, Takayama Y, Covell JW. Transverse Shear Along Myocardial Cleavage Planes Provides a Mechanism for Normal Systolic Wall Thickening. *Circ Res*. 1995;77(1):182-193. doi:10.1161/01.RES.77.1.182

114. Costa KD, Takayama Y, McCulloch AD, Covell JW. Laminar fiber architecture and three-dimensional systolic mechanics in canine ventricular myocardium. *Am J Physiol - Hear Circ Physiol*. 1999;276(2 45-2). doi:10.1152/ajpheart.1999.276.2.h595

115. Kong C-R, Bursac N, Tung L. Mechanoelectrical excitation by fluid jets in monolayers of cultured cardiac myocytes. *J Appl Physiol*. 2005;98(6):2328-2336. doi:10.1152/japplphysiol.01084.2004

116. Milstein ML, Musa H, Balbuena DP, et al. Dynamic reciprocity of sodium and potassium channel expression in a macromolecular complex controls cardiac excitability and arrhythmia. *Proc Natl Acad Sci*. 2012;109(31):E2134-E2143. doi:10.1073/pnas.1109370109

117. Verkerk AO, van Ginneken ACG, van Veen TAB, Tan HL. Effects of heart failure on brain-type Na+ channels in rabbit ventricular myocytes. *EP Eur*. 2007;9(8):571-577. doi:10.1093/europace/eum121

118. Lin X, Liu N, Lu J, et al. Subcellular heterogeneity of sodium current properties in adult cardiac ventricular myocytes. *Hear Rhythm*. 2011;8(12):1923-1930. doi:10.1016/j.hrthm.2011.07.016

119. Shy D, Gillet L, Abriel H. Targeting the Sodium Channel NaV1.5 to Specific Membrane Compartments of Cardiac Cells: Not a Simple Task! *Circ Res*. 2014;115(11):901-903. doi:10.1161/CIRCRESAHA.114.305305

120. Eichel CA, Beuriot A, Chevalier MYE, et al. Lateral Membrane-Specific MAGUK CASK Down-Regulates NaV1.5 Channel in Cardiac Myocytes. *Circ Res*. 2016;119(4):544-556. doi:10.1161/CIRCRESAHA.116.309254

121. Hund TJ, Koval OM, Li J, et al. A βIV-spectrin/CaMKII signaling complex is essential for membrane excitability in mice. *J Clin Invest*. 2010;120(10):3508-3519. doi:10.1172/JCI43621

122. Mohler PJ, Rivolta I, Napolitano C, et al. Nav1.5 E1053K mutation causing Brugada syndrome blocks binding to ankyrin-G and expression of Nav1.5 on the of cardiomyocytes. *Proc Natl Acad Sci U S A*. 2004;101(50):17533-17538. doi:10.1073/pnas.0403711101

123. Mukhopadhyay D, Riezman H. Proteasome-independent functions of ubiquitin in endocytosis and signaling. *Science*. 2007;315(5809):201-205.

doi:10.1126/science.1127085

124. Foot N, Henshall T, Kumar S. Ubiquitination and the regulation of membrane proteins. *Physiol Rev*. 2017;97(1):253-281. doi:10.1152/physrev.00012.2016

125. Van Bemmelen MX, Rougier JS, Gavillet B, et al. Cardiac voltage-gated sodium channel Nav1.5 is regulated by Nedd4-2 mediated ubiquitination. *Circ Res*. 2004;95(3):284-291. doi:10.1161/01.RES.0000136816.05109.89

126. Wang Y, Du Y, Luo L, et al. Alterations of Nedd4-2-binding capacity in PY-motif of NaV1.5 channel underlie long QT syndrome and Brugada syndrome. *Acta Physiol*. 2020;229(2):e13438. doi:10.1111/apha.13438

127. Cortada E, Verges M. Alterations in ubiquitin-mediated degradation of NaV1.5 can cause arrhythmia. *Acta Physiol*. 2020;229(2):5-7. doi:10.1111/apha.13459

128. Landrum MJ, Lee JM, Benson M, et al. ClinVar: Improving access to variant interpretations and supporting evidence. *Nucleic Acids Res*. 2018;46(D1):D1062-D1067. doi:10.1093/nar/gkx1153

129. Bateman A. UniProt: a worldwide hub of protein knowledge. *Nucleic Acids Res*. 2019;47(D1):D506-D515. doi:10.1093/nar/gky1049

130. Das S, Gilchrist J, Bosmans F, Van Petegem F. Binary architecture of the Nav1.2-β2 signaling complex. *Elife*. 2016;5(February2016):1-21. doi:10.7554/eLife.10960

131. Bouza AA, Philippe JM, Edokobi N, et al. Sodium channel β1 subunits are post-translationally modified by tyrosine phosphorylation, S -palmitoylation, and regulated intramembrane proteolysis. *J Biol Chem*. 2020;295(30):10380-10393. doi:10.1074/jbc.RA120.013978

132. Makita N, Behr E, Shimizu W, et al. The E1784K mutation in SCN5A is associated with mixed clinical phenotype of type 3 long QT syndrome. *J Clin Invest*. 2008;118(6):2219-2229. doi:10.1172/JCI34057

133. Valdivia CR, Medeiros-Domingo A, Ye B, et al. Loss-of-function mutation of the SCN3B-encoded sodium channel 3 subunit associated with a case of idiopathic ventricular fibrillation. *Cardiovasc Res*. 2010;86(3):392-400. doi:10.1093/cvr/cvp417

134. Zimmer T, Biskup C, Bollensdorff C, Benndorf K. The b1 Subunit but not the b2 Subunit Colocalizes with the Human Heart Na+ Channel (hH1) already within the Endoplasmic Reticulum. *J Membr Biol*. 2002;186(1):13-21. doi:10.1007/s00232-001-0131-0

135. Hart GW. Glycosylation. *Curr Opin Cell Biol*. 1992;4(6):1017-1023. doi:10.1016/0955-0674(92)90134-X

136. Vergés M, Sebastián I, Mostov KE. Phosphoinositide 3-kinase regulates the role of retromer in transcytosis of the polymeric immunoglobulin receptor. *Exp Cell Res*. 2007;313(4):707-718. doi:10.1016/j.yexcr.2006.11.010

137. Cortada E, Brugada R, Verges M. N-Glycosylation of the voltage-gated sodium channel β2 subunit is required for efficient trafficking of NaV1.5/β2 to the plasma membrane. *J Biol Chem*. 2019;294(44):16123-16140. doi:10.1074/jbc.RA119.007903

138. Breitfeld PP, Casanova JE, Harris JM, Simister NE, Mostov KE. Expression and analysis of the polymeric immunoglobulin receptor in Madin-Darby canine kidney cells using retroviral vectors. *Methods Cell Biol*. 1989;32(C):329-337. doi:10.1016/S0091-679X(08)61178-4

139. Dulsat G, Palomeras S, Cortada E, Riuró H, Brugada R, Vergés M. Trafficking and localisation to the plasma membrane of Na v 1.5 promoted by the β2 subunit is defective due to a β2 mutation associated with Brugada syndrome. *Biol Cell*. 2017;109(7):273-291. doi:10.1111/boc.201600085

140. Cuartero Y, Mellado M, Capell A, Alvarez-Dolado M, Verges M. Retromer regulates postendocytic sorting of β-secretase in polarized Madin-Darby canine kidney cells. *Traffic*. 2012;13(10):1393-1410. doi:10.1111/j.1600-0854.2012.01392.x

141. Huet G, Hennebicq-Reig S, De Bolos C, et al. GalNAc-α-O-benzyl inhibits NeuAcα2-3 glycosylation and blocks the intracellular transport of apical glycoproteins and mucus in differentiated HT-29 cells. *J Cell Biol*. 1998;141(6):1311-1322. doi:10.1083/jcb.141.6.1311

142. Lippincott-Schwartz J, Liu W. Online Article: Insights into COPI coat assembly and function in living cells. *Trends Cell Biol*. 2006;16(10). doi:10.1016/j.tcb.2006.08.008

143. Zidovetzki R, Levitan I. Use of cyclodextrins to manipulate plasma membrane cholesterol content: Evidence, misconceptions and control strategies. *Biochim Biophys Acta - Biomembr*. 2007;1768(6):1311-1324. doi:10.1016/j.bbamem.2007.03.026

144. Cenedella RJ. Cholesterol Synthesis Inhibitor U18666A and the Role of Sterol Metabolism and Trafficking in Numerous Pathophysiological Processes. *Lipids*. 2009;44(6):477-487. doi:10.1007/s11745-009-3305-7

145. Alberts AW. Discovery, biochemistry and biology of lovastatin. *Am J Cardiol*. 1988;62(15):J10-J15. doi:10.1016/0002-9149(88)90002-1

146. Fenton R, Kung H, Longo D, Smith M. Regulation of intracellular actin polymerization by prenylated cellular proteins. *J Cell Biol*. 1992;117(2):347-356. doi:10.1083/jcb.117.2.347

147. Reverter M, Rentero C, de Muga SV, et al. Cholesterol transport from late

endosomes to the Golgi regulates t-SNARE trafficking, assembly, and function. *Mol Biol Cell*. 2011;22(21):4108-4123. doi:10.1091/mbc.E11-04-0332

148. Drisdel RC, Green WN. Labeling and quantifying sites of protein palmitoylation. *Biotechniques*. 2004;36(2):276-285. doi:10.2144/04362rr02

149. Wan J, Roth AF, Bailey AO, Davis NG. Palmitoylated proteins: Purification and identification. *Nat Protoc*. 2007;2(7):1573-1584. doi:10.1038/nprot.2007.225

150. Mellado M, Cuartero Y, Brugada R, Verges M. Subcellular localisation of retromer in post-endocytic pathways of polarised Madin-Darby canine kidney cells. *Biol cell*. 2014;106(11):377-393. doi:10.1111/boc.201400011

151. Capell A, Steiner H, Willem M, et al. Maturation and pro-peptide cleavage of β-secretase. *J Biol Chem*. 2000;275(40):30849-30854. doi:10.1074/jbc.M003202200

152. Haft CR, de la Luz Sierra M, Bafford R, Lesniak MA, Barr VA, Taylor SI. Human orthologs of yeast vacuolar protein sorting proteins Vps26, 29, and 35: assembly into multimeric complexes. *Mol Biol Cell*. 2000;11(12):4105-4116. doi:10.1091/mbc.11.12.4105

153. Füllekrug J, Shevchenko AA, Simons K. Identification of glycosylated marker proteins of epithelial polarity in MDCK cells by homology driven proteomics. *BMC Biochem*. 2006;7:8. doi:10.1186/1471-2091-7-8

154. Stevenson BR, Siliciano JD, Mooseker MS, Goodenough DA. Identification of ZO-1: A high molecular weight polypeptide associated with the tight junction (Zonula Occludens) in a variety of epithelia. *J Cell Biol*. 1986;103(3):755-766. doi:10.1083/jcb.103.3.755

155. Bolte S, Cordelières FP. A guided tour into subcellular colocalization analysis in light microscopy. *J Microsc*. 2006;224(3):213-232. doi:10.1111/j.1365-2818.2006.01706.x

156. Dunn KW, Kamocka MM, McDonald JH. A practical guide to evaluating colocalization in biological microscopy. *Am J Physiol - Cell Physiol*. 2011;300(4). doi:10.1152/ajpcell.00462.2010

157. Leo-Macias A, Agullo-Pascual E, Delmar M. The cardiac connexome: Non-canonical functions of connexin43 and their role in cardiac arrhythmias. *Semin Cell Dev Biol*. 2016;50:13-21. doi:10.1016/j.semcdb.2015.12.002

158. Janich P, Corbeil D. GM1 and GM3 gangliosides highlight distinct lipid microdomains within the apical domain of epithelial cells. *FEBS Lett*. 2007;581(9):1783-1787. doi:10.1016/j.febslet.2007.03.065

159. Phair RD, Gorski S a., Misteli T. Measurement of Dynamic Protein Binding to

Chromatin In Vivo, Using Photobleaching Microscopy. *Methods Enzymol*. 2004;375(2000):393-414. doi:10.1016/S0076-6879(03)75025-3

160. Kang M, Day CA, Kenworthy AK, DiBenedetto E. Simplified equation to extract diffusion coefficients from confocal FRAP data Minchul. *Traffic*. 2012;29(6):997-1003. doi:10.1016/j.biotechadv.2011.08.021.Secreted

161. Dessau RB, Pipper CB. [’’R"--project for statistical computing]. *Ugeskr Laeger*. 2008;170(5):328-330.

162. Mostov KE, Verges M, Altschuler Y. Membrane traffic in polarized epithelial cells. *Curr Opin Cell Biol*. 2000;12(4):483-490. doi:10.1016/S0955-0674(00)00120-4

163. Weisz OA, Rodriguez-Boulan E. Apical trafficking in epithelial cells: signals, clusters and motors. *J Cell Sci*. 2009;122(23):4253-4266. doi:10.1242/jcs.032615

164. Stoops EH, Caplan MJ. Trafficking to the apical and basolateral membranes in polarized epithelial cells. *J Am Soc Nephrol*. 2014;25(7):1375-1386. doi:10.1681/ASN.2013080883

165. Isom LL, Ragsdale DS, De Jongh KS, et al. Structure and function of the β2 subunit of brain sodium channels, a transmembrane glycoprotein with a CAM motif. *Cell*. 1995;83(3):433-442. doi:10.1016/0092-8674(95)90121-3

166. Freeze HH, Kranz C. Endoglycosidase and glycoamidase release of N-linked glycans. *Curr Protoc Mol Biol*. 2010;2010. doi:10.1002/0471142727.mb1713as89

167. Vagin O, Kraut JA, Sachs G. Role of N-glycosylation in trafficking of apical membrane proteins in epithelia. *Am J Physiol - Ren Physiol*. 2009;296(3). doi:10.1152/ajprenal.90340.2008

168. Aicart-Ramos C, Valero RA, Rodriguez-Crespo I. Protein palmitoylation and subcellular trafficking. *Biochim Biophys Acta - Biomembr*. 2011;1808(12):2981-2994. doi:10.1016/j.bbamem.2011.07.009

169. Füllekrug J, Simons K. Lipid Rafts and Apical Membrane Traffic. *Ann N Y Acad Sci*. 2004;1014(1):164-169. doi:10.1196/annals.1294.017

170. Simons K, Sampaio JL. Membrane Organization and Lipid Rafts. *Cold Spring Harb Perspect Biol*. 2011;3(10):a004697-a004697. doi:10.1101/cshperspect.a004697

171. Kusumi A, Fujiwara TK, Tsunoyama TA, et al. Defining raft domains in the plasma membrane. *Traffic*. 2020;21(1):106-137. doi:10.1111/tra.12718

172. Le Bivic A, Garcia M, Rodriguez-Boulan E. Ricin-resistant Madin-Darby canine kidney cells missort a major endogenous apical sialoglycoprotein. *J*

Biol Chem. 1993;268(10):6909-6916.

173. Sprague BL, McNally JG. FRAP analysis of binding: Proper and fitting. *Trends Cell Biol*. 2005;15(2):84-91. doi:10.1016/j.tcb.2004.12.001

174. Head BP, Patel HH, Insel PA. Interaction of membrane/lipid rafts with the cytoskeleton: Impact on signaling and function. *Biochim Biophys Acta - Biomembr*. 2014;1838(2):532-545. doi:10.1016/j.bbamem.2013.07.018

175. Gómez-Llobregat J, Buceta J, Reigada R. Interplay of cytoskeletal activity and lipid phase stability in dynamic protein recruitment and clustering. *Sci Rep*. 2013;3(1):1-8. doi:10.1038/srep02608

176. Bao Y, Willis BC, Frasier CR, et al. Scn2b Deletion in Mice Results in Ventricular and Atrial Arrhythmias. *Circ Arrhythmia Electrophysiol*. 2016;9(12). doi:10.1161/CIRCEP.116.003923

177. Malhotra J, Chen C, Rivolta I, et al. Characterization of sodium channel alpha- and beta-subunits in rat and mouse cardiac myocytes. *Circulation*. 2001;103(9):1303-1310. doi:10.1161/01.cir.103.9.1303

178. Zimmer T, Biskup C, Dugarmaa S, et al. Functional Expression of GFP-linked Human Heart Sodium Channel (hH1) and Subcellular Localization of the a Subunit in HEK293 Cells and Dog Cardiac Myocytes. *J Membr Biol*. 2002;186(1):1-12. doi:10.1007/s00232-001-0130-1

179. Mercier A, Clément R, Harnois T, Bourmeyster N, Bois P, Chatelier A. Nav1.5 channels can reach the plasma membrane through distinct N-glycosylation states. *Biochim Biophys Acta - Gen Subj*. 2015;1850(6):1215-1223. doi:10.1016/j.bbagen.2015.02.009

180. Ponce-Balbuena D, Guerrero-Serna G, Valdivia CR, et al. Cardiac Kir2.1 and NaV1.5 Channels Traffic Together to the Sarcolemma to Control Excitability. *Circ Res*. 2018;122(11):1501-1516. doi:10.1161/CIRCRESAHA.117.311872

181. Pérez-Hernández M, Matamoros M, Alfayate S, et al. Brugada syndrome trafficking-defective Nav1.5 channels can trap cardiac Kir2.1/2.2 channels. *JCI insight*. 2018;3(18). doi:10.1172/jci.insight.96291

182. O'Malley HA, Isom LL. Sodium Channel β Subunits: Emerging Targets in Channelopathies. *Annu Rev Physiol*. 2015;77(1):481-504. doi:10.1146/annurev-physiol-021014-071846

183. Stockley JH, O'Neill C. Understanding BACE1: essential protease for amyloid-β production in Alzheimer's disease. *Cell Mol Life Sci*. 2008;65(20):3265-3289. doi:10.1007/s00018-008-8271-3

184. Rodriguez-Boulan E, Macara IG. Organization and execution of the epithelial polarity programme. *Nat Rev Mol Cell Biol*. 2014;15(4):225-242. doi:10.1038/nrm3775

185. Zurzolo C, Simons K. Glycosylphosphatidylinositol-anchored proteins: Membrane organization and transport. *Biochim Biophys Acta - Biomembr*. 2016;1858(4):632-639. doi:10.1016/j.bbamem.2015.12.018

186. Delacour D, Koch A, Jacob R. The role of galectins in protein trafficking. *Traffic*. 2009;10(10):1405-1413. doi:10.1111/j.1600-0854.2009.00960.x

187. Gottlieb TA, Ivanov IE, Adesnik M, Sabatini DD. Actin microfilaments play a critical role in endocytosis at the apical but not the basolateral surface of polarized epithelial cells. *J Cell Biol*. 1993;120(3):695-710. doi:10.1083/jcb.120.3.695

188. Verkade P, Harder T, Lafont F, Simons K. Induction of caveolae in the apical plasma membrane of Madin-Darby canine kidney cells. *J Cell Biol*. 2000;148(4):727-739. doi:10.1083/jcb.148.4.727

189. Phair RD, Misteli T. Kinetic modelling approaches to in vivo imaging. *Nat Rev Mol Cell Biol*. 2001;2(12):898-907. doi:10.1038/35103000

190. Cortada E. Effects of the D211G mutation in membrane dynamics of the cardiac voltage-gated sodium channel beta2 subunit. In: *Master's Report*. University of Girona; 2015:1-35.

191. Peran M, Hicks BW, Peterson NL, Hooper H, Salas R. Lateral mobility and anchoring of recombinant GABA A receptors depend on subunit composition. *Cell Motil Cytoskeleton*. 2001;50(2):89-100. doi:10.1002/cm.1043

192. Bao Y, Isom LL. NaV1.5 and Regulatory β Subunits in Cardiac Sodium Channelopathies. *Card Electrophysiol Clin*. 2014;6(4):679-694. doi:10.1016/j.ccep.2014.07.002

193. Pralle a., Keller P, Florin EL, Simons K, Hörber JKHH. Sphingolipid-cholesterol rafts diffuse as small entities in the plasma membrane of mammalian cells. *J Cell Biol*. 2000;148(5):997-1007. doi:10.1083/jcb.148.5.997

194. Agarwal SR, Yang PC, Rice M, et al. Role of membrane microdomains in compartmentation of cAMP signaling. *PLoS One*. 2014;9(4). doi:10.1371/journal.pone.0095835

195. Marlar S, Arnspang EC, Pedersen GA, Koffman JS, Nejsum LN. Measuring localization and diffusion coefficients of basolateral proteins in lateral versus basal membranes using functionalized substrates and kICS analysis. *Biochim Biophys Acta - Biomembr*. 2014;1838(10):2404-2411. doi:10.1016/j.bbamem.2014.06.005

196. Shvartsman DE, Gutman O, Tietz A, Henis YI. Cyclodextrins but not compactin inhibit the lateral diffusion of membrane proteins independent of cholesterol. *Traffic*. 2006;7(7):917-926. doi:10.1111/j.1600-0854.2006.00437.x

197. Remme CA. Cardiac sodium channelopathy associated with SCN5A mutations: electrophysiological, molecular and genetic aspects. *J Physiol*. 2013;591(17):4099-4116. doi:10.1113/jphysiol.2013.256461

198. Shy D, Gillet L, Abriel H. Cardiac sodium channel NaV1.5 distribution in myocytes via interacting proteins: The multiple pool model. *Biochim Biophys Acta - Mol Cell Res*. 2013;1833(4):886-894. doi:10.1016/j.bbamcr.2012.10.026

199. Schmidt JW, Catterall WA. Biosynthesis and processing of the α subunit of the voltage-sensitive sodium channel in rat brain neurons. *Cell*. 1986;46(3):437-445. doi:10.1016/0092-8674(86)90664-1

200. Rook MB, Evers MM, Vos MA, Bierhuizen MFA. Biology of cardiac sodium channel Nav1.5 expression. *Cardiovasc Res*. 2012;93(1):12-23. doi:10.1093/cvr/cvr252

201. Veerman CC, Wilde AAM, Lodder EM. The cardiac sodium channel gene SCN5A and its gene product NaV1.5: Role in physiology and pathophysiology. *Gene*. 2015;573(2):177-187. doi:10.1016/j.gene.2015.08.062

202. Hull JM, Isom LL. Voltage-gated sodium channel β subunits: The power outside the pore in brain development and disease. *Neuropharmacology*. 2018;132:43-57. doi:10.1016/j.neuropharm.2017.09.018

203. Jiang D, Shi H, Tonggu L, et al. Structure of the Cardiac Sodium Channel. *Cell*. 2020;180(1):122-134.e10. doi:10.1016/j.cell.2019.11.041

204. Salvage SC, Huang CLH, Jackson AP. Cell-Adhesion Properties of β-Subunits in the Regulation of Cardiomyocyte Sodium Channels. *Biomolecules*. 2020;10(7):989. doi:10.3390/biom10070989

205. Curran J, Mohler PJ. Alternative Paradigms for Ion Channelopathies : Disorders of Ion Channel Membrane Trafficking and Posttranslational Modification. 2015;(September 2014):1-20. doi:10.1146/annurev-physiol-021014-071838

206. Malhotra J, Koopmann MC, Kazen-Gillespie KA, Fettman N, Hortsch M, Isom LL. Structural requirements for interaction of sodium channel beta1 subunits with ankyrin. *J Biol Chem*. 2002;277(29):26681-26688. doi:10.1074/jbc.M202354200

207. Balse E, Steele DF, Abriel H, Coulombe A, Fedida D, Hatem SN. Dynamic of Ion Channel Expression at the Plasma Membrane of Cardiomyocytes. *Physiol Rev*. 2012;92(3):1317-1358. doi:10.1152/physrev.00041.2011

208. Kaufmann SG, Westenbroek RE, Zechner C, et al. Functional protein expression of multiple sodium channel α- and β-subunit isoforms in neonatal cardiomyocytes. *J Mol Cell Cardiol*. 2010;48(1):261-269.

doi:10.1016/j.yjmcc.2009.04.017

209. Malhotra JD, Kazen-Gillespie K, Hortsch M, Isom LL. Sodium Channel β Subunits Mediate Homophilic Cell Adhesion and Recruit Ankyrin to Points of Cell-Cell Contact. *J Biol Chem*. 2000;275(15):11383-11388. doi:10.1074/jbc.275.15.11383

210. Campuzano O, Sarquella-Brugada G, Fernandez-Falgueras A, et al. Genetic interpretation and clinical translation of minor genes related to Brugada syndrome. *Hum Mutat*. 2019;40(6):749-764. doi:10.1002/humu.23730